IMPACT RESPONSE OF LAMINATED COMPOSITE SKEWED HYPAR SHELL ROOF BY FINITE ELEMENT APPROACH

Thesis Submitted
by

Sanjoy Das Neogi

Doctor of Philosophy (Engineering)

Civil Engineering Department
Faculty Council of Engineering & Technology
Jadavpur University
Kolkata, India
2019

JADAVPUR UNIVERSITY

KOLKATA – 700 032, INDIA

INDEX NO. 289/12/E

1. **Title of the thesis:** Impact Response of Laminated Composite Skewed Hypar Shell Roofs by Finite Element Approach

2. **Name, Designation & Institution of the Supervisor/s:** Dr. Dipankar Chakravorty, Professor, Jadavpur University.
   Dr. Amit Karmakar, Associate Professor, Jadavpur University.

3. **List of publications:**

   International Journal Papers:

   a) Sanjoy Das Neogi, Amit Karmakar, Dipankar Chakravorty, Impact Response of Simply Supported Skewed Hypar Shell Roofs by Finite Element, *Journal of Reinforced Plastics and Composites*, 2011, 30(21)1795-1805, ISSN: 0731-6844

   b) Sanjoy Das Neogi, Amit Karmakar, Dipankar Chakravorty, An investigation of impact induced response of a multilayered composite hypar shell roof-A finite element approach *International Journal of Material Research, Electronics and Electrical Systems,* 2012, 5 (1) ISSN: 0974-6978

   c) Sanjoy Das Neogi , Amit Karmakar, Dipankar Chakravorty, Finite Element Analysis of Corner-Supported Composite Skewed Hypar Shell Roof Impacted by a Solid Striker, *International Journal of Engineering Research and Technology,* 2012 1(9) 1-8 ISSN 2278-018

   d) Sanjoy Das Neogi, Amit Karmakar, Dipankar Chakravorty, Behaviour of multilayered simply supported composite hypar shell roof impacted by a solid striker- A finite element approach, *Journal of Structural Engineering,* 2013 Special Issue, ISSN 0970-0137, Issue no 40.1

   e) Sanjoy Das Neogi, Amit Karmakar, Dipankar Chakravorty, Study of dynamic behavior of multilayered clamped composite skewed hyper shell roofs under impact load, Journal of Engineering, 2013, 2013 Article ID 192176 /dx.doi.org/10.1155/2013/192176

f) Sanjoy Das Neogi, Amit Karmakar, Dipankar Chakravorty, Finite Element Analysis of Laminated Composite Skewed Hypar Shell Roof Under Oblique Impact with Friction, *Procedia* Engineering, Elsevier, 2017, 173, 314-322, Doi 10.1016/j.proeng.2016.12.023

International Conference Publications:

a) Sanjoy Das Neogi, Amit Karmakar, Dipankar Chakravorty, Study of dynamic behavior of multilayer composite skewed hyper shell roofs under impact load , *56th Congress of ISTAM,* SVNIT, Surat 2011.

b) Sanjoy Das Neogi, Amit Karmakar, Dipankar Chakravorty, Behavioral study of multilayered clamped composite hypar shell roof impacted by solid striker, *The 19th International Congress of Sound and Vibration,* Lithuania 2012.

c) Sanjoy Das Neogi, Amit Karmakar, Dipankar Chakravorty, Behavior of clamped composite hypar shell roof impacted by a solid striker- A finite element approach, *3rd Asian Conference on Mechanics of Functional Materials and Structures*, IIT Delhi December, 2012.

d) Sanjoy Das Neogi, Amit Karmakar, Dipankar Chakravorty, Behaviour of multilayered simply supported composite hypar shell roof impacted by a solid striker- A finite element approach, *Fourth International Congress on Computational Mechanics and Simulation,* IIT Hydrabad, December 2012.

e) Sanjoy Das Neogi, Amit Karmakar, Dipankar Chakravorty, Analysis of point supported hypar shell roofs under impact load- A selection guideline, *International Conference on Materials Science and Chemical Engineering (MSCE 2013),* Singapur, February 2013.

f) Sanjoy Das Neogi, Amit Karmakar, Dipankar Chakravorty, Vibration Characteristics of Point-Supported Composite Skewed Hypar Shell Roof under Sudden Impact, *20th International Congress on Sound and Vibration (ICSV20)*, Bangkok, Thailand, July 2013.

g) Sanjoy Das Neogi, Amit Karmakar, Dipankar Chakravorty,Dynamic Analysis of Simply Supported Laminated Composite Hypar Shell Roof Subjected to Oblique Impact by Finite Element, *17th International Conference of Composite Structures (ICCS17),* Portugal, May 2013.

h) Sanjoy Das Neogi, Amit Karmakar, Dipankar Chakravorty, Dynamics of laminated composite hypar shell roof due to Oblique impact with friction, *58 Congress of ISTAM*, December 2013, BESU, Shibpur.

i) Sanjoy Das Neogi, Amit Karmakar, Dipankar Chakravorty, Finite Element Analysis of Composite Hyper Shell Roof Due to Oblique Impact, *5th International Congress*

on Computational Mechanics and Simulation (ICCMS-2014) December 2014, CSIR-Structural Engineering Research Centre, Chennai.

j) Sanjoy Das Neogi, Amit Karmakar, Dipankar Chakravorty, Finite Element Analysis of Laminated Composite Skewed Hypar Shell Roof Under Oblique Impact with Friction, *11th International Symposium on Plasticity and Impact Mechanics, Implast* 2016, December 2016 Department of Civil Engineering IIT Delhi.

k) Sanjoy Das Neogi, Amit Karmakar, Dipankar Chakravorty, Finite Element Application in Analysis and Design of Corner-Supported Composite Skewed Hypar Shell Roof under Low-Velocity Impact- Selection Guide Lines, International Conference on Computational Mechanics and Structures (ICCMS-2017), December 27 - 29, 2017 Department of Civil Engineering, IIT Hyderabad.

4. **List of Patents**: No.

5. **List of Presentations in National/International**:

International Presentations:

a) Sanjoy Das Neogi, Amit Karmakar, Dipankar Chakravorty, Behavior of clamped composite hypar shell roof impacted by a solid striker- A finite element approach, *3rd Asian Conference on Mechanics of Functional Materials and Structures*, IIT Delhi December, 2012.

b) Sanjoy Das Neogi, Amit Karmakar, Dipankar Chakravorty, Dynamics of laminated composite hypar shell roof due to Oblique impact with friction, *58 Congress of ISTAM*, December 2013, BESU, Shibpur.

c) Sanjoy Das Neogi, Amit Karmakar, Dipankar Chakravorty, Finite Element Analysis of Composite Hyper Shell Roof Due to Oblique Impact, *5th International Congress on Computational Mechanics and Simulation (ICCMS-2014)* December 2014, CSIR-Structural Engineering Research Centre, Chennai.

d) Sanjoy Das Neogi, Amit Karmakar, Dipankar Chakravorty, Finite Element Analysis of Laminated Composite Skewed Hypar Shell Roof Under Oblique Impact with Friction, *11th International Symposium on Plasticity and Impact Mechanics, Implast* 2016, December 2016 Department of Civil Engineering IIT Delhi.

e) Sanjoy Das Neogi, Amit Karmakar, Dipankar Chakravorty, Finite Element Application in Analysis and Design of Corner-Supported Composite Skewed Hypar Shell Roof under Low-Velocity Impact- Selection Guide Lines, International Conference on Computational Mechanics and Structures (ICCMS-2017), December 27 - 29, 2017 Department of Civil Engineering, IIT Hyderabad.

CERTIFICATE FROM THE SUPERVISOR

*This is to certify that the thesis entitled "**Impact Response of Laminated Composite Skewed Hypar Shell Roof by Finite Element Approach**" submitted by Shri Sanjoy Das Neogi, who got his name registered on 28.3.2012 for the award of Ph.D. (Engg.) degree of Jadavpur University is absolutely based upon his own work under the supervision of Dr. Dipankar Chakravorty and Dr. Amit Karmakar and that neither his thesis nor any part of the thesis has been submitted for any degree/diploma or any other academic award anywhere before.*

.....…… …….....

Dr. Dipankar Chakravorty
Professor ,
Civil Engineering Department
Jadavpur University, Kolkata.

Dr. Amit Karmakar
Associate Professor,
Department of Mechanical Engineering
Jadavpur University, Kolkata.

CERTIFICATE

The foregoing thesis is hereby approved as a creditable study of an engineering subject carried out and presented in a manner satisfactory to warrant its acceptance as a prerequisite to the Ph.D. degree (Engineering) for which it has been submitted. It is understood that by this approval the undersigned do not necessarily endorse or approve any statement made, opinion expressed or conclusion drawn therein, but approve the thesis only for the purpose for which it is submitted.

Final Examination for

Evaluation of Thesis

1. _____

2. _____

3. _____

(Signatures of Examiners)

ACKNOWLEDGEMENT

The author owes his most sincere thanks and profound gratitude to his supervisors, Prof. Dr. Dipankar Chakravorty and Prof. Dr. Amit Karmakar for their indispensable advice and inspiration rendered at each phase of the research work. Their valuable suggestions, constructive criticism and critical evaluation throughout the research work are thankfully acknowledged.

The author is grateful to the Head of the Department and to all the faculty members of Civil Engineering Department for their cooperation. The author also expresses his gratitude to staff members of the departmental library and the central library of Jadavpur University.

The excellent cooperation and support of the co-researchers are thankfully acknowledged.

It would not have been possible for the author to pursue the research work without the constant effort, sacrifices and encouragement of his parents from the very first day of his student life till date.

The author is deeply indebted to his parents for their blessing and good wishes that have always encouraged him. The author should acknowledge his wife and his children for their love, encouragement, inspiration and help to ensure his full-time devotion to research by relieving him of household activities.

The author is thankful to all those, whose efforts either directly or indirectly have contributed substantially during the course of this thesis work.

Signature of the Candidate:

Date:

Place: Kolkata

TABLE OF CONTENTS

LIST OF FIGURES

LIST OF TABLES

NOTATIONS

The following notations are used in the text of the thesis. The symbols which are not listed in the following are explained where they appear for the first time.

1. VARIABLES IN MATRIX FORM

$[B]$	Strain-displacement matrix
$[D]$	Constitutive relationship matrix
$[J]$	The Jacobian matrix
$[K_e]$	Element stiffness matrix

2. VARIABLES AS VECTORS

$\{d_i\}$	Element nodal displacement vector
$\{d\}$	Global displacement vector of the shell
$\{F\}$	Force vector for impact
$\{F_c\}$	Contact force

3. OTHER VARIABLES

A_0-A_7	Constant terms of displacement polynomial
a,b	Length and width of shell in plan
E_{11}, E_{22}	Elastic moduli
F_{cki}	Contact force in k^{th} direction at i^{th} iteration
G_{12}, G_{13}, G_{23}	Shear moduli
H_h, H_l	Higher and lower height of conoidal shell
h	Shell thickness
M_x, M_y	Moment resultants per unit length of the shell
M_{xy}	Torsional moment resultant per unit length of the shell
m_i	Mass of impactor

N_1 to N_8	Shape functions for first to eight nodes of the element
N_x, N_y	In-plane normal force resultants per unit length of the shell
N_{xy}	In-plane shear force resultant per unit length of shell
Q_x, Q_y	Transverse shear resultants per unit length of shell
q	Intensity of uniformly distributed load
R_{xy}	Radius of cross curvature of conoidal shell
R_{xx}	Radius of curvature along global x-axis of the shell
R_{yy}	Radius of curvature along global y-axis of the shell
t_c	Time instant of contact
u, v, w	Translational degrees of freedom along global x, y and z axes of the shell, respectively
x, y, z	Global co-ordinates of the laminate
z_k , z_{k-1}	Top and bottom distance of the k^{th} ply from mid-plane of a laminate
α,β	Rotations about y and x axes, respectively
α_i	indentation parameter at any i^{th} iteration
α_m	Maximum local indentation
α_{cr}	Critical indentation beyond which permanent indentation occurs
γ_{xy} ,γ_{xz}, γ_{yz}	In-plane and transverse shear strains, respectively
ε_x, ε_y	In-plane strains along x and y axes of the shell
θ	Orientation of fibers in a lamina with respect to the global x-axis of shell
θ_i	Angle of impact with z-direction
μ_x, μ_y	coefficients of friction in global x and y-direction of graphite-epoxy composite

ν_{ij}	Poisson's ratio which characterizes compressive strain along x_j direction produced by a tensile strain applied in x_i direction
ξ, η, ζ	Natural co-ordinates of isoparametric elements
σ_x, σ_y	Normal stresses
$\tau_{xy}, \tau_{xz}, \tau_{yz}$	Shear stresses
k_x, k_y, k_{xy}	Curvature changes of the shell due to loading
k	Contact stiffness
w_i	Vertical displacement of impactor due to contact
w_s	Displacement of shell due to impact
x_c, y_c	Coordinate of point of contact

ABSTRACT

Man has related himself with shell structures through natural examples from the very first dawn of civilization. Enhanced load carrying capacity of curve surfaces have facilitated mankind and the earliest balloons, tyres, pressure cookers and domes were conceptualized imitating the natural examples of human skull, egg shell etc. The application, fabrication, construction and research on shell structures have sailed a long way and researchers are now engaged in analyzing and designing shell structures with laminated composites. Successful implementation of laminated composites in fabrication of shell surfaces requires understanding of its behavioral characteristics comprehensively. To attain this, understanding the current status of shell research and indentifying the areas which has not been explored are mandatory requirements. With this aim, the literature on laminated composites is reviewed thoroughly to identify the broad scope which needs to be addressed. The actual scope of the present study is defined subsequently from the broad scope and the skewed hypar graphite-epoxy shell is picked up for present study. A finite element formulation is developed using an eight noded curved quadrilateral element. The modified Harzian contact law is used to model the contact mechanics and the dynamic equation of equilibrium is solved using Newmark's time integration scheme. The present code is validated through solution of a number of benchmark problems.

A number of other problems with a number of practical parametric variations like stacking sequences and boundary conditions are solved. Both normal and oblique low velocity impact are considered. The results are presented systematically in form of tables and figures. The results are meticulously examined to extract meaningful conclusion of engineering significance. The conclusions are presented systematically at the end of the chapters.

Scope of future research is indicated at the end of the thesis.

ORGANISATION OF THE THESIS

The thesis is divided into nine chapters and one appendix. Chapter 1 contains the general introduction, course of development of shell structure and research importance of present study. In Chapter 2, the review of the existing literature is reported meticulously. The available literature is thoroughly analyzed and critically discussed to identify the lacunae present therein. Based on the elaborate review exercise, the actual scope of the present work is outlined and presented in Chapter 3. Having defined the scope, Chapter 4 contains the mathematical formulation employed in the present analysis. A wide spectrum of author's own problems are taken up and solved with different practical parametric variations and are discussed in details in Chapters 5, 6, 7 and 8. Results are also obtained for some specific benchmark problems solved by earlier investigators to establish the validity of the present formulation in relevant chapters. Chapter 5 deals with impact response of simply supported laminated composite skewed hypar shells. Chapter 6 reports impact response of laminated composite skewed hypar shells with clamped boundary condition. Chapter 7 proposes some design guidelines for point supported laminated composite skewed hypar shells considering the dynamic behavior due to impact load. Response of simply supported laminated skewed hypar shell due to oblique impact is presented in Chapter 8 considering dry friction between the impactor and shell surface. Chapter 9 discusses about the future scope of the present study. The references are presented in the Appendix.

Chapter 1

INTRODUCTION

1.1 GENERAL

Man has been a keen observer of nature from very ancient times and the natural examples of shell structures did not escape his notice. He also understood it well that nature spontaneously evolves means of load transfer mechanism which can guide him to conceptualise and design different structural elements.

Egg and nut shell, animal skulls are natural examples of shell structures imitating which man developed the Chou vases and Greek Urns in shape of shells. With the passage of time, balloons, pressure cookers, various containers and pipes were fabricated as shell structures and the trend is continuing till today.

Section 1.2 briefly captures the developmental course of shell structures and highlights the importance of the present study.

1.2 COURSE OF DEVELOPMENT OF SHELL STRUCTURES AND THE RESEARCH IMPORTANCE OF PRESENT STUDY

Apart from primitive examples of shell structures, more massive structures of shells came into being as early as AD 538 when the mosque of Santa Sofia was built in Istanbul. This mosque was an example of shell structure being used in civil engineering followed by the Pantheon of Rome, having a large span built as early as AD 125. Application of shell structures in other engineering fields gained importance also as a result of which the first prototype submarine was

built in 1620 followed by the earliest pressure cooker being fabricated in 1888. The first half of the eighteenth century saw the introduction of thin walled pressure vessels together with the evolution of pneumatic tyre in 1845. As the course of human civilization attained maturity, shell structures also increasingly found places in different civil engineering applications. Shell structures started being used as roofing units, foundation components, drain storage structures, chimneys, water tanks and cooling towers.

The design of shell structures of different complicated forms necessitated elaborate mathematical treatment and closed form series solution got proposed but for limited class of shells.

Apart from the simple cylindrical and spherical configurations strong and aesthetically appealing elliptical, hyperbolic and conoidal shells started getting places in the industry. These shell configurations with complicated boundary and loading conditions do not admit closed form solutions and the approximate methods like weighted residual method, finite difference method, Rayleigh-Ritz method, and Galerkin method started getting applied to analyse the shell structures. The advent of high-speed computers and the efficiency of the finite element approach to analysis a wide spectrum of shell problems started getting utilised by the researchers and engineers in obtaining solutions of shells with complicated loading and boundary conditions.

The hunt of advanced materials in the weight sensitive branches of engineering resulted in the introduction of laminated composites in the second half of the last century. These composites started getting applied to fabricate aerospace,

naval and civil engineering shell forms. Success of finite element method, the use of high speed computer and the efficiency of the laminated composites collectively created a thrust of wide spread application of composite shell structures with different loading and boundary conditions.

With the increasing acceptability of the laminated composites the researchers and engineers concentrated also on appropriate characterisation of these materials together with studying the different vulnerable aspects, performance of laminated composites in environment having hygro-thermal gradient, behaviour of these materials with low transverse shear strength under impact, delamination, First ply failure of these structures due to fabrication defect or overloading attracted the attention of the researchers also.

Efficient and confident use of laminated composite shells requires knowledge about their performance under different adverse conditions out of which impact response is one of the important areas. A composite civil engineering shell structure may undergo impact effects induced due to snowfall, air bone debris and drop hammer incidents in shop floors. The present study realises the importance of analysing the impact behaviour of laminated composite shells and the industrially popular skewed hypar shell form has been taken up for the study. They are doubly ruled, easy to fabricate, aesthetically pleasant skewed hypar shells have been studied under normal and oblique low velocity impacts to extract meaningful engineering conclusions that may directly being used by practicing engineers.

Chapter 2

REVIEW OF LITERATURE

2.1 GENERAL

Impact is a high force or shock generated over a short period of time when two or more bodies collide. In such occurrence, the time of load application is less than the one third of the lowest natural time period of vibration of the parts. Such a force usually has a greater effect than a force of lower magnitude applied over a proportionately longer period.

Impact on structural elements may be induced due to a number of reasons. Air born debris strikes the adjacent structures causing an impact. Impact is also caused by drop hammer cases in industrial floors and when aircraft strikes flying objects. Research awareness on impact analysis dates back to the nineteenth century when Hertz (1881) proposed a classical contact law for impact between two elastic solids.

Among the different improved sophisticated materials that have been introduced to cast and fabricate structural elements, the laminated composites are one of the most preferred ones. Use of laminated composites in fabricating structural units started from the second half of the last century and has gained great importance due to the versatility of these improved materials. Despite having a number of advantages these materials being weak in transverse shear are susceptible to damage under impact loading.

Keeping in view the importance of research on impact and the necessity of confident use of the laminated composites in the industry, the first step of this research effort is to scrutinise the published

papers on impact particularly those related to impact on composite structures. The review of literature to follow focuses on this.

"Historical Review" presented in Section 2.2 gives a picture of the course of development of research related to impact on structures, which started in the first half of twentieth century (1913). Section 2.3 critically discusses the volume of published literature reported here to identify the areas which require research attention.

2.2 HISTORICAL REVIEW

2.2.1 Normal Impact

Impact may be defined as collision between two or more bodies and is encountered in many fields of science and technology. Classical rigid-body impact dynamics was founded on Newton's laws of motion. Newton (1687) offered the kinematic definition of the coefficient of restitution. Poisson (1817) predicted that an impact generally consists of separate compression and restitution phases.

It is quite obvious, that a proper contact law is indispensable to model an impact problem. The classical contact law between elastic solids was derived by Hertz (1881). He addressed the problem of contact of the elastic bodies under normal loading without friction for isotropic material. Based on some simple assumptions, he confirmed that the contact pressure distribution is hemispherical between two contacting smooth spheres. He also showed that the contact zone of elastic solids with curved profiles in contact is in the shape of an ellipse and non-linearly varying deformation with the normal load. Timoshenko (1913) proposed the basic approach of this theory. Combining the Euler beam theory and Hartzian contact law he studied the low velocity impact problem between a steel ball and an elastic beam. He extended the problem further to solve the impact problem of isotropic plate and shell. Classical contact law proposed by Hertz was used by Goldsmith (1960) to study impact occurrence on homogeneous isotropic material. Sun and Chottopadhyay (1975) proposed an analytical treatment of

the impact performance of composite plate. This may be regarded as one of the earliest analytical work of impact investigation, applying of Mindlin plate theory. Dobyns (1981) pursued similar model among the others, to study the impact response of laminated composite plates.

The problem turned out to be more complicated in case of anisotropic materials like the laminated composites. The classical contact law proposed by Hertz, for homogeneous isotropic material, was found to be inadequate in case of laminated composite. Yang and Sun (1982) conducted tests on static indentation induced by steel balls and proposed a power law for the contact phenomenon based on their study. Tan and Sun (1985) undertook an experimental and analytical study on a laminated composite graphite epoxy plate. They found that the static contact law proposed by Yang and Sun also holds well in case of dynamic impact. Time histories of contact force and displacement were reported by Sun and Chen (1985) for simply supported plate under impact using steel ball as an impactor using the modified Hatzian contact law proposed by Tan and Sun (1985).

Elber (1983) reported that due to low-velocity impact, thin laminates undergo large deformations. Impact induced damage initiation and propagation was investigated by Cantwell and Morton (1985). High velocity impact on laminated composite plate was considered in their analysis. Keer et al. (1986) adopted non Hertzian contact law to describe indentation due to impact. Local deformation of the target structure and the impactor in the contact area was considered to evaluate the response of transversely isotropic beams and plate. Investigation on transient response due to impact on a cylindrical shell was reported by Ramkumar and Thakur (1987). Fourier series solution technique was applied in the analysis to describe transient response. Wu and Chang (1989) considered the impact response of a steel plate with clamped boundary condition at four edges. They concluded that contact duration depends on the mass of the impactor and contact stiffness as well. An iterative three-dimensional finite element technique was formulated by Hwang and Sun (1989) for failure analysis of laminated composites.

Response of a simply supported orthotropic cylindrical shell was reported by Christiforou and Swamson (1990) subjected to low velocity impact. Local indentation of the target and the striker was neglected in the formulation, and therefore validation of the model remained restricted within loading and unloading phase only. Lin and Lee (1990) examined the impact response of laminated composite plates and shell considering modified Hertzian contact law proposed by Tan and Sun (1985) considering local indentation. Wang and Yew (1990) predicted the damage in thin circular laminates due to low-velocity impact by using energy principles.

Interaction between matrix cracking and delaminations was studied by Choi et al. (1991) due to low velocity impact. They concluded that cracks in outside layers are vertical and caused by bending effects, although in inside layers they are inclined and mainly caused by shear effects. In a later work (1992), the authors proposed a double failure criterion identifying separately, the matrix rupture and delamination. An extensive review of impact response of laminated composite structures was reported by Abrate (1991,1994). Analysis of a laminated composite open cylindrical shell was reported by Gong et al. (1994) under low velocity impact. They considered permanent indentation during impact event following modified Hertzian contact law. Impact analysis of shell structure was formulated by Toh et al. (1995) for an orthotropic laminated cylindrical shell under low velocity impact targeted by a solid striker. Shim et al. (1996) predicted an elastic response of glass/epoxy laminated composite ogival shells subjected to low velocity impact at any arbitrary location by a solid striker. They proposed an analytic bi-harmonic polynomial solution. A numerical analysis procedure was performed by Vaziri et al. (1996) to estimate the impact response of laminated composite plates and cylindrical shell. Hertzian contact law was utilized to describe the impact behavior. An effort to predict the inter-laminar stresses and failure was made by Ganapathy and Rao (1997, 1998) via Kirchhoff-Love shell theory along with Green's tensor. Finite element models, with and without geometric nonlinearity were compared by

Kistler and Waas (1998) for a laminated composite cylindrical shell subjected to transverse central impact. Chun and Lam (1998) reported impact response of fully clamped laminated composite plate. Schoeppner and Abrate (2000) investigated load level causing delamination in composites due to impact. They defined it as delamination threshold load. After studying various models available for analyzing the impact dynamics, Abrate (2001) proposed selection guidelines for choosing an appropriate model for each particular impact event. Krishnamurty et al. (2001, 2003) presented a parametric study of impact response and damage of laminated cylindrical composite shells. They illustrated that the degenerated shell element is sufficiently accurate to be used in impact-damage analysis. Saravanos and Christoforou (2002) formulated the theoretical framework for analyzing low-energy impacts on laminated shells of double curvature with distributed piezoelectric actuator and sensor layers. Contact law was formulated using exact in-plane Ritz solutions by them. Johnson and Holzapfel (2003) reviewed recent progress on material modeling and numerical simulation of soft body impact on fiber reinforced composite structures. Applicability of explicit finite element analysis codes to model composite shell struck by highly deformable soft impactors was also investigated. A finite element analysis strategy was implemented by Mahanta et al. (2004) for estimation of contact force history and stresses in FRP composite laminates subjected to transverse impact. Her and Liang (2004) utilized ANSYS and LS DYNA to investigate the contact force induced impact damage for a laminated composite shell subjected to low velocity impact. While reviewing the current damage mechanics and fracture methods for predicting delamination under impact available in the literature, Elder et al. (2003, 2004) concluded that additional development is required for current techniques before a definitive predictive delamination method be made available. Choi and Lim (2004) compared a linearized contact law with modified Hertzian contact law for low velocity impact analysis of composite laminates. High-order impact model of sandwich beams was developed by Mijia and Pizhong (2005) for impact analysis

of sandwich panels with transversely flexible cores. The system consists of multiple small impactors with small masses. The dynamic response of the composite shells was considered by Jafari et al. (2005) due to transverse impact and axial compressive loads. Convolution integral technique was utilized for solution of the shell under the given loading conditions. A higher-order dynamic impact theory was developed by Malekzadeh (2006) to analyze the low-velocity impact on composite sandwich panel with transversely flexible core hit by multiple small impactors of small masses.

Impact damage is a major issue in the design of laminated composite structures. Delaminations are particularly serious since they are formed at relatively low loads and have a major influence on flexural stiffness and stability against buckling. Li et al. (2006) undertook an experimental program to predict the modes of damage of laminated composites under low-velocity impact. They found that the most common modes of damage are transverse cracking and delamination. A continuum damage mechanics (CDM) model for fabric reinforced composites was proposed by Johnson and Holzapfel (2006) to model both in-ply damage and delamination failure during impact. Delamination criteria were fixed allowing the interfaces to damage and fracture as delamination failure energy criterion was reached. A criterion was derived by Olsson 2006) for delamination inception in transversely isotropic laminated plates under small mass causing high velocity impact. They reported that the resulting delamination threshold load was about 21% higher than the corresponding quasi-static threshold load. Zheng et al. (2006) proposed a kinetic theory and related damage criterion for the composite laminated structures. Finite element code considering geometric nonlinearity was functional to examine the impact mechanical behavior of the composite filament cylindrical vessel. A 3D finite element formulation was carried out by Chakraborty (2007) to evaluate delamination at the interfaces of graphite/epoxy laminated fiber reinforced composites due to low velocity impact of multiple cylindrical impactors. Newmark-β method was used for numerical integration along with Hertzian contact law for transient

dynamic finite element analysis. Zhao and Cho (2007) investigated low-velocity impact-induced damage initiation and propagation in laminated composite shells. Inter-laminar stress distribution and progressive failure were described using three-dimensional eight-noded non-conforming element. A computational model was proposed by Icardi (2007) to explore the local extent and the through-the-thickness position of the damage generated due to low velocity impact on laminated composite plate. Puente et al. (2007) formulated an analytical model to study the impact progression of a spherical projectile indenting into a carbon/epoxy woven laminate at high velocity. The kinetic energy of the projectile was assumed to be absorbed by the laminate by three different mechanisms: laminate crushing, linear momentum transfer and tensile fiber failure. An elasto-plastic contact law was used, by Zheng and Binienda (2007) which accounted for permanent indentation and damage effects, to study small mass impact on laminated composite plates. After of results analysis they opined that damage can change the dynamic response significantly with escalating impact velocity.

Xu et al. (2008) simulated a three-dimensional peridynamic model to forecast delamination and matrix damage patterns. Results were validated with experimentally observed correlation of damage area and impact energy. An investigation on laminated composite thin disks of epoxy resin reinforced by carbon fiber under low velocity impact was performed by Tia et al. (2008). Influence of stacking sequence and energy impact on load–time histories, displacement–time histories and energy–time histories were investigated. Farooq and Gregory (2009) studied the initiation and propagation of barely visible impact damage (BVID) and static-load deflection behavior of fibrous composite panels struck by variable shape indentors using computational model. Setoodeh et al. (2009) coupled three-dimensional elasticity based approach with layer wise laminated plate theory to execute low velocity impact analyses of fiber reinforced laminated composite plates. Yokoyama et al. (2010) formulated an energy-based failure model to work out the impact resistance of composite shells. The damage model formulation combined

stress-based continuum damage mechanics and fracture mechanics approaches. Charpy impact test was chosen by Ghasemnejad et al. (2010) to study the energy absorbing capacity of delaminated carbon/epoxy composite beam. It was shown that composite beams with closer position of delamination to impacted surface are able to absorb more energy in comparison with other delamination positions in hybrid and non-hybrid ones. The generalized ray method (GRM) was employed by Liu (2011) to study beams and layered media under the influence of transient elastic wave. The study was extended to investigate transient response of laminated composite cylindrical shell under impact load. Zhang et al. (2013) performed some experimental and numerical simulations on the vulnerability of laminated glass windows subjected to windborne wooden block impact. Wooden debris of different impact energy were considered. A contact law was proposed by He et al. (2013) to predict the permanent indentation due to low-velocity impact on laminated composites, considering anisotropic elasto-plasticity. Their experimental results showed that fiber failure is primary responsible for failure in composite laminates due to low-velocity impact. A computational model based on the subsection displacement theory and the large deflection analysis was formulated by Wang et al. (2013). They illustrated the dynamic response of isotropic laminated circular plates impacted by a soft body. The model took into account the inter-laminar shear deformation induced in the middle weak layer. Malik et al. (2013) performed a sensitivity analysis to ascertain the degree of influence of various mechanical and material parameters on the impact behavior of the composite laminated plates. Effort was made to pick up the parameter which is needed to be considered more critically in design based on the normalized sensitivity coefficients of each individual parameter. Perez et al. (2013) used a finite element formulation to predict of the impact generated internal damage in composite laminates. Micro-mechanical approach was adopted to estimate the performance of the composite.

Small pieces of gravel impacting a car windshield can cause micro-cracks, which may propagate and lead to dangerous glass fracture events. Marcon et al. (2014), while scrutinizing the fracture mechanics of micro-cracks in the laminated glass plates of car windshields, concluded that cyclic fatigue is not a controlling factor in crack propagation in impacted glass. Farooq and Myler (2014) carried out physical testing and numerical simulations of flat and round nose drop-weight impact on carbon fibre-reinforced laminated composite panels to predict ply level failure. Xiao et al. (2014) reported an analytical approach for measuring the damaged area of a laminate introduced by low velocity impact. Their method was computationally cheaper than the nonlinear three dimensional Finite element analyses. Low-velocity impact responses and impact-induced damages were evaluated by Li et al. (2014) for the stiffened composite laminated plates based on the progressive failure model and layer-wise/solid-elements method (LW/SE). Hertzian contact law was adopted for the analysis. Evci (2015) investigated low velocity impact induced damage properties such as damage thresholds, critical energy thresholds and damage process of laminated composites. Damage thresholds of Hertzian failure of woven and unidirectional Glass Fiber Reinforced Polymer laminates of varying thicknesses were determined through impact tests. Kavousi et al. (2015) analyzed laminated composite beams theoretically for low-velocity impact with arbitrary lay-ups and different boundary conditions subjected to repetitive impacts of multiple masses. Higher-order shear deformation beam theory and modified Hertzian contact law were used for modeling. Numerical examples showed that the time of impact played an important role in determining contact forces, beam displacements, and energies absorbed by the beam. Liu et al. (2015) explored the effect of different failure criteria, including Puck, Hashin and Chang–Chang criteria, on the dynamic progressive failure properties of carbon fiber composite laminates. A unified theoretical framework was presented considering intra-laminar damage and inter-

laminar delamination of composites based on the variational form of the initial value problem with an interface discontinuity.

Repair or reinforcement of damaged part of the composite structure is essential to improve its service life. Energy absorption and impact damage of the repaired laminates were recorded by Chen et al. (2016) when subjected to projectile impact by a gas gun above ballistic velocity at different locations from centre of the patch. Numerical replications were also carried out to detect energy absorbing capability of the repaired composite laminates. Farooq and Myler (2016) formulated a dynamic computational model of low velocity drop-weight impacts on fibre-reinforced laminated composite panels. The model established that flat nose impacts caused localized barely visible internal damage that severely reduces compressive residual strength which might result in catastrophic failure during operation. Haro et al. (2016) investigated ballistic impact behavior of hybrid composite laminates synthesized for armor protection. The energy dissipation potential of the hybrid composite was compared with the initial impact energy of low caliber weapons to determine the protection level achieved by the developed hybrid laminates. Ivancevic and Smojver (2016) proposed a multi-scale impact damage prediction methodology based on a micromechanical model damage formulation for laminated composite structures. They proposed a numerical approach for explicit finite element analyses which was employed for modeling high-velocity impact damage in laminated composites. Transient response of a composite laminated plate and cylindrical shells were studied numerically by Choi (2016) under the action of low-velocity impact. A geometrically nonlinear finite element program was developed using the shear deformation theory of a doubly curved shell and von Karman's large deflection theory. An experimental program was undertaken by Yang et al. (2017) to predict fracture and impact properties of laminated composites. The double cantilever beam configuration was considered to investigate the fracture properties. Impacted composite laminates were mainly carried out

ignoring the local stress non-uniformity and strength difference between the fiber and matrix according to the macro-mechanics-based homogenous strength theories. A multi scale analysis scheme was proposed by Lou et al. (2017) which combined the micromechanics of failure (MMF) theory for intra-laminar damage and cohesive model for inter-laminar failure. Impact fatigue of square plates with holes was studied by Santos et al. (2017) for different relative positions of the point of impact with respect to that of the hole. They observed experimentally that for small relative distances the damage progresses relatively faster. Boria et al. (2017) illustrated the results of an experiment done on a fully thermoplastic composite, where both the reinforcement and the matrix were made with polypropylene. The target structure was examined under different impact loading conditions using a drop weight testing machine. The influence of the impact or mass and velocity on the energy absorption capability of the material was discussed by them. Liao and Liu (2017) reported dynamic mechanical responses and damage mechanisms of plastic fiber-reinforced polymer matrix composite laminate under low velocity impact. They concluded that the plastic damage model leads to higher precision than the elastic damage model as the impact energy becomes relatively large.

Hossoon et al. (2017) formulated a finite element code to predict the behavior of damaged composite wedges under slamming impact. Results were interpreted by assessing the hydro-elastic influence both on kinematic effect owing to deflection of the composite panel and dynamic effect caused due the fluid-structure interaction. An experimental study was carried out by Yang (2017) to explore fracture and impact properties of novel Auxetic Kevlar laminated composites. Auxetic Kevlar reinforced composites depicted a considerable reduction in damaged area compared to the woven counterpart under impact test. Fan and Wang (2017) considered the low-velocity impact response of a shear deformable laminated plate containing both carbon nano-tube reinforced composite layers and fiber reinforced composite layers. A refined self-consistent model was selected allowing for the effect of matrix cracks

to portray the degraded stiffness of the plate. A numerical solution was proposed by Natsuki et al. (2017) to evaluate low velocity impact response of laminated plates having an elastic medium layer. The elastic material present between the laminates was replicated by spring model with constant elastic stiffness. The influences of impactor parameters, such as velocity and mass, on the impact response were also look into.

2.2.2 Oblique Impact

In most of the practical situations the impacts that occur are oblique in nature. Sliding of such impactor over the target surface may cause a frictional drag. Dry friction considered conventionally, depends on normal pressure of contact but is nearly independent of sliding speed. Rickerby and Macmillan (1979) proposed an iterative solution to work out the equation of motion of a spherical impactor and to compute the volume it brushes out over the target surface during the impact event. The model was validated with experimental results. An experimental program was undertaken by Suderarajan and Shewmon (1986) on six different ductile target materials with different levels of impact velocities considering different angles of inclination. A hard steel ball was used as the impactor in experiment. They measured the crater volume created, the rebound velocity and its angle as well. Gupta and Madhu (1991) performed a series of experiments on mild steel plate, subjected to both normal and oblique impact force, fired by spinning armor piercing projectile. A parametric study on residual velocity as well as the damage created due different impact velocities and target thicknesses was presented. Experiments on aluminum alloy cantilever beam were carried out by Shu et al. (1992). Madjidi et al. (1996) carried out an experimental program on reinforced polyester laminates for low velocity oblique impact. They concluded that, between two orthogonal effects of impacts – normal and tangential, the effect of the former is far more significant than that of the latter. An experimental study on normal and oblique impact was reported by Gupta and Madhu (1997). A high velocity impact was fired on single

and layered plate made with mild steel and aluminum. Nature of damage that occurred on the target and residual velocity as well was reported. Tu and Chao (1998) studied oblique impact behavior of a simply supported laminated plate struck by a rigid impactor. Moving boundary problem was considered which consists of an undetermined contact area and undetermined contact stress distribution with anisotropic friction. Energy variation and contact mechanics approach was utilized in the solution method. Spottswood and Palazotto (2001) determined the physical response including material failure of thin curved composite panel intended to resist transverse loading. A nonlinear finite element code was implemented to predict the cause of failure. Luo et al. (2001) reported impact damage initiation and propagation in composite plates. They confirmed that impact damage could be predicted by introducing both threshold strength and propagation strength of matrix cracking. Abrate (2001) compared different mathematical model to portray the impact event. He also compared between simple and complex dynamic model of impact load. An extension of this approach by Rajbhandari (2003) included an additional virtual delamination ply with a reduced shear capacity between the actual plies. This provided better results where axial based damage modes were minimal.

Puente et al. (2008) used a finite element model for carbon/epoxy woven laminates to calculate residual velocity and extend of damaged area under high velocity impact. Experiments using a gas gun were conducted to validate the model. A morphological analysis was also made to investigate the different breakage mechanisms that appear during the indentation. Greve et al. (2008) proposed a simulation technique of stable fragmentation in fibre reinforced composite structures under dynamic compressive loading. An explicit crash code was applied to implement a hybrid modeling technique, in which two distinct material models act simultaneously. A numerical experiment using finite element technique was reported by Mills et al. (2009) to predict the rotational and linear acceleration of a head-form, representing a motorcyclist's head, considering the effects of friction at the head/helmet and

helmet/road interfaces. Oblique impact effect on the skin of the helicopter blade was studied by Navarro et al. (2012) both experimentally and through numerical modelling. A sandwich panel made up of a foam core covered with a thin woven composite skin was utilized as the target material. Damage mechanisms in the skin due to this kind of loading were studied including propagation of damage. Paruka et al. (2013) scrutinized energy absorbed by a square tube made of fiber E-glass and polyester composite to cause a collapse. Quasi-static impacts with four angles of laminates were applied on each specimen to observe the crush behaviors. They concluded that the tube material and structure absorb more energy as the composite suffer more crushing before collapse. Energy absorbed in the tube decreased significantly with increase in impact angle. Ivanez et al. (2015) formulated an experimental study of low-velocity oblique impact on composite sandwich plates. Several impact angles and impact energies were selected to study their influence on the maximum contact force, maximum contact time, absorbed energy and maximum displacement of the impactor and damaged area. They established that peak load and energy absorption rose with increasing impact energy and impact angle, while the contact time remained almost constant. Crushing due to dynamic axial and oblique load on circular tubes with externally press-fitted ring around the outer tube surface was investigated by Isaac et al. (2016). A finite element simulation tool for analysis was functioned. The study establised the potential of improving the energy absorption capacity of a ring strips, fitted around the tube surface. Xie et al. (2016) reported the impact generated perforation behavior of carbon fiber reinforced plastics. Ballistic impact tests were executed on the composite using an one-stage gas gun at different impact angles and impact velocities varying from 70 to 280 m/s. A simple energy model was adopted to study the effect of the impact angle and ballistic limit on the energy dissipated by the laminate at velocity close to the ballistic limit. Tabacu (2016) concentrated on the collapse mode of circular tubes with multi-cell insert due to oblique impact. The material assigned to the structures was such that the material strain-rate

sensitivity could be neglected. Experimental and numerical analyses was performed by Ansari and Chakrabarti (2017) to study the behavior of unidirectional glass fiber reinforced cross ply laminate. Different projectile nose shapes, incidence velocities, incidence angles and laminate thicknesses were considered in the study. Velocity and acceleration-time histories of projectile along with ballistic limit, energy absorption and damage pattern on the target plate were presented. Ansari et al. (2017) studied the ballistic performance of Glass Fiber Reinforced Polymer (GFRP) composite struck by conical nosed steel projectiles. A parametric study on target thicknesses, geometry and boundary conditions was made against contact force, residual velocity and induced damage.

2.3 CRITICAL DISCUSSION

Dynamic response of initially stressed laminated plates was reported by Sun and Chottopadhayay (1975) who also reported the energy transferred to the striking mass during impact. Sun and Chen (1985) also worked on impact on initially stressed composite laminates. Static indentation laws were used for low velocity impact analysis of laminated composite plates by Tan and Sun (1985), while Christiforou and Swamson (1990) chose simply supported orthotropic cylindrical shells for impact analysis. The shells that were considered were complete cylinders and cylindrical shell panels were not studied. Low velocity impact response was studied experimentally by Choi et al. (1991) and Gong et al. (1994) worked on low velocity impact response of composite shell panels using spring mass model. Impact analysis of orthotropic laminated shell panels continued to be studied by Toh et al. (1995) who concentrated on transient stresses. Vaziri et al. (1996) analyzed plates and complete cylinders under impact loads. Cylindrical composite shell panel received attention from Krishnamurty et al. (2001,2003) who worked on impact induced damage. Similar work on impact induced damage initiation and progression was carried out by Zhao and Cho (2007) for cylindrical shell panels. Geometrically non-linear transient dynamic analysis of composite plates and shells was studied by Choi

(2016) for different shell curvatures. Progressive failure of laminated composites under low velocity impact was reported recently by Liao and Liu (2017) using a finite element model.

It is evident from the review of literature that impact response of composite plates has received adequate attention from the researchers, while cylindrical shell panels have found place in very few research articles. The little work that has been reported on the impact response of composite shell panels deals with only with cylindrical shells. A number of industrially preferred shell configurations like spherical, skewed hypar and the conoidal shell panels have not been studied in depth in terms of their behavior under impact loading.

The present study is aimed at fulfilling a part of this lacuna by focusing on impact response of industrially important skewed hypar shell panels.

Chapter 3

SCOPE OF PRESENT STUDY

3.1 GENERAL

Based on the detail review of literature, it is evident that researchers have engaged themselves in exploring different behavioral aspects of laminated composite shells from the second half of the last century. Many important aspects related to direct application of this exotic material in different weight sensitive branches of engineering have been reported as research articles. Still it is felt that successful implementation of this material in fabricating civil engineering shell structures requires a deeper understanding of the impact behavior particularly because these materials are weak in transverse shear.

The present research aims to fulfill this lacuna considering the skewed hypar shell geometry. Section 3.2 outlines the systematic steps that are adopted to fulfill the scope.

3.2 PRESENT SCOPE

A finite element formulation of impact problem is presented employing an eight noded curved quadrilateral element. Strain displacement relationship of thin shell are used to develop the contact forces in the different phases of loading , unloading and reloading. The Newmark's time integration scheme is utilized for solving the dynamic equation of equilibrium.

Response of simply supported and clamped skewed hypar shells subjected to low velocity impact are studied in details. Apart from these, the practical boundary condition of point supports is also considered which does not normally receive attention but has wide practical applications. Both normal impactandoblique impact cases are studied considering the friction between the impactor and the shell surface. The results that are obtained for different stacking

sequences and boundary conditions are studied in details to extract meaningful conclusions of engineering significance.

Chapter 4 presents the mathematical formulation while Chapter 5 to Chapter 8 contain the different problems, related detailed discussion and the significant conclusions. General conclusion, significant contribution and future scope of the present study are indicated in Chapter 9.

Chapter 4

MATHEMATICAL FORMULATION

4.1 GENERAL

This chapter presents the mathematical formulation and solution techniques for study of vibration characteristics of laminated composite hypar shell under normal and oblique impact forces.

The finite element formulation is presented in Section 4.2. The impact formulation adopted is furnished in Section 4.3. Section 4.4 describes the solution technique adopted.

4.2 FINITE ELEMENT FORMULATION

4.2.1 Shell Element

A general shallow skewed hypar shell of plan dimension 'a x b' as shown in Figure 4.1 is considered. The surface defined by Equation 4.4, has only the cross curvature. The equation of the middle surface of a general shell, referred to the Cartesian coordinate system (x, y, z) is expressed as:

$$z = f(x, y) \tag{4.1}$$

A shell is defined as shallow if any infinitesimal line element of its middle surface is approximated by the length of its projection on the XY plane. This implies that

$$\left(\frac{\partial z}{\partial x}\right)^2 << 1\,; \quad \left(\frac{\partial z}{\partial y}\right)^2 << 1\,; \quad \left(\frac{\partial z}{\partial x}\right)\left(\frac{\partial z}{\partial y}\right) << 1 \tag{4.2}$$

Moreover, the lateral boundary of a shallow shell is approximated by its projection on the XY plane with regard to its boundary conditions. According to Vlasov (1958), the above

conditions are practically satisfied for shells with a rise to span ratio less than 1/5 and the curvatures are approximately represented as:

$$\frac{1}{R_x}=\frac{\partial^2 z}{\partial x^2},\ \frac{1}{R_y}=\frac{\partial^2 z}{\partial y^2},\ \frac{1}{R_{xy}}=\frac{\partial^2 z}{\partial x \partial y} \tag{4.3}$$

The skewed hypar shell with only $\frac{1}{R_{xy}}$ has surface equation as follows.

$$z=\frac{4c}{ab}(x-a/2)(y-b/2) \tag{4.4}$$

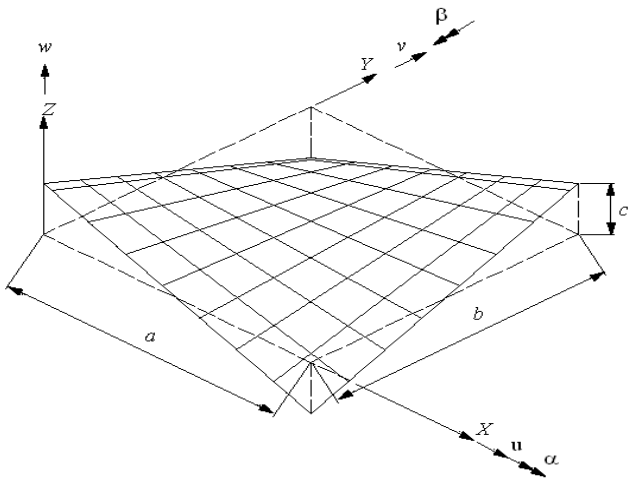

Figure 4.1 Surface of a skewed hypar shell and degrees of freedom

4.2.2 Selection of the shell element

In finite element approach the structure has to be discretized into a number of elements connected at the nodal points. Element shall be such that it can properly characterize the behaviour of the structure. An eight noded curved quadratic isoparametric element is chosen in the present analysis having all three radii of curvature. The quadrilateral element has four corner nodes and four mid side nodes. The isoparametric element (Figure 4.2) is oriented in the natural coordinate system (ξ,η,ζ) and is mapped to the

Cartesian coordinate system using the Jacobian matrix. The local coordinate of the hypar shell is shown in Figure 4.3 in Cartesian coordinate system.

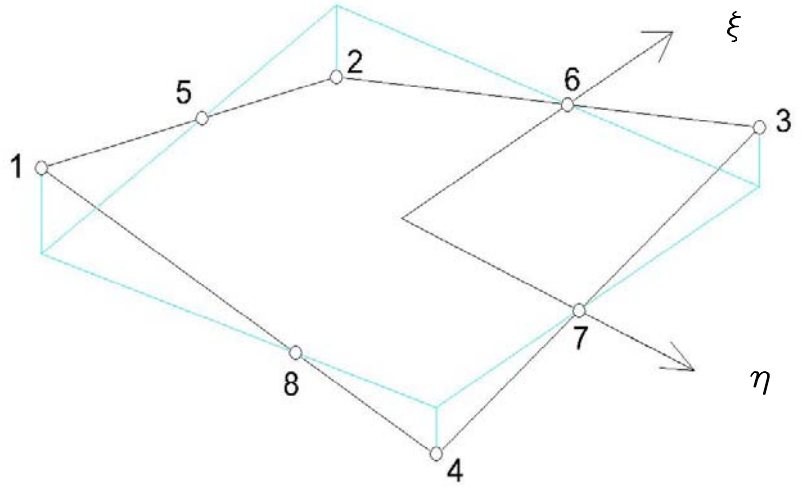

Figure 4.2 The shell element with isoparametric coordinates

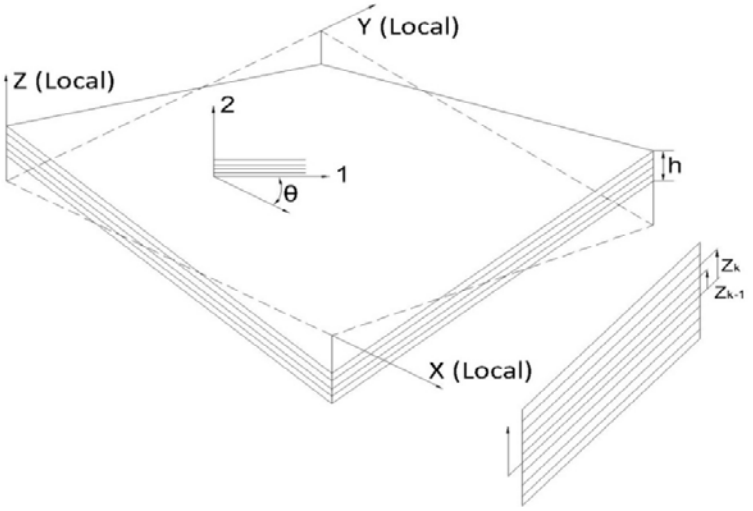

Figure 4.3 The composite skewed hypar shell element with Cartesian coordinates

The full surface of the shell has to be discretized into finite elements. The order of numbering of elements and nodes over the plan area of a typical skewed hypar surface is shown in Figure 4.4 for a typical 8x8 mesh.

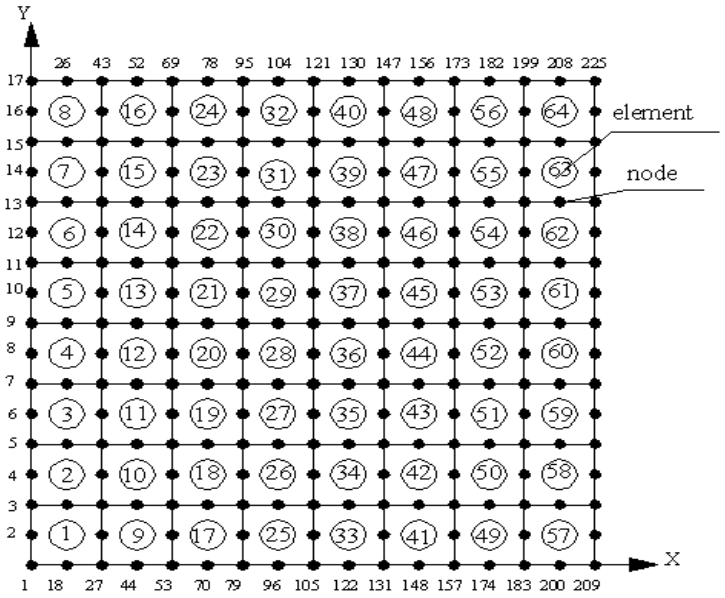

Figure 4.4 A typical discretization of 8x8 mesh on plan area with element and node numbers

4.2.3 Selection of the shape functions

The shape functions or interpolation functions are polynomials of natural coordinates (ξ, η, ζ) which relate the generalized displacements at any point within an element to the nodal values of the displacements. These are derived from an interpolation polynomial in terms of the natural coordinates so that the displacement fields are satisfactorily represented. For the analysis of thin shells, where the final element is assumed to have mid-surface nodes only, the interpolation polynomial is a function of ξ and η and has the following form:

$$u(\xi,\eta) = A_0 + A_1\xi + A_2\eta + A_3\xi^2 + A_4\xi\eta + A_5\eta^2 + A_6\xi^2\eta + A_7\xi\eta^2 \qquad (4.5)$$

The shape functions derived from interpolation polynomial are:

$$N_i = (1+\xi\xi_i)(1+\eta\eta_i)(\xi\xi_i + \eta\eta_i - 1)/4 \qquad \text{for } i=1, 2, 3, 4$$

$$N_i = (1 + \xi\xi_i)(1 - \eta^2)/2 \qquad \text{for } i=5,7$$

$$N_i = (1 + \eta\eta_i)(1 - \xi^2)/2 \qquad \text{for } i=6,8 \qquad (4.6)$$

where, N_i denotes the shape function at ith node having natural coordinates ξ_i and η_i.

The correctness of the shape functions is checked from the relations

$$\sum N_i = 1,\ \sum \frac{\partial N_i}{\partial \xi} = 0 \text{ and } \sum \frac{\partial N_i}{\partial \eta} = 0 \qquad (4.7)$$

In an isoparametric formulation the generalised displacements and coordinates are interpolated from their nodal values by the same set of shape functions. Hence, the coordinates (x, y) of any point within an element are obtained as:

$$x = \sum_{i=1}^{n} N_i x_i \quad y = \sum_{i=1}^{n} N_i y_i \ . \qquad (4.8)$$

where x_i and y_i are the coordinates of the ith node.

4.2.4 Selection of the generalized displacement fields and nodal displacements

Three dimensional solid elements can be operated for modeling of any shell surface. When the thickness of the entity is considerably smaller than the other dimensions, the nodes along the thickness direction contribute additional degrees of freedom than those looked-for and hence are not preferred. Thus five degrees of freedom including three translations (u, v, w) and two rotations (α, β) are attached to each node. The final element has mid-surface nodes only and a line in the thickness direction remains straight but not necessarily normal to the mid-surface after deformation. The directions of the generalized displacements are shown in Figure 4.1.

The following expressions establish the relations between the displacement at any point with respect to the co-ordinates ξ and η and the nodal degrees of freedom.

$$u=\sum_{i=1}^{8}N_i u_i \qquad v=\sum_{i=1}^{8}N_i v_i \qquad w=\sum_{i=1}^{8}N_i w_i \qquad \alpha=\sum_{i=1}^{8}N_i \alpha_i \qquad \beta=\sum_{i=1}^{8}N_i \beta_i \quad (4.9)$$

The generalized displacement vector of an element is expressed in terms of the shape functions and nodal degrees of freedom as:

$$[d_e]=[N]\{d_i\} \tag{4.10}$$

$$\text{i.e., } \{d_e\}=\begin{Bmatrix} u \\ v \\ w \\ \alpha \\ \beta \end{Bmatrix}=\sum_{i=1,8}\begin{bmatrix} [N_i] & & & & \\ & [N_i] & & & \\ & & [N_i] & & \\ & & & [N_i] & \\ & & & & [N_i] \end{bmatrix}\begin{Bmatrix} u_i \\ v_i \\ w_i \\ \alpha_i \\ \beta_i \end{Bmatrix} \tag{4.11}$$

where,

$$[N_i]=[N_1 \quad N_2 \quad N_3 \quad . \quad . \quad . \quad . \quad N_8] \tag{4.12}$$

$$[u_i]=[u_1 \quad u_2 \quad u_3 \quad . \quad . \quad . \quad . \quad u_8] \text{ etc.} \tag{4.13}$$

4.2.5 Strain displacement equations

The strain-displacement relations on the basis of improved first order approximation theory for thin shells are established as:

$$\{\varepsilon\}=\begin{Bmatrix} \varepsilon_x \\ \varepsilon_y \\ \gamma_{xy} \\ \gamma_{xz} \\ \gamma_{yz} \end{Bmatrix}=\begin{Bmatrix} \varepsilon_x^0 \\ \varepsilon_y^0 \\ \gamma_{xy}^0 \\ \gamma_{xz}^0 \\ \gamma_{yz}^0 \end{Bmatrix}+z\begin{Bmatrix} k_x \\ k_y \\ k_{xy} \\ k_{xz} \\ k_{yz} \end{Bmatrix} \tag{4.14}$$

where, the first vector is the mid-surface strain and the second vector is the curvature and are related to degrees of freedom as:

$$\begin{Bmatrix} \varepsilon_x^0 \\ \varepsilon_y^0 \\ \gamma_{xy}^0 \\ \gamma_{xz}^0 \\ \gamma_{yz}^0 \end{Bmatrix} = \begin{Bmatrix} \partial u/\partial x \\ \partial v/\partial y \\ \partial u/\partial y + \partial v/\partial x - 2w/R_{xy} \\ \alpha + \partial w/\partial x \\ \beta + \partial w/\partial y \end{Bmatrix} \tag{4.15}$$

and

$$\begin{Bmatrix} k_x \\ k_y \\ k_{xy} \\ k_{xz} \\ k_{yz} \end{Bmatrix} = \begin{Bmatrix} \partial\alpha/\partial x \\ \partial\beta/\partial y \\ \partial\alpha/\partial y + \partial\beta/\partial x \\ 0 \\ 0 \end{Bmatrix} \tag{4.16}$$

The strain components of the Equation 4.15 and Equation 4.16 are to be judged together for generalized illustration of the three-dimensional strain field and are put across in the following form

$$\{\varepsilon\} = [H]\{d_e\} \tag{4.17}$$

where

$$\{d_e\} = \left\{ \frac{\partial u}{\partial x} \quad \frac{\partial u}{\partial y} \quad \frac{\partial u}{\partial z} \quad \frac{\partial v}{\partial x} \quad \frac{\partial v}{\partial y} \quad \frac{\partial v}{\partial z} \quad . \quad . \quad . \quad . \quad u \quad v \quad w \quad \alpha \quad \beta \right\}^T \tag{4.18}$$

and $[H]$ is an 8×20 matrix of the form given in Table 4.1

In the isoparametric formulation the displacements are interpolated from nodal values via shape functions and therefore the derivatives of the displacements are obtained with respect to the natural coordinates and then appropriate transformation technique is functioned.

Table 4.1 Elements of [*H*]

	1	2	3	4	5	6	7	8	9	10	11	12	13	14	15	16	17	18	19	20
1	1																			
2					1															
3		1		1														$-1/R_{xy}$		
4										1										
5														1						
6											1		1							
7							1												1	
8								1												1

Thus, the vector $\{d_e\}$ is expressed in terms of natural coordinates as:

$$\{d_e\} = [J]^{-1}\{d_n\} \tag{4.19}$$

where,

$$\{d_n\} = \left\{ \frac{\partial u}{\partial \xi} \quad \frac{\partial u}{\partial \eta} \quad \frac{\partial u}{\partial \zeta} \quad \frac{\partial v}{\partial \xi} \quad \frac{\partial v}{\partial \eta} \quad \frac{\partial v}{\partial \zeta} \quad . \quad . \quad . \quad . \quad u \quad v \quad w \quad \alpha \quad \beta \right\}^T \tag{4.20}$$

and $[J]$ is Jacobian matrix expressed as

$$[J]=\begin{bmatrix} \frac{\partial x}{\partial \xi} & \frac{\partial y}{\partial \xi} & \frac{\partial z}{\partial \xi} \\ \frac{\partial x}{\partial \eta} & \frac{\partial y}{\partial \eta} & \frac{\partial z}{\partial \eta} \\ \frac{\partial x}{\partial \zeta} & \frac{\partial y}{\partial \zeta} & \frac{\partial z}{\partial \zeta} \end{bmatrix} \tag{4.21}$$

From Equation 4.20 it is evident that the vector $\{d_n\}$ is obtained on multiplying the nodal displacement vector $\{\delta_i\}$ by a matrix $[\Lambda]$ containing the shape functions and derivatives with respect to the natural coordinates.

Thus,

$$\{d_n\}=[\Lambda]_{20\times 5n}\{\delta_i\}_{5n\times 1} \tag{4.22}$$

where, n is the number of nodes in the element and $\{\delta_i\}$ is given by

$$\{\delta_i\}=\{u_1 \quad v_1 \quad w_1 \quad \alpha_1 \quad \beta_1 \quad . \quad . \quad . \quad . \quad . \quad u_n \quad v_n \quad w_n \quad \alpha_n \quad \beta_n\}^T \tag{4.23}$$

Combining the equations 4.17, 4.19 and 4.20 one gets

$$\begin{aligned} \{\varepsilon\}_{8\times 1} &= [H]_{8\times 20}\{d_e\}_{20\times 1} = [H]_{8\times 20}[J]^{-1}_{20\times 20}\{d_n\}_{20\times 1} \\ &= [H]_{8\times 20}[J]^{-1}_{20\times 20}[\Lambda]_{20\times 5n}\{\delta_i\}_{5n\times 1} = [B]_{8\times 5n}\{\delta_i\}_{5n\times 1} \end{aligned} \tag{4.24}$$

where $[B]$ is the strain displacement matrix.

4.2.6 Force-strain relationship

To establish the relationship between the forces and strains, the shell thickness is assumed to be made of a composite laminate which in turn consists of a number of thin laminae. The principal material axes are designated by 1 and 2 and the moduli of elasticity of a

lamina along these two directions are E_{11} and E_{22} respectively. If the major and minor Poisson's ratios are ν_{12} and ν_{21}, then using the reciprocal relation one obtains

$$\nu_{21} = \left(E_{22} / E_{11}\right)\nu_{12} \tag{4.25}$$

The on-axis elastic constant matrix corresponding to the fibre direction is given by

$$\left[Q_{ij}\right]_{on} = \begin{bmatrix} Q_{11} & Q_{12} & 0 \\ Q_{12} & Q_{22} & 0 \\ 0 & 0 & Q_{66} \end{bmatrix} \tag{4.26}$$

where, $Q_{11} = \left(1 - \nu_{12}\nu_{21}\right)^{-1} E_{11}$,

$$Q_{22} = \left(1 - \nu_{12}\nu_{21}\right)^{-1} E_{22} \ ,$$

$$Q_{12} = \left(1 - \nu_{12}\nu_{21}\right)^{-1} E_{11}\nu_{21},$$

$$Q_{66} = G_{12} \tag{4.27}$$

For obtaining the elastic constant matrix corresponding to any arbitrary principal axes, making an angle θ with the fiber direction, appropriate transformation is necessary. Thus the off-axis elastic constant matrix is formulated from the on-axis elastic constant matrix as:

$$\left[Q_{ij}\right]_{off} = \begin{bmatrix} Q_{11} & Q_{12} & Q_{16} \\ Q_{12} & Q_{22} & Q_{26} \\ Q_{16} & Q_{26} & Q_{66} \end{bmatrix} = [T]^T \left[Q_{ij}\right]_{on} [T] \tag{4.28}$$

in which

$$[T]=\begin{bmatrix} m^2 & n^2 & mn \\ n^2 & m^2 & -mn \\ -2mn & 2mn & m^2-n^2 \end{bmatrix} \tag{4.29}$$

and m=cosθ and n =sinθ (4.30)

The transverse shear deformation, is modeled in the off-axis elastic constant matrix given as:

$$[Q_{ij}]=\begin{bmatrix} Q_{44} & Q_{45} \\ Q_{45} & Q_{55} \end{bmatrix} \tag{4.31}$$

where,

$$Q_{44} = G_{13}m^2 + G_{23}n^2$$

$$Q_{45} = (G_{13} - G_{23})mn$$

$$Q_{55} = G_{13}n^2 + G_{23}m^2 \tag{4.32}$$

where, G_{13} and G_{23} are the shear moduli in the transverse direction, i.e., normal to the laminate plane.

The stress-strain relations are given by

$$\begin{Bmatrix} \sigma_x \\ \sigma_y \\ \tau_{xy} \end{Bmatrix} = \begin{bmatrix} Q_{11} & Q_{12} & Q_{16} \\ Q_{12} & Q_{22} & Q_{26} \\ Q_{16} & Q_{26} & Q_{66} \end{bmatrix} \left\{ \begin{Bmatrix} \varepsilon_x^0 \\ \varepsilon_y^0 \\ \varepsilon_{xy}^0 \end{Bmatrix} + z \begin{Bmatrix} k_x \\ k_y \\ k_{xy} \end{Bmatrix} \right\} \tag{4.33}$$

and $$\begin{Bmatrix} \tau_{xz} \\ \tau_{yz} \end{Bmatrix} = \begin{bmatrix} Q_{44} & Q_{45} \\ Q_{45} & Q_{55} \end{bmatrix} \begin{Bmatrix} \gamma_{xz}^0 \\ \gamma_{yz}^0 \end{Bmatrix} \tag{4.34}$$

The force and moment resultants (refer Figure 4.5) are obtained from the stresses as

$$\{F\} = \begin{Bmatrix} N_x \\ N_y \\ N_{xy} \\ M_x \\ M_y \\ M_{xy} \\ Q_x \\ Q_y \end{Bmatrix} = \int_{-h/2}^{h/2} \begin{Bmatrix} \sigma_x dz \\ \sigma_y dz \\ \tau_{xy} dz \\ \sigma_x z dz \\ \sigma_y z dz \\ \tau_{xy} z dz \\ \tau_{xz} dz \\ \tau_{yz} dz \end{Bmatrix} \tag{4.35}$$

where σ_x and σ_y are the normal stresses along *X* and *Y* directions, respectively and τ_{xy}, τ_{xz} and τ_{yz} are shear stresses in *XY*, *XZ* and *YZ* planes, respectively. The thickness of a laminate is denoted by *h*. In the present case upward deflection, tensile inplane forces, hogging moments and inplane shears tending to rotate the shell element anti-clockwise are taken as positive.

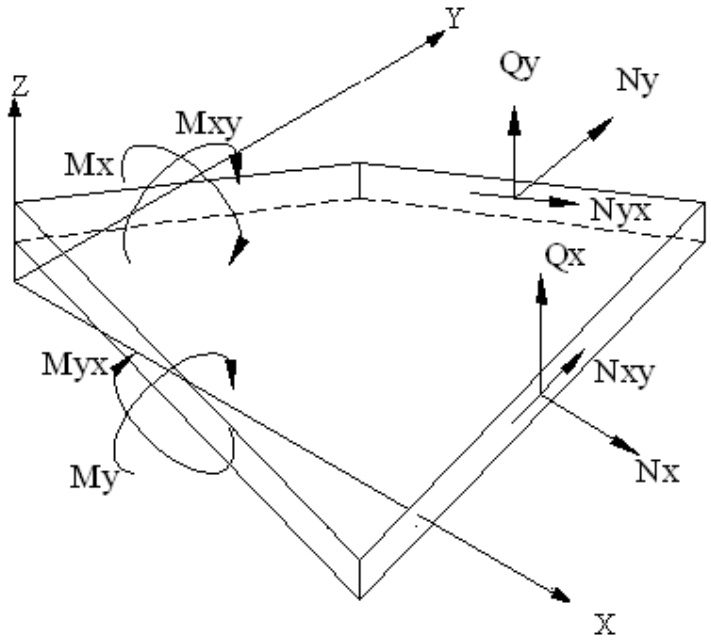

Figure 4.5 Generalized force and moment resultants

Since the laminate consists of a number of laminae, the total stress resultants of an *np*-layer laminate are expressed as

$$\begin{Bmatrix} N_x \\ N_y \\ N_{xy} \end{Bmatrix} = \sum_{k=1}^{np} [Q_{ij}] \left\{ \int_{z_{k-1}}^{z_k} \begin{Bmatrix} \varepsilon_x^0 \\ \varepsilon_y^0 \\ \gamma_{xy}^0 \end{Bmatrix} dz + \int_{z_{k-1}}^{z_k} \begin{Bmatrix} k_x \\ k_y \\ k_{xy} \end{Bmatrix} z dz \right\} \tag{4.36}$$

$$\begin{Bmatrix} M_x \\ M_y \\ M_{xy} \end{Bmatrix} = \sum_{k=1}^{np} [Q_{ij}] \left\{ \int_{z_{k-1}}^{z_k} \begin{Bmatrix} \varepsilon_x^0 \\ \varepsilon_y^0 \\ \gamma_{xy}^0 \end{Bmatrix} z dz + \int_{z_{k-1}}^{z_k} \begin{Bmatrix} k_x \\ k_y \\ k_{xy} \end{Bmatrix} z^2 dz \right\}; \quad \text{i, j=1,2,6} \tag{4.37}$$

$$\begin{Bmatrix} Q_x \\ Q_y \end{Bmatrix} = \sum_{k=1}^{np} [Q_{ij}] \left\{ \int_{z_{k-1}}^{z_k} \begin{Bmatrix} \gamma_{xz}^0 \\ \gamma_{yz}^0 \end{Bmatrix} dz \right\}; \quad \text{i,j = 4,5} \tag{4.38}$$

Equations 4.34, 4.35 and 4.36 are combined to obtain

$$\begin{Bmatrix} N_x \\ N_y \\ N_{xy} \\ M_x \\ M_y \\ M_{xy} \\ Q_x \\ Q_y \end{Bmatrix} = \begin{bmatrix} A_{11} & A_{12} & A_{16} & B_{11} & B_{12} & B_{16} & 0 & 0 \\ A_{12} & A_{22} & A_{26} & B_{12} & B_{22} & B_{26} & 0 & 0 \\ A_{16} & A_{26} & A_{66} & B_{16} & B_{26} & B_{66} & 0 & 0 \\ B_{11} & B_{12} & B_{16} & D_{11} & D_{12} & D_{16} & 0 & 0 \\ B_{12} & B_{22} & B_{26} & D_{12} & D_{22} & D_{26} & 0 & 0 \\ B_{16} & B_{26} & B_{66} & D_{16} & D_{26} & D_{66} & 0 & 0 \\ 0 & 0 & 0 & 0 & 0 & 0 & S_{11} & S_{12} \\ 0 & 0 & 0 & 0 & 0 & 0 & S_{12} & S_{22} \end{bmatrix} \begin{Bmatrix} \varepsilon_x^0 \\ \varepsilon_y^0 \\ \gamma_{xy}^0 \\ k_x \\ k_y \\ k_{xy} \\ \gamma_{xz}^0 \\ \gamma_{yz}^0 \end{Bmatrix} \tag{4.39}$$

or $\{F\}=[D]\{\varepsilon\}$ (4.40)

where,

$$A_{ij} = \sum_{k=1}^{np} (Q_{ij})_k (z_k - z_{k-1}) \; B_{ij} = \frac{1}{2} \sum_{k=1}^{np} (Q_{ij})_k (z_k^2 - z_{k-1}^2)$$

$$D_{ij} = \frac{1}{3} \sum_{k=1}^{np} (Q_{ij})_k (z_k^3 - z_{k-1}^3) \; i,j=1,2,6$$

$$S_{ij} = \sum_{k=1}^{np} F_i F_j (G_{ij})_k (z_k - z_{k-1})\, i,j=1,2 \tag{4.41}$$

In the above equations z_k and z_{k-1} are the distances measured from the midsurface of a laminate to the bottom of the kth and (k-1)th laminate, respectively. $(Q_{ij})_k$ is the off-axis elastic constant matrix for the kth lamina. The 8×8 matrix in Equation 4.39 is termed as the laminate stiffness matrix [D]. Fi and F_j are two shear connection factors presently taken as unity for thin shell.

4.2.7 Element stiffness matrix

The element stiffness and mass matrices and element load vector are derived by using the minimum energy principle. The element stiffness matrix is

$$[K_e] = \iint [B]^T [D][B] dxdy \tag{4.42}$$

The two-dimensional integral is converted to isoparametric coordinates and is carried out by 2×2 Gauss quadrature because the shape functions are derived from a cubic interpolation polynomial and it is an established fact that a polynomial of degree 2n-1 is integrated exactly by n point Gauss quadrature.

4.2.8 Element mass matrix

The generalised inertia matrix per unit area consists of translatory and rotatory inertia terms. The mass and moment of inertia are respectively the measures of translatory and rotatory inertial resistances and are given by the following equations respectively. Mass per unit area is denoted by P and is given by

$$P = \sum_{k=1}^{np} \int_{z_{k-1}}^{z_k} \rho dz \tag{4.43}$$

Moment of inertia per unit area is denoted by I and is given by

$$I = \sum_{k=1}^{np} \int_{z_{k-1}}^{z_k} z\rho dz \tag{4.44}$$

Incorporating both the translatory and rotatory inertia terms, the generalised inertia matrix takes the following form,

$$[M_e] = \iint [N]^T [\rho][N] dxdy\,, \tag{4.45}$$

where,

$$[N] = \sum_{i=1}^{8} \begin{bmatrix} N_i & 0 & 0 & 0 & 0 \\ 0 & N_i & 0 & 0 & 0 \\ 0 & 0 & N_i & 0 & 0 \\ 0 & 0 & 0 & N_i & 0 \\ 0 & 0 & 0 & 0 & N_i \end{bmatrix}, \quad [\rho] = \sum_{i=1}^{8} \begin{bmatrix} \rho & 0 & 0 & 0 & 0 \\ 0 & \rho & 0 & 0 & 0 \\ 0 & 0 & \rho & 0 & 0 \\ 0 & 0 & 0 & I & 0 \\ 0 & 0 & 0 & 0 & I \end{bmatrix}, \tag{4.46}$$

4.3 IMPACT FORMULATION

Impact is a simple occurrence with various complicated consequences, and what appears as a logical conclusion in one situation seems to be completely opposite in another. During the life period of a structure, impacts due to foreign objects are probable to occur during manufacturing, service and maintenance operations. An example of in-service impact is due to wind born debris in cyclone prone areas. During the manufacturing process or during maintenance, tools may drop on the structural floors. In this case, impact velocities are small but the mass of the projectile is large. Laminated composite structures are more susceptible to impact damage than similar metallic structures due to the low transverse shear capacity of composites. In composites, impacts generate internal damage, which is hidden within the plies and which frequently cannot be perceived by visual assessment. This internal damage can cause inexorable diminution in strength

which can mature under load. Therefore, the effects of foreign object impacts on composite structures must be appreciated, and proper measures should be taken in the design process to account for these likely events.

4.3.1 Contact Law

A simple relationship connecting the contact force and the indentation is termed as the contact law. Local deformations in the contact region must be accounted for in the analysis in order to accurately predict the contact force history. The indentation, defined as the difference between the displacement of the projectile and that of the back face of the target body, can be of the same order as or larger than the overall displacement of the laminate. A detailed description of the contact between the impactor and the structure during an impact event would be difficult to assess and is not required as part of the impact dynamics analysis. Instead, what is needed is a contact law relating the contact force to the indentation, which is defined as the motion of the projectile relative to that of the target. With the material systems commonly used, strain rate effects are negligible such that static and dynamic contact laws are identical, and so statically determined contact laws can be used in the dynamic analysis. If k be the contact stiffness and α_m be the maximum local indentation, the contact force F_c during loading is given by (modified Hertzian contact law)

$$F_c = k\alpha_i^{1.5} \quad 0 < \alpha_i \leq \alpha_m \tag{4.47}$$

The indentation parameter α_i at any i^{th} iteration depends on the difference of the displacements of the impactor and the target structure at any instant of time, and the contact force as well i.e. the values of α_i keeps changing with time with time-varying

displacements of both the rigid impactor and the target structure. In the present analysis where oblique impact is also considered along with the normal impact, effect of friction generated due to sliding of the impactor over the surface of the target structure has been considered along with the vertical disarticulation while calculating the indentation parameter and the contact force at each time step. Considering displacements along any arbitrary global directions for oblique impact, the indentation α_i at any ith iteration is given as

$$\alpha_i = w_i(t)\cos\theta_i - w_s(x_c, y_c, t_c) \quad (4.48)$$

where w_i and w_s are displacement of impactor and target shell displacement along global z direction at the point of impact (x_c ,y_c), at any time instant t_c.

Thus, with the maximum indentation taking place, the maximum contact force is attained, followed by the displacement of the impactor reaching its maximum W. Goldmith (1960). Subsequently the displacement of the impactor gradually decreases, but the target point displacement keeps on changing and finally increases to a maximum and then comes a time when these two displacements become equal. This leads to zero value of indentation. Eventually the contact force becomes zero when the impactor loses contact with the target. This process of attaining the maximum contact force till the reduction of the same to zero is fundamentally referred to as unloading. The indentation process introduces damage and permanent deformations in the contact zone; as a result, the unloading curve differs from the loading curve. Provided that the mass of the impactor is not very small, a second impact may occur upon the rebound of the target structure leading to an identical phenomenon of contact deformation and attainment of the maximum. This is known as reloading. In many cases, multiple impacts occur and the reloading curve is again different. If F_m be the maximum contact force at the onset of unloading and α_m be the

maximum indentation during loading, the contact force F_c for unloading and reloading are expressed as. [As proposed by Sun and Chen (1985)]

Unloading phase: $$F_c = F_m \left[\frac{\alpha - \alpha_0}{\alpha_m - \alpha_0} \right]^{2.5} \quad (4.49)$$

Reloading phase: $$F_c = F_m \left[\frac{\alpha - \alpha_0}{\alpha_m - \alpha_0} \right]^{1.5} \quad (4.50)$$

where α_0 denotes the permanent indentation in a loading-unloading cycle and is determined as Sun and Chen (1985)

$\alpha_0 = \beta_c (\alpha_m - \alpha_p)$ if $\alpha_m \geq \alpha_{cr}$ (4.51)

$\alpha_0 = 0$ if $\alpha_m < \alpha_{cr}$ (4.52)

where $\beta_c$is a constant and α_{cr} is the critical indentation beyond which permanent indentation occurs, and the values are 0.094 and .01667cm respectively for graphite-epoxy composite as taken by Sun and Chen (1985).

4.4 SOLUTION TECHNIQUE

4.4.1 Formulation of Dynamic Equation

The dynamic equilibrium equation of the target shell for low velocity impact is given by the following equation:

$$[M]\{\ddot{\delta}\} + [K]\{\delta\} = \{F\} \quad (4.53)$$

where [M] and [K] are global mass and elastic stiffness matrices, respectively. {δ} is the global displacement vector. For the impact problem {F}, the force vector is given as

$$\{F\} = \{0\ 0\ 0\ \ldots . F_c \ldots\ldots 0\ 0\ 0\}^T \quad (4.54)$$

Here F_c is the contact force given by the indentation law and the equation of motion of the rigid impactor is given as:

$$m_i \ddot{\omega}_i + F_C = 0 \tag{4.55}$$

where mi and $\ddot{\omega}_i$ are the mass and acceleration of the impactor respectively. Since the author dealt with impact load in the present thesis, a lumped load scheme has been utilized. The concentrated load is applied at the central node after global numbering, corresponding to the third degree of freedom for that node in the negative direction for normal impact.

However, for oblique impact if μ_x, μ_y be the coefficients of friction in global x and y-direction of graphite-epoxy composite, whereas θ_i be the angle of impact with z-direction. F_{cki} be the contact force in k^{th} direction at i^{th} iteration then we have

$$F_{cz(i+1)}=F_{cz(i)}(t)\cos\theta_i \tag{4.56}$$

$$F_{cx(i+1)}=F_{cx(i)}(t)\sin\theta_i - \mu_x F_{cz(i)}(t)\cos\theta_i \tag{4.57}$$

$$F_{cy(i+1)}=F_{cy(i)}(t)\sin\theta_i - \mu_y F_{cz(i)}(t)\cos\theta_i \tag{4.58}$$

4.4.2 Solution using Newmark's time integration scheme

Aim of the numerical integration of finite element system equilibrium equations is to appraise a good approximation to the actual dynamic response of the structure under consideration. In order to predict the dynamic response of the structure accurately it is required to solve all the system equilibrium equation accurately. Equation 4.53, 4.54 and 4.55 are solved using Newmark constant- acceleration time integration algorithm in the present analysis. Equation 4.42 may be expressed in iteration form at each time step.

$$\left[\bar{K}\right]\{\Delta\}_{t+\Delta t}^{i+1} = \frac{\Delta t^2}{4}\{F\}_{t+\Delta t}^{i} + [M]\{b\}_i \tag{4.59}$$

Where

$$\left[\bar{K} \right] = \frac{\Delta t^2}{4}[K] + [M] \tag{4.60}$$

$$\{b\}_t = \{\Delta\}_t + \Delta t \left\{ \dot{\Delta} \right\}_t + \frac{\Delta t^2}{4} \left\{ \ddot{\Delta} \right\}_t \tag{4.61}$$

The same solution scheme is also utilized for solving the equation of motion of the impactor, i.e. Equation (4.55). It is to be noted that a modified contact force $F^i_{t+\Delta t}$ obtained from the previous iteration is used to solve the current response $\{\Delta\}^{i+1}_{t+\Delta t}$. The iteration procedure is continued until the equilibrium criterion is met.

Chapter 5

IMPACT RESPONSE OF SIMPLY SUPPORTED SKEWED HYPAR SHELL: A NUMERICAL STUDY

5.1 GENERAL

The mathematical formulation presented in Chapter 4 is applied to carry out a number of numerical experimentations considering simply supported composite hypar shells. Numerical examples considered and the corresponding validation are presented in Section 5.2. Section 5.3 contains the important results and the corresponding discussions. The salient findings from this exercise are presented as conclusions in Section 5.4.

5.2 NUMERICAL EXAMPLES

Problems are solved with two different objectives. The present formulation is applied to solve natural frequencies of cantilever graphite-epoxy twisted plates which are structurally similar to skewed hypar shells. This problem is expected to validate both the stiffness and mass matrix formulation of present finite element code. A problem, solved earlier by Sun and Chen[1985] regarding the impact response of composite plate , is taken up as the benchmark problem to validate the impact formulation. The details of the benchmark problems are furnished in Table 5.1 and Figure 5.1

Table 5.1 Non-dimensional fundamental frequencies ($\bar{\omega}$) for three layer graphite-epoxy cantilever twisted plates, [θ/-θ/θ] laminate

Angle of twist θ (deg)		0	15	30	45	60	75	90
$\phi = 15^{\circ}$	Qatu and Lessia[1991]	1.0035	0.9296	0.7465	0.5286	0.3545	0.2723	0.2555
	Present formulation	0.9990	0.9257	0.7445	0.5279	0.3542	0.2720	0.2551
$\phi = 30^{\circ}$	Qatu and Lessia[1991]	0.9566	0.8914	0.7205	0.5149	0.3443	0.2606	0.2436
	Present formulation	0.9490	0.8842	0.7181	0.5142	0.3447	0.2613	0.2444

a/b=1, a/h=100; E_{11}=138 GPa, E_{22}=8.96 GPa, G_{12}=7.1 GPa, ν_{12}=0.3

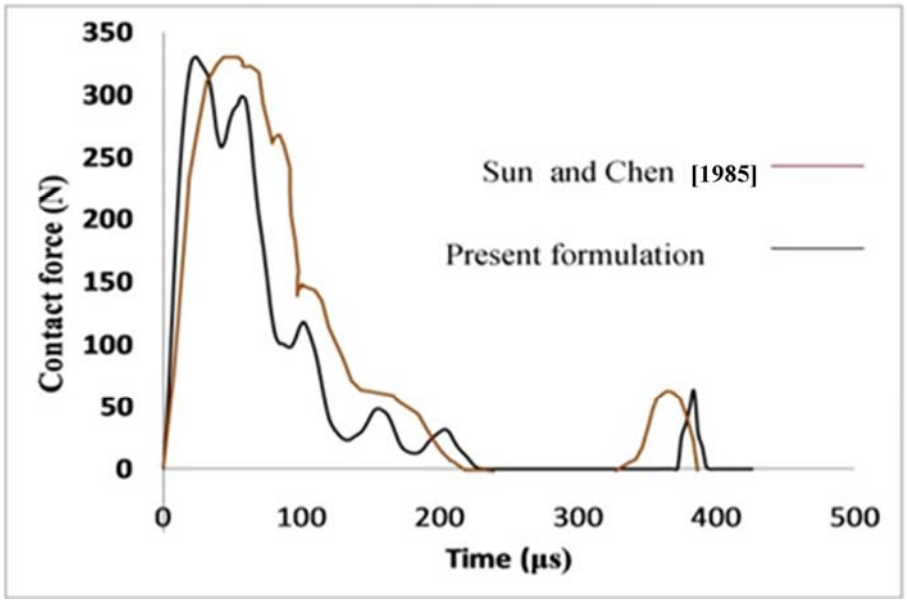

E_{11}=120 GPa, E_{22}= 7.9 GPa, G_{12}= G_{23}=G_{13}=5.5 GPa, ν_{12} =0.30,
ρ=1.58x 10-5 N-sec^2/cm^2
Plate size=20cm x 20cm. x 0.269cm.; Ply orientation = [$0^0/45^0/0^0/-45^0/0^0]^{2s}$ Velocity of impactor = 3m/s; Mass density of impactor = 7.96x10-5 N-sec/cm^4

Figure 5.1 Contact force history of simply supported plate under low velocity impact

Apart from the problems mentioned above, impact response of skewed hypar shells being impacted at the central point are also studied for simply supported boundary condition, different laminations and impact velocities. The details of the problems which are the author's own are given below.

(i)	Boundary condition :-	Simply supported (SS)
(ii)	Lamination:-	$+45^0/-45^0$ (AP), $0^0 / 90^0$ (CP)
(iii)	Velocity of impact (m/s):-	1, 2, 3, 5, 7, 10
(iv)	Details of shell geometry :-	a = 1.0m, b =1.0m, t=0.02m, c=0.2m
(v)	Material details :-	E11=120GPa, E22= 7.9 GPa,
		G12= G23= G13= 5.5GPa
		$\nu_{12} = 0.30$, ρ = 1.58x10-5N-sec^2/cm^4

5.3 RESULTS AND DISCUSSIONS

The results in Table 5.1 show that the fundamental frequency values of the twisted plates obtained by the present formulation agree very closely to those reported by Qatu and Lessia [1991]. This agreement validates the correct incorporation of stiffness and mass matrix formulation in the present code. Figure 5.1 shows the time variation of the contact force induced in a composite plate under low velocity impact previously reported by Sun and Chen [1985]. The values obtained by the present formulation are also presented graphically in the same figure in a different style. Here again excellent agreement of results is observed which establishes the correctness of impact formulation.

To study the impact response of simply supported (SS) angle ply (AP) shell Figure 5.2 to 5.7 and Table 5.2 are studied. All the results of contact force and displacement that are

presented in either graphical or tabular form are arrived at after the study of time step convergence. The finite element mesh adopted is also based on force and displacement convergence criteria. When low velocity normal impact response of simply supported angle ply shell is studied being struck by the spherical impactor centrally, it is observed that the contact force shows a sort of parabolic variation with a single peak. After a given time span which is 100μs or less, the contact force converges to a null value. It is interesting to note that higher the impactor velocity higher is the contact force as expected, but the force dies down to a null value earlier. This behavior may be attributed to the fact that the higher the velocity more rapid is the elastic rebound of the impactor followed by detachment which causes contact force to decay out. It is also very interesting to observe that the time instant corresponding to peak contact force and that for peak displacement do not match. This is because the resultant displacement at any time instant is a cumulative effect of the instantaneous contact force value and the inertia effect of the previous instant. The figure showing the transient displacement reflects the fact that vibration continues even after the force dies down with successively occurring peak though the peak values are less in magnitude than the highest peak which occurs a bit after the instant of maximum contact force but before the full decay of it.

To estimate the equivalent static load (ESL) corresponding to a particular impactor velocity , a concentrated load at the centre (point of impact) is applied and adjusted the yield a central displacement equal to the maximum dynamic displacement. It is further explored to estimate the magnitude of the central displacement when the peak contact force is applied at the point of impact as a static concentrated load. The central displacement obtained under such a load when divides the maximum dynamic displacements yields dynamic magnification factor

(DMF). The variations of maximum contact force, maximum dynamic displacement and equivalent static load (ESL) with impactor velocity are almost linear and of three above mentioned values are increasing functions of impactor velocity. However the dynamic magnification factor (DMF) and the impactor velocity shows a logarithmic relation and the DMF is a decreasing function of velocity.

The behavior of the impact response of simply supported (SS) cross ply (CP) shell may be studied through Figure 5.9 to 5.14 and Table 5.2. The nature of contact force and dynamic displacement for this class (SS/ CP) of shell is more or less similar to what is discussed before for SS/AP shell. One interesting difference is that for SS/ CP shell the peak dynamic displacement does not only show a phase lag with respect to the peak contact force but by time displacement value reaches the peak the contact force value dies down totally. This shows that the after-effect of impact are some times more severe than the shell response during the impact and study of displacement variation even after the contact force decays to a null value is absolutely necessary. However, after passage of some more time the subsequent local maxima which are obtained do not touch the peak.

The dependence of the maximum contact force, the peak dynamic displacement and the equivalent static load (ESL) on the impactor velocity in case of simply supported cross ply (SS /CP) shell are similar to what is observed in case of simply supported angle ply (SS/AP) shell. The same is shown in Figure 5.8 for supported angle ply (SS/AP) shell and in Figure 5.13 for simply supported cross ply (SS /CP) shell.

It is further noted that the maximum value of contact force and displacement for SS /AP and SS /CP shells are almost equal for any given velocity of the impactor. It is further noted that the value of ESL and DMF are higher in case of SS /AP shell.

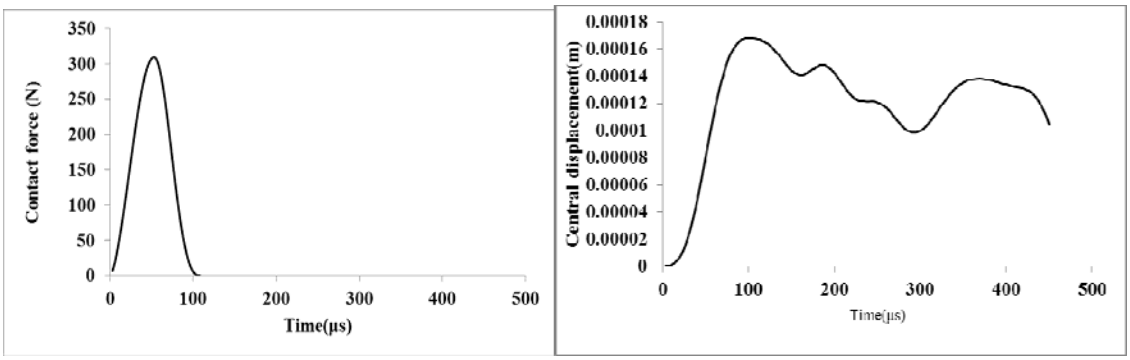

Figure 5.2 Impact response of simply supported angle ply (SS/AP) composite hypar shells for impact velocity 1m/**s**

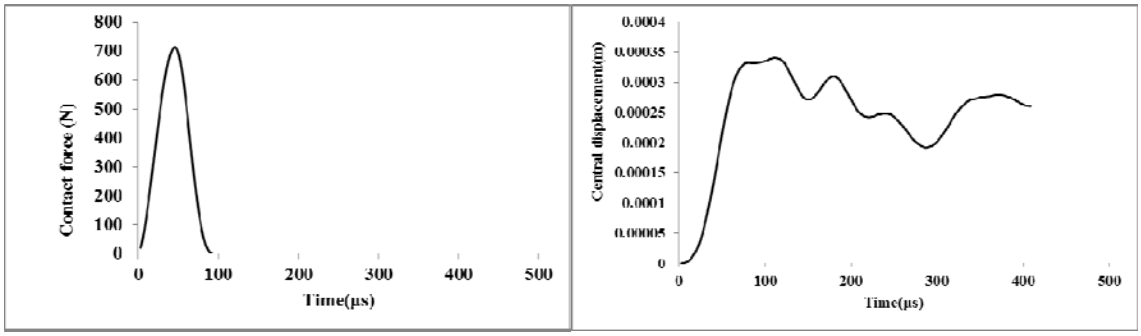

Figure 5.3 Impact response of simply supported angle ply (SS/AP) composite hypar shells for impact velocity 2m/s

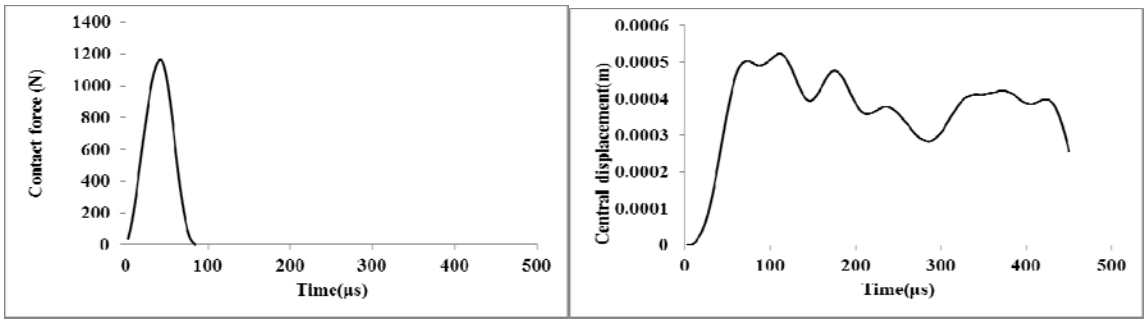

Figure 5.4 Impact response of simply supported angle ply (SS/AP) composite hypar shells for impact velocity 3m/s

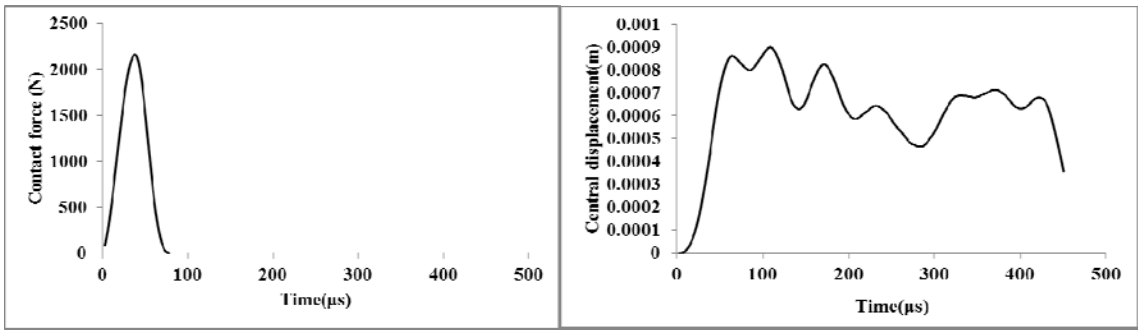

Figure 5.5 Impact response of simply supported angle ply (SS/AP) composite hypar shells for impact velocity 5m/s

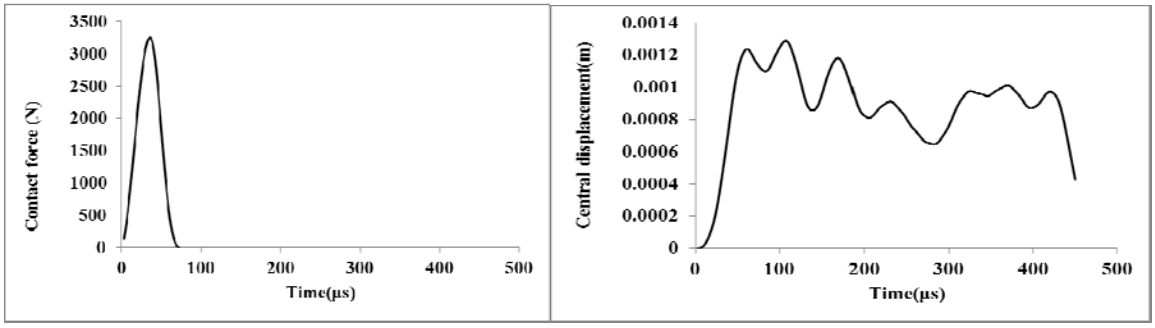

Figure 5.6 Impact response of simply supported angle ply (SS/AP) composite hypar shells for impact velocity 7m/s

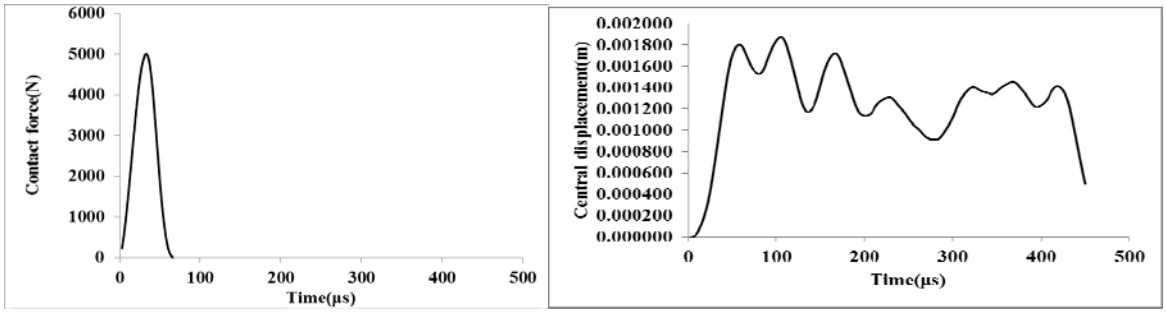

Figure 5.7 Impact response of simply supported angle ply (SS/AP) composite hypar shells for impact velocity 10m/s

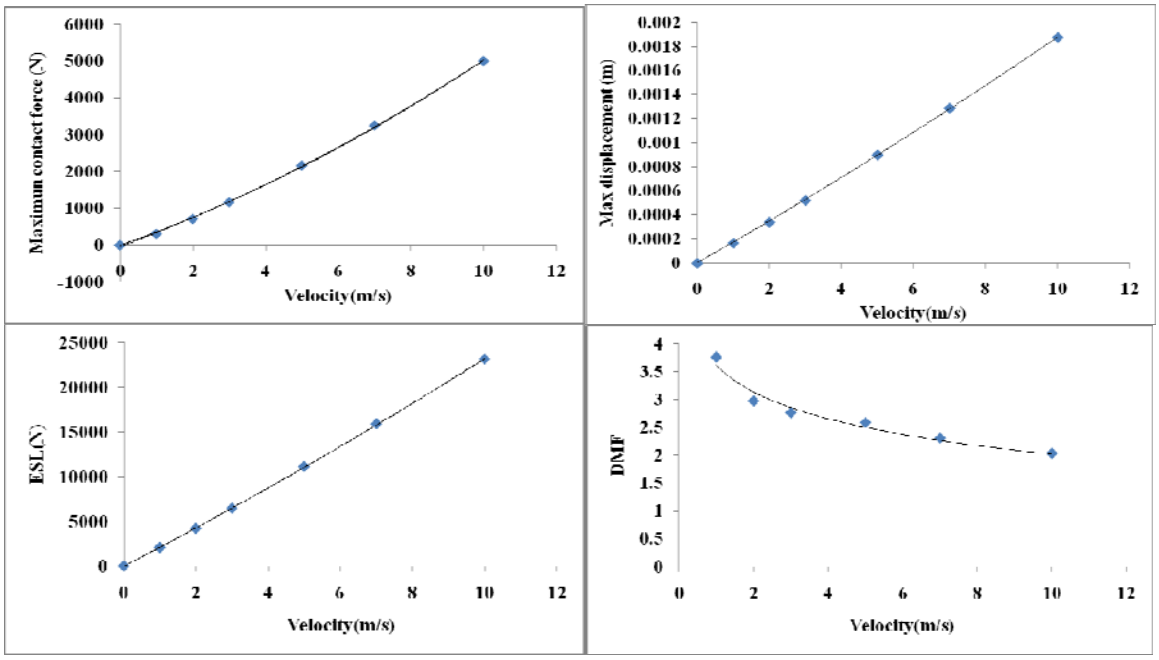

Figure-5.8 Variation of maximum impact load, maximum displacement, equivalent static load and dynamic magnification factor with velocity for simply supported angle ply (SS/AP) composite hypar shells

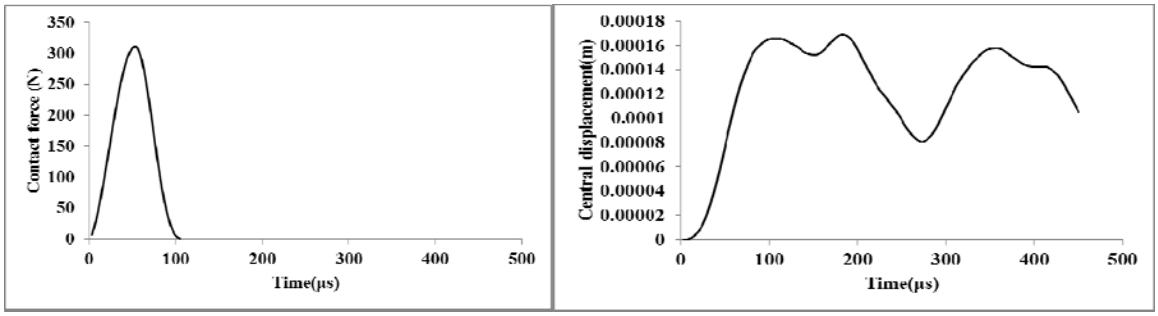

Figure 5.9 Impact response of simply supported cross ply (SS/CP) composite hypar shells for impact velocity 1m/s

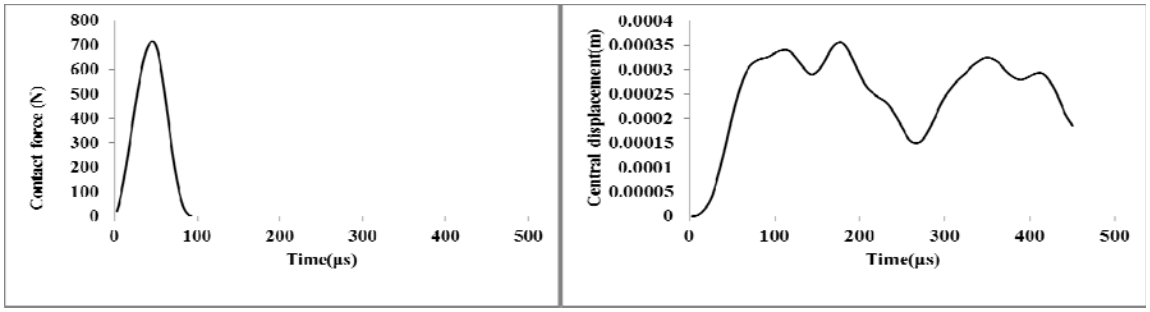

Figure 5.10 Impact response of simply supported cross ply (SS/CP) composite hypar shells for impact velocity 2m/s

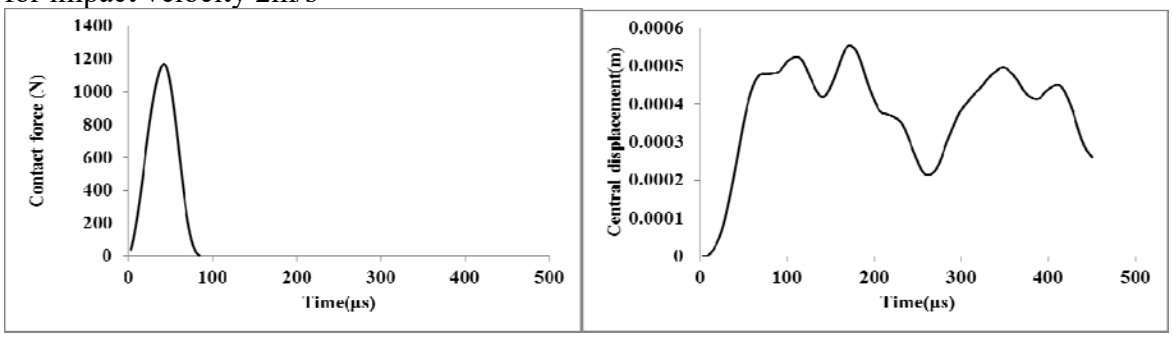

Figure 5.11 Impact response of simply supported cross ply (SS/CP) composite hypar shells for impact velocity 3m/s

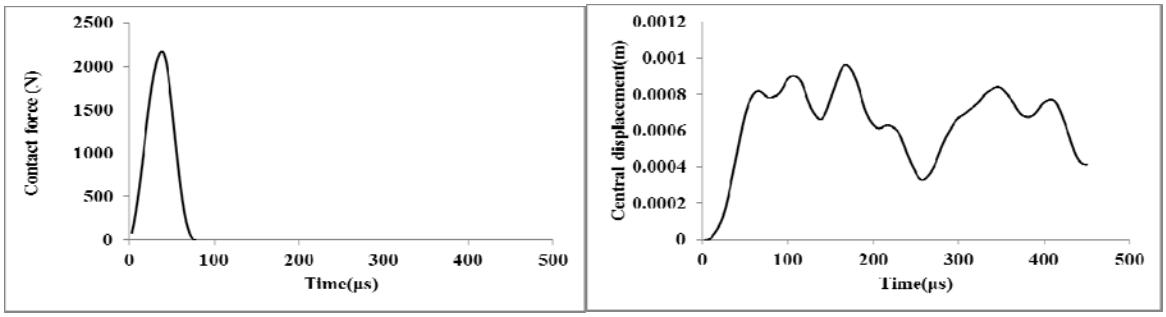

Figure 5.12 Impact response of simply supported cross ply (SS/CP) composite hypar shells for impact velocity 5m/s

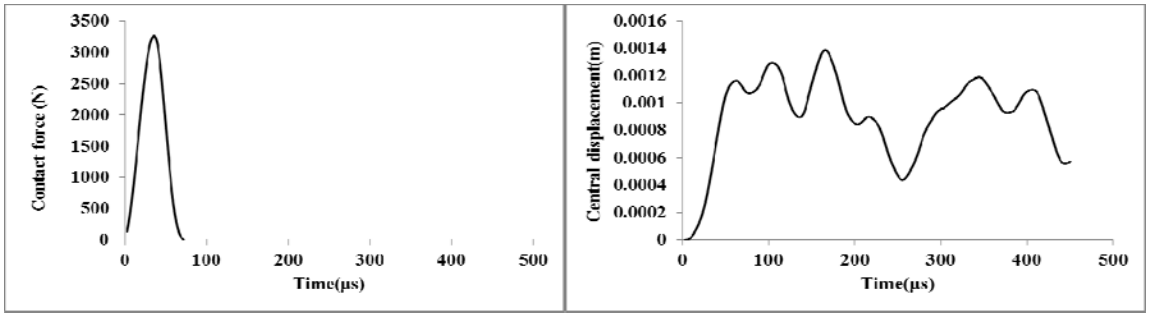

Figure 5.13 Impact response of simply supported cross ply (SS/CP) composite hypar shells for impact velocity 7m/s

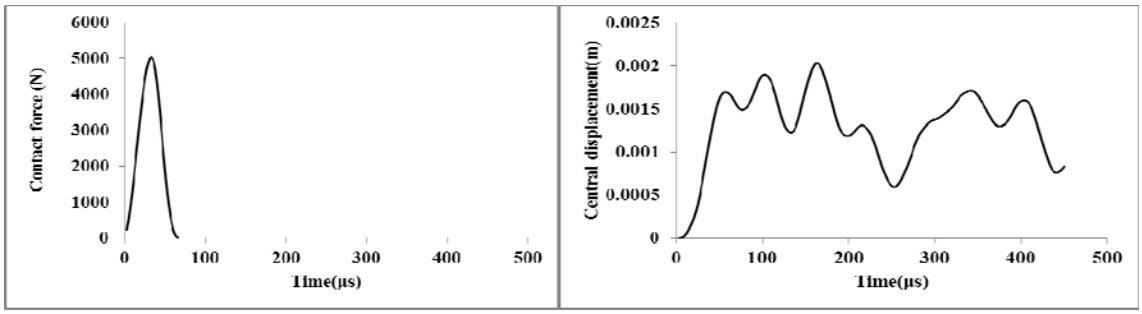

Figure 5.14 Impact response of simply supported cross ply (SS/CP) composite hypar shells for impact velocity 10m/s

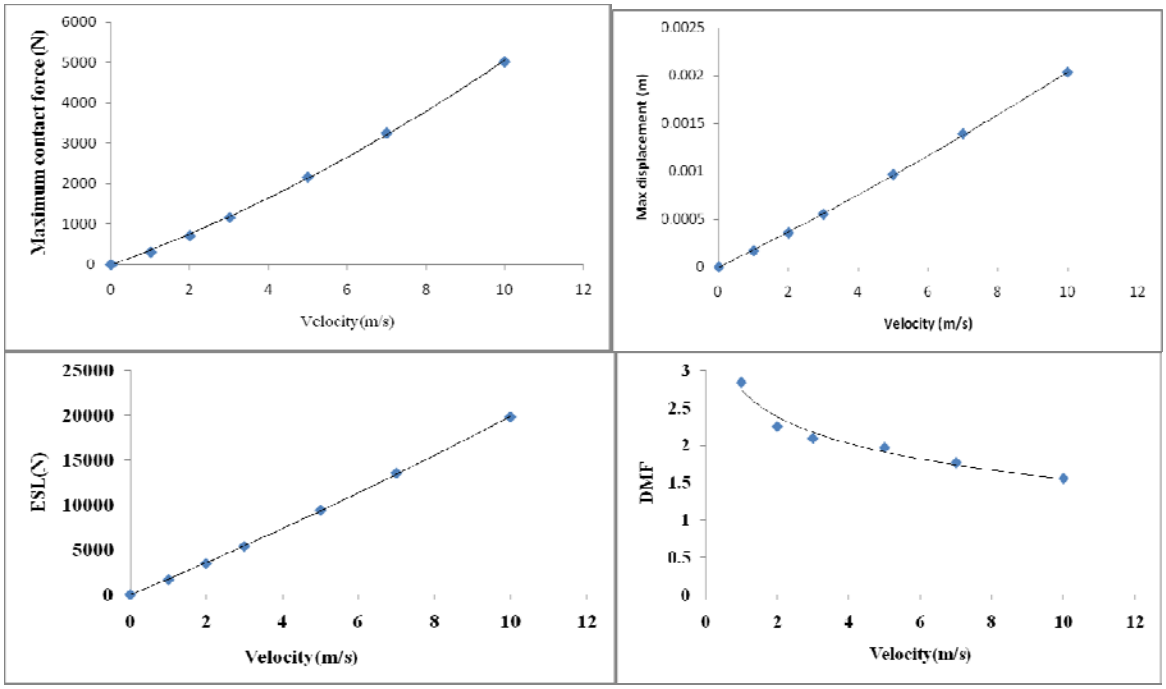

Figure-5.15 Variation of maximum impact load, maximum displacement, equivalent static load and dynamic magnification factor with velocity for simply supported cross ply (SS/CP) composite hypar shells

Table 5.2 Maximum contact force, maximum dynamic displacement, equivalent static load, dynamic magnification factor due to different impact velocities for anti-symmetric ply shell

Boundary condition and ply orientation		Velocity(m/s)	Maximum impact load(N)	Maximum displacement(m)	Equivalent static load (N)	Dynamic magnification factor
Simply supported	$0^0/90^0$	0	0	0	0	0
		1	310.1821	0.000169	1654	2.84
		2	715.7551	0.000356	3484	2.25
		3	1169.577	0.000552	5398	2.10
		5	2169.126	0.000965	9434	1.97
		7	3261.304	0.001390	13593	1.77
		10	5025.045	0.002031	19863	1.56
	$+45^0/-45^0$	0	0	0	0	0
		1	309.2766	0.000168	2080	3.76
		2	713.6038	0.000341	4210	2.97
		3	1165.866	0.000523	6460	2.76
		5	2162.327	0.00090	11100	2.58
		7	3252.504	0.001287	15900	2.31
		10	5010.827	0.001875	23200	2.03

5.4 CONCLUSIONS

The following conclusions may be derived from the present study.

1. The close agreement of the results obtained by the present method with those available in the published literature establishes the correctness of the approach used here .
2. Under the influence of normal low velocity impact the contact force shows a parabolic combined loading and unloading curve with a single peak for the practical class of shells considered here. Higher magnitude of impact velocity results in higher value of the peak contact force. However, due to a sharp elastic rebound the total duration of contact force is less for higher velocity of impactor.

3. The time instants at which the maximum contact force and the maximum dynamic displacement occur show a phase difference and interestingly in some cases the maximum displacement and hence stresses may occur even after the contact force dies down totally .Thus it is concluded that the study should be continued only after when the major peaks of the dynamic displacement die down and not after the full decay of the contact force only.
4. The maximum contact force, the peak dynamic displacement and the equivalent static load are all increasing functions of impactor velocity, the relations being almost linear. However, the dynamic magnification factor shows a logarithmically decreasing tendency with increase of the velocity of impact.

Chapter 6

IMPACT PERFORMANCE OF COMPOSITE HYPAR SHELL ROOF WITH CLAMPED BOUNDARY CONDITION

6.1 GENERAL

Impact response of fully clamped skewed hypar shell roofs is presented in this chapter. Section 6.2 describes the numerical examples considered, while results are reported and discussed in Section 6.3. The conclusions of engineering significance are presented in Section 6.4.

6.2 NUMERICAL EXAMPLES

A problem solved earlier by Chun and Lam [1998], related to the impact response of clamped composite plate, is taken up as the benchmark to validate the impact formulation for clamped boundary condition and the results are furnished as Figure 6.1.

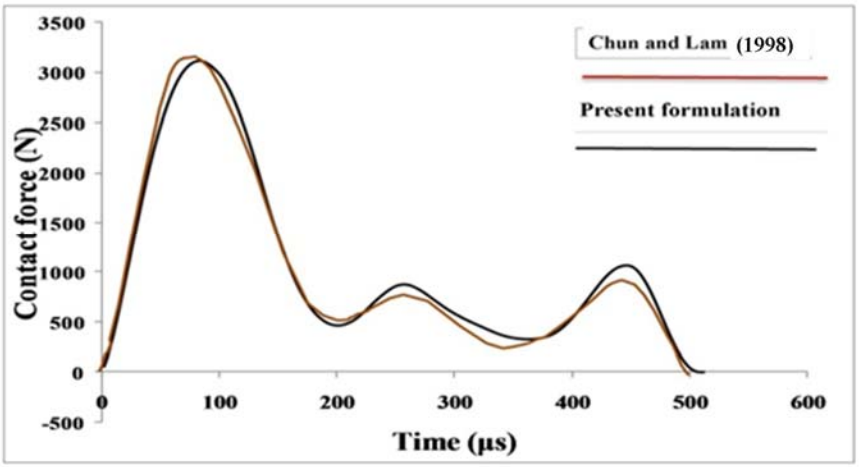

E_{11}=142.73GPa, E_{22}= 13.79GPa, G_{12}=4.64GPa, ν_{12} = 0.30, ρ = 1.61x10^{3}kg/m^3, a=b=0.14m, h=3.81x10^{-3}m, mass of striker=0.014175kg, velocity of striker= 22.6m/s, contact stiffness k_c =1x10^{8}N/m$^{1.5}$

Figure 6.1 Contact force history of clamped plate

Apart from the problem mentioned above, impact response of skewed hypar shells being impacted at the central point is also studied for clamped boundary condition, different laminations and impact velocities. The details of the problems which are the author's own are given below.

(i) Boundary condition :- Clamped (CL)

(ii) Lamination:- $+45^0/-45^0$ (AP), $0^0/90^0$ (CP)

(iii) Velocity of impact in (m/s):- 1, 2, 3, 5, 7, 10

(iv) Details of shell geometry :- a = 1.0m, b =1.0m, h=0.02m, c=0.2m

(v) Material details :- E_{11}=120GPa, E_{22}= 7.9 GPa,

G_{12}= G_{23}= G_{13}= 5.5GPa

ν_{12} = 0.30, ρ = 1.58x10^{-5}N-sec^2/cm^4

The converged value of time step $\Delta t=3\mu s$ is adopted for the present analysis.

6.3 RESULTS AND DISCUSSION

Figure 6.1 shows the time variation of the contact force induced in a composite plate under low velocity impact as obtained by Chun and Lam [1998]. The values obtained by the present formulation are also presented graphically in the same figure in a different style. Excellent agreement of results is observed which establishes the correctness of impact formulation.

To study the impact response of clamped (CL) angle ply (AP) shell Figure 6.2 to 6.7 and Table 6.1 are to be studied. All the results of contact force and displacement that are presented, in either graphical or tabular form, are arrived at after a study of time step convergence. The finite element mesh adopted is also based on force and displacement convergence criteria. When low velocity normal impact response of clamped angle ply shell is studied being struck by the spherical impactor centrally it is observed that the contact force shows a sort of parabolic variation with a single peak. After a given time span of 100μs or less, the contact force dies down to a null value. It is interesting to note that higher the impactor velocity higher is the contact force as expected, but the force dies down to a null value earlier. This behavior may be attributed to the fact that higher the velocity, more rapid is the elastic rebound of the impactor followed by detachment which causes the contact force to decay out. It is also very interesting to observe that the time instant corresponding to peak contact force and that for peak displacement do not match. This is because the resultant displacement at any time instant is a cumulative effect of the instantaneous contact force value and the inertia effect of the previous instant. Figures showing the transient displacements reflect the fact that vibration continues even after the force dies down with successively occurring peaks though, the peak values are less in magnitude than the highest

peak which occurs a bit after the instant of maximum contact force but before the full decay of it.

To estimate the equivalent static load (ESL) corresponding to a particular impactor velocity , a concentrated load at the centre (point of impact) is applied and adjusted to yield a central displacement equal to the maximum dynamic displacement. The magnitude of the central displacement is calculated with the peak contact force applied at the point of impact as a static concentrated load. The central displacement obtained under such a load when divides the maximum dynamic displacements yields dynamic magnification factor (DMF). The variations of maximum contact force, maximum dynamic displacement and equivalent static load (ESL) with impact velocity are almost linear and all of the three above mentioned values are increasing functions of the impact velocity. However the dynamic magnification factor (DMF) and the impact velocity shows a logarithmic relation and the DMF is a decreasing function of velocity of impact.

The behavior of the impact response of clamped (CL) cross ply (CP) may be studied from Figure 6.9 to 6.14 and Table 6.1. The nature of contact force and dynamic displacement for this class (CL/ CP) of shell is more or less similar to what is discussed before for CL/AP shell. One interesting difference is that for CL/ CP shell the peak dynamic displacement does not only show a phase lag with respect to the peak contact force but by the time , displacement value reaches the peak , the contact force value dies down totally. This shows that the after-effect of impact is some times more severe than the shell response during the impact and study of displacement variation even after the contact force decays to a null value is absolutely necessary. However, after passage of some more time the subsequent local maxima which are obtained do not touch the peak.

The dependence of the maximum contact force, the peak dynamic displacement and the equivalent static load (ESL) on the impactor velocity in case of clamped cross ply (CL /CP) (Figure 6.15) shell are similar to what is observed in case of clamped angle ply (CL/AP) shell (Figure 6.8).

It is further noted that the maximum value of the contact force and displacement for CL /AP and CL /CP shells are almost equal for any given velocity of the impactor but the value of ESL and DMF are higher in case of CL /AP shell.

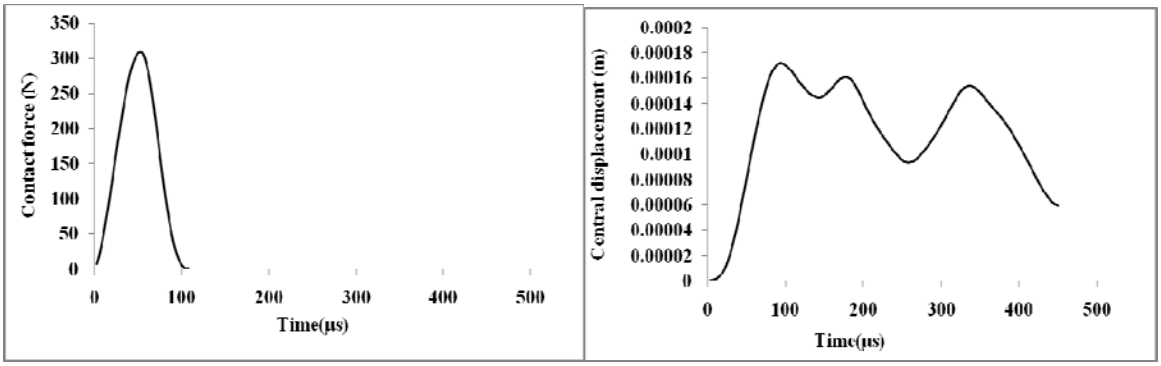

Figure- 6.2 Impact response of clamped angle ply (CL/AP) composite hypar shells for impact velocity 1m/s

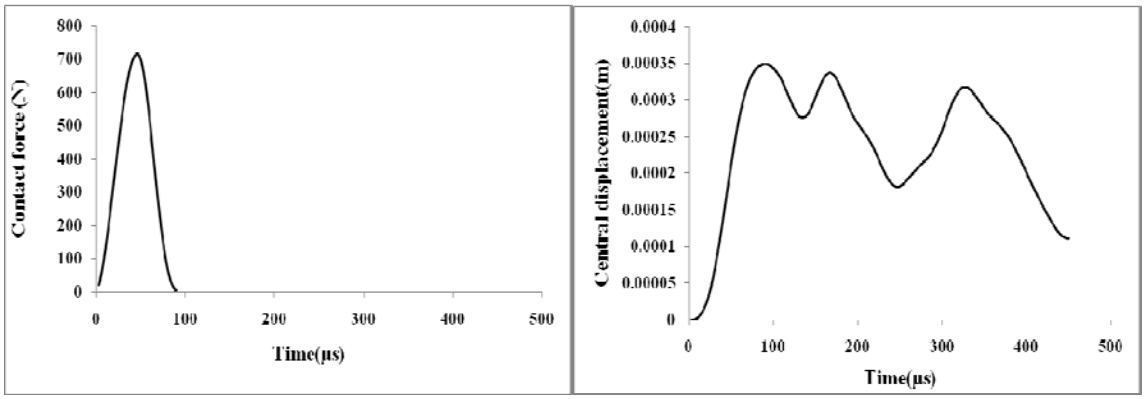

Figure 6.3 Impact response of clamped angle ply (CL/AP) composite hypar shells for impact velocity 2m/s

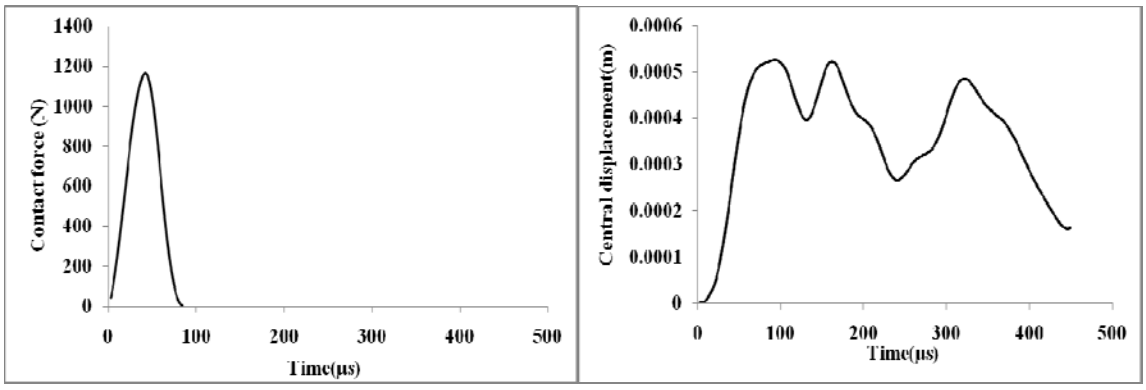

Figure 6.4 Impact response of clamped angle ply (CL/AP) composite hypar shells for impact velocity 3m/s

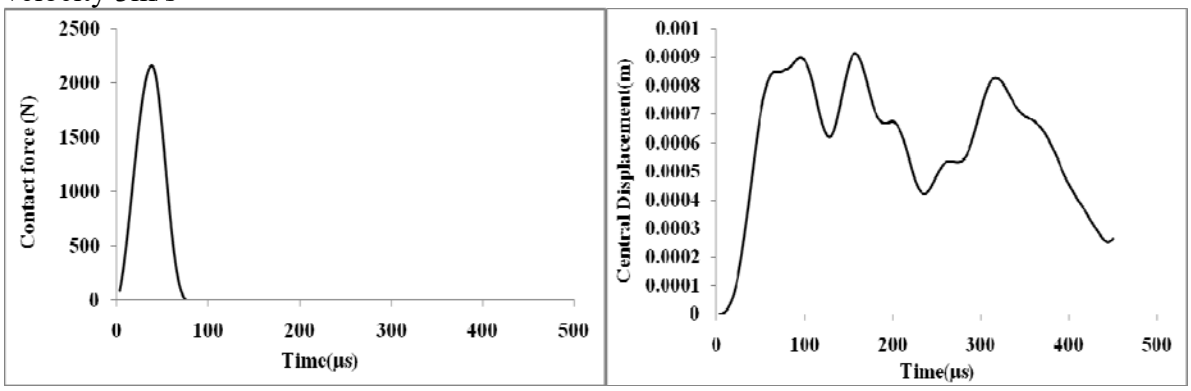

Figure 6.5 Impact response of clamped angle ply (CL/AP) composite hypar shells for impact velocity 5m/s

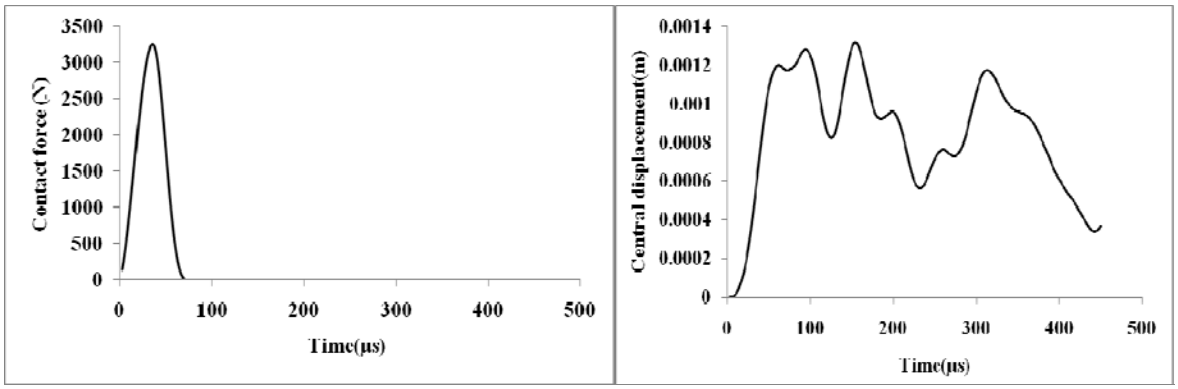

Figure 6.6 Impact response of clamped angle ply (CL/AP) composite hypar shells for impact velocity 7m/s

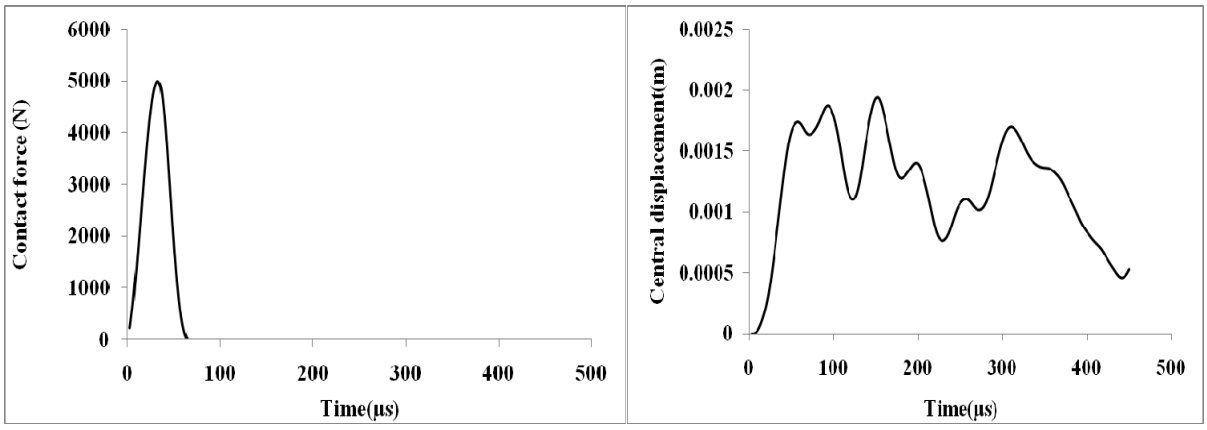

Figure 6.7 Impact response of clamped angle ply (CL/AP) composite hypar shells for impact velocity 10 m/s

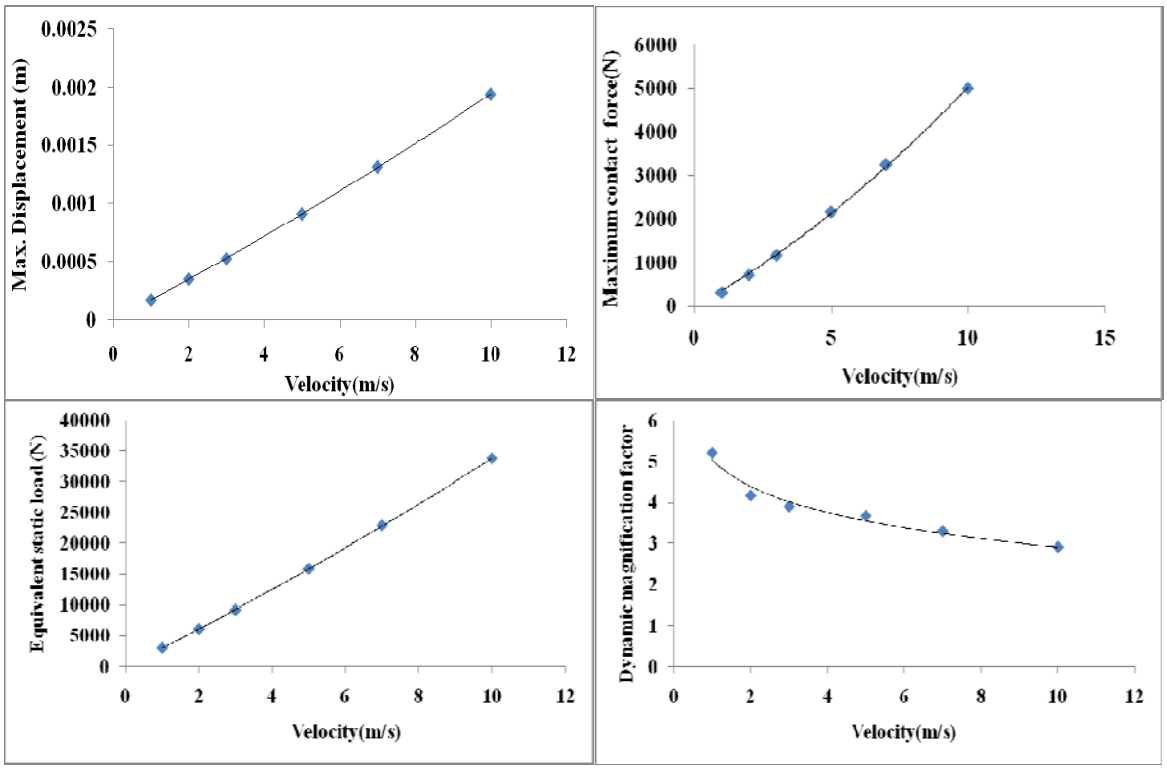

Figure 6.8 Variation of maximum impact load, maximum displacement, equivalent static load and dynamic magnification factor with velocity for clamped angle ply (CL/AP) composite hypar shells

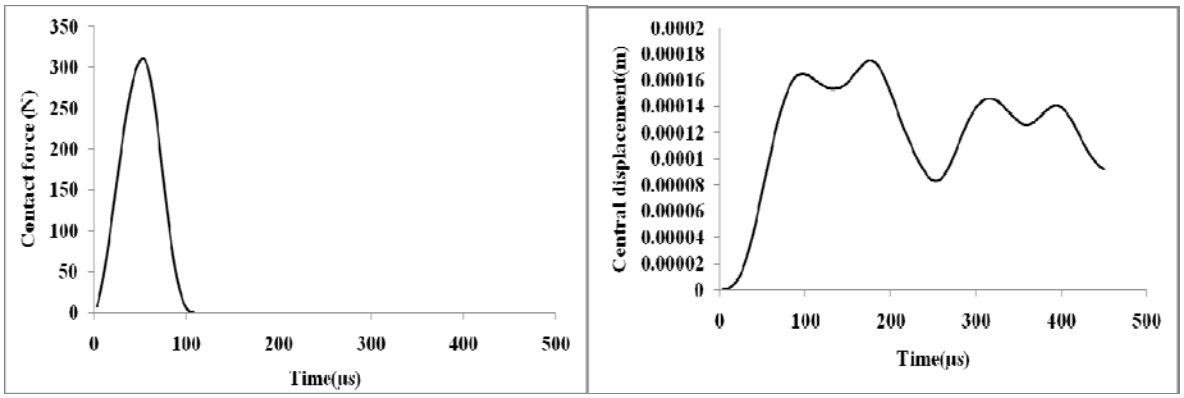

Figure 6.9 Impact response of clamped cross ply (CL/CP) composite hypar shells for impact velocity 1m/s

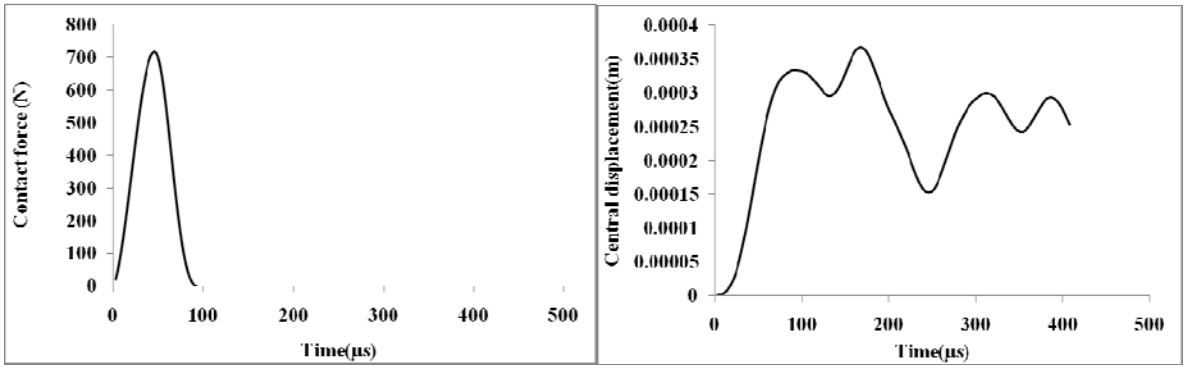

Figure 6.10 Impact response of clamped cross ply (CL/CP) composite hypar shells for impact velocity 2m/s

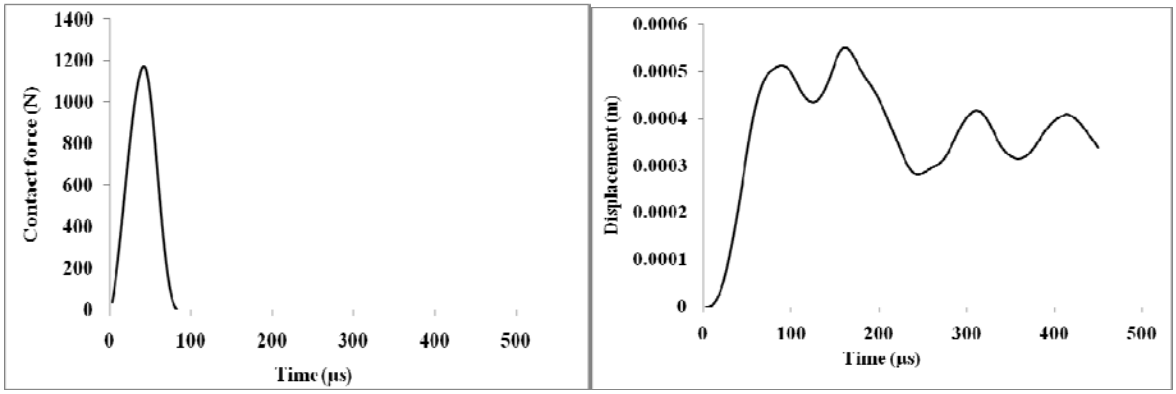

Figure 6.11 Impact response of clamped cross ply (CL/CP) composite hypar shells for impact velocity 3m/s

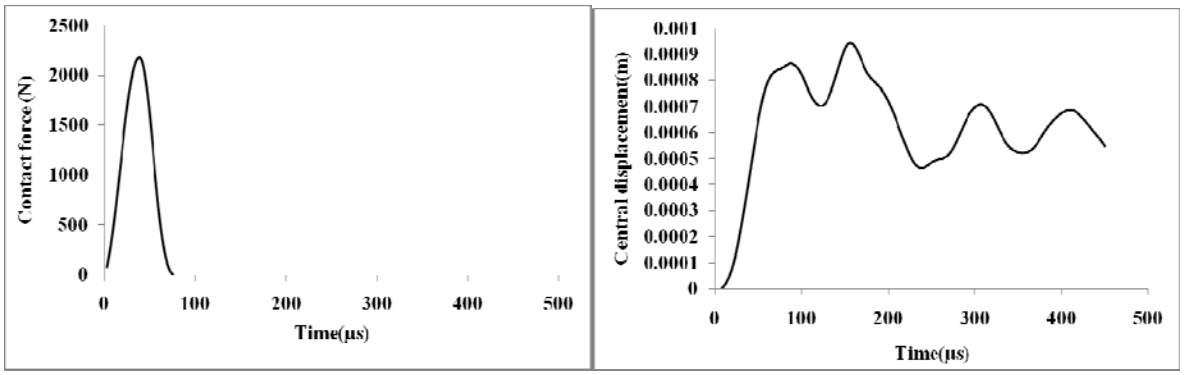

Figure 6.12 Impact response of clamped cross ply (CL/CP) composite hypar shells for impact velocity 5m/s

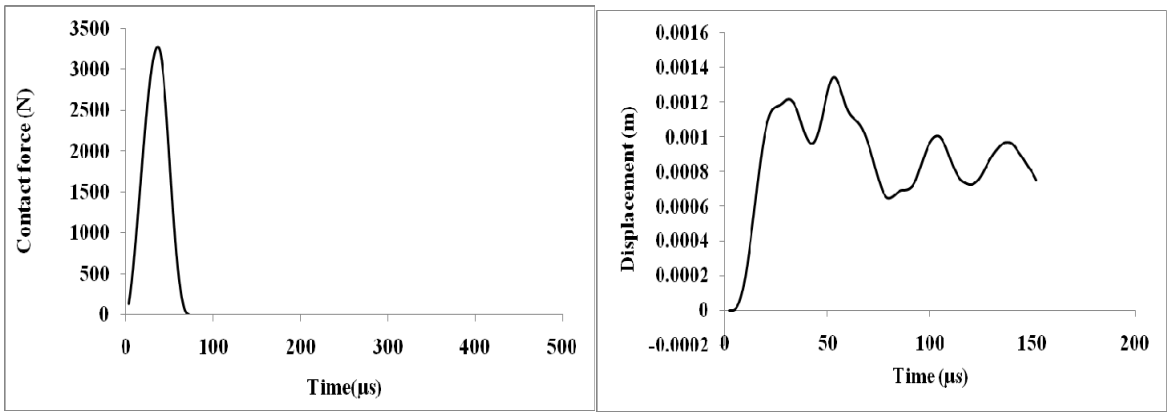

Figure 6.13 Impact response of clamped cross ply (CL/CP) composite hypar shells for impact velocity 7m/s

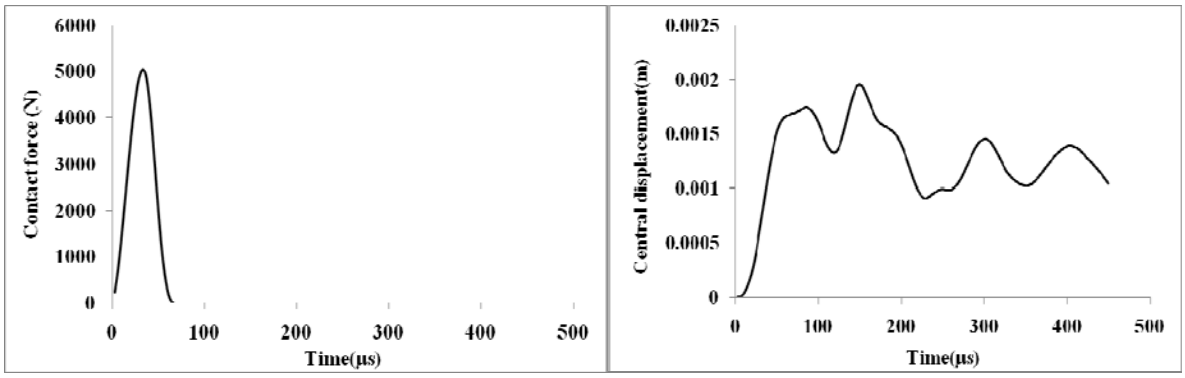

Figure 6.14 Impact response of clamped cross ply (CL/CP) composite hypar shells for impact velocity 10m/s

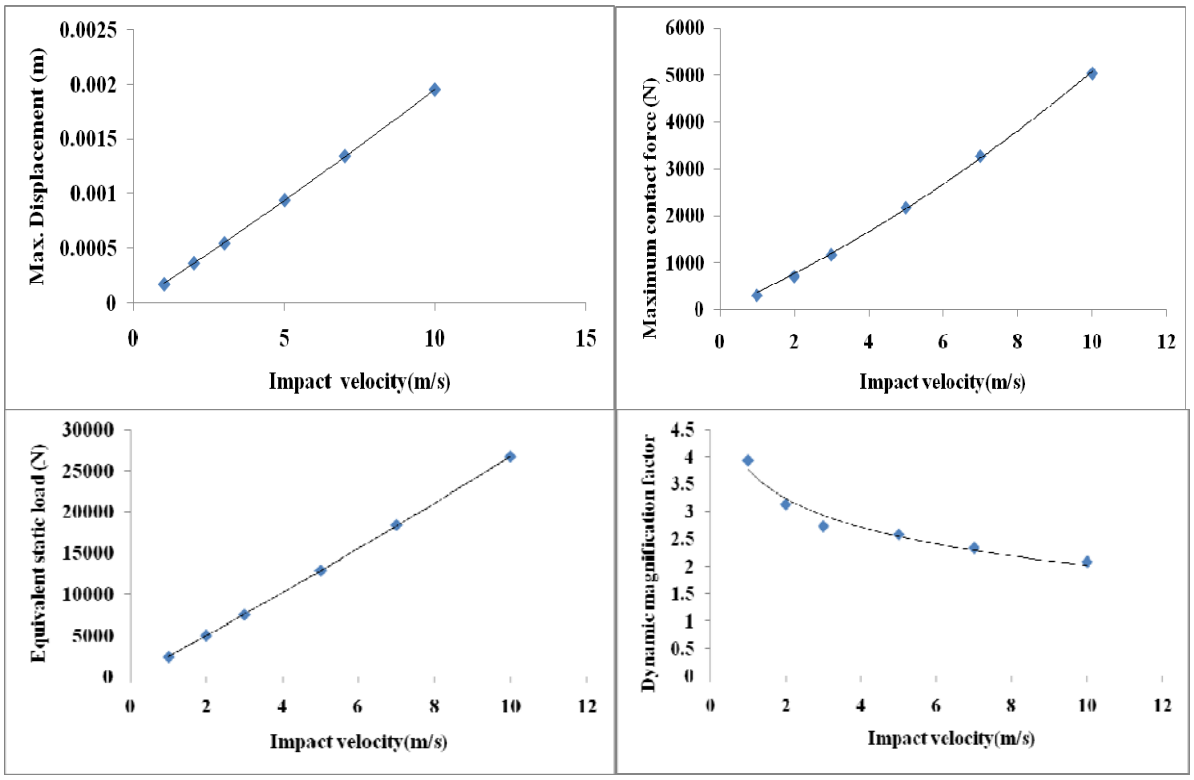

Figure-6.15 Variation of maximum impact load, maximum displacement, equivalent static load and dynamic magnification factor with velocity for clamped cross ply (CL/CP) composite hypar shells

Table 6.1 Maximum contact force, maximum dynamic displacement, equivalent static load, dynamic magnification factor for different impact velocities

Boundary condition and ply orientation	Velocity(m/s)	Maximum impact load (N)	Maximum displacement (m)	Equivalent static load (N)	Dynamic magnification factor
Clamped $0^0/90^0$	0	0	0	0	0
	1	310.4116	0.000175	2401.84	3.93
	2	716.0525	0.000368	5031.99	3.14
	3	1175.383	0.000549	7518.80	2.73
	5	2180.685	0.000944	12916.88	2.58
	7	3277.516	0.001346	18427.72	2.33
	10	5043.874	0.001953	26739.72	2.09
Clamped $+45^0/-45^0$	0	0	0	0	0
	1	309.6553	0.000172	3001.077	5.22
	2	713.8558	0.000349	6079.476	4.18
	3	1165.725	0.000526	9167.109	3.91
	5	2160.912	0.000911	15883.056	3.68
	7	3248.894	0.001316	22938.054	3.30
	10	5003.201	0.001941	33829.285	2.91

6.4 CONCLUSIONS

The following conclusions may be derived from the present study.

1. The close agreement of the results obtained by the present method with those available in the published literature establishes the correctness of the approach used here.
2. Under the influence of normal low velocity impact, the contact force shows a parabolic combined loading and unloading curve with a single peak for the practical class of shells considered here. Higher magnitude of impact velocity results in higher value of the peak contact force but due to a sharp elastic rebound, the total duration of contact force is less for higher velocity of impactor.

3. The time instants at which the maximum contact force and the maximum dynamic displacement occur show a phase difference and interestingly in some cases the maximum displacement and hence stresses may occur even after the contact force dies down totally .Thus it is concluded that the study may be stopped only after when the major peaks of the dynamic displacement die down and not after the full decay of the contact force only.
4. The maximum contact force, the peak dynamic displacement and the equivalent static load are all increasing functions of impactor velocity, the relations being almost linear. However, the dynamic magnification factor shows a logarithmically decreasing tendency with increase of the velocity of impact.

Chapter 7

ANALYSIS AND DESIGN GUIDELINES OF POINT-SUPPORTED COMPOSITE SKEWED HYPAR SHELL ROOF

7.1 GENERAL

Using the mathematical formulation presented in Chapter 4, impact response parameters are evaluated and design aspects of corner supported composite skewed hypar shell under low velocity impact are high-lighted in this chapter. A number of problems are solved for validation of the present approach and to explore the impact behavior of the class of shells mentioned above which are presented in Section 7.2. Section 7.3 contains the important results and related discussion while conclusions are presented in Section 7.4.

7.2 NUMERICAL EXAMPLES

Natural frequencies obtained by the present approach are compared with those reported by Narita and Leissa [1984] for a point supported isotropic cylindrical shell. This was solved to validate the correct incorporation of the point supported boundary condition in the present computer code. In this problem, the author has taken the liberty of applying the formulation developed for composite shells to the isotropic case by making the moduli of elasticity and shear equal in all directions. Appropriate changes in curvature terms are done to model the cylindrical geometry. The detail of the benchmark problem is furnished in Table 7.1.

Table 7.1 First four non-dimensional natural frequencies $\left[\bar{\omega} = \omega_n a^2 \sqrt{\left(\frac{\rho h}{D}\right)}\right]$ of isotropic corner-point supported cylindrical shell

Narita and Leissa (1984)	Present formulation
19.76	19.758
31.48	31.45
41.94	41.90
55.74	55.77

a/b =1, a_I/a=1, a/h=100, a/R= 0.5, $\nu = 0.3$

Apart from the problems mentioned above, impact responses of skewed hypar shells being impacted at the central point are also studied for eight different shell options combining two boundary conditions and four laminations. Six impact velocities are considered. The details of the problems which are the author's own are given below.

(i) Boundary condition- Two different boundary conditions having different arrangements of point supports along four edges, designated as BD-1 and BD-2 are adopted (Figure 7.2). BD-1 shells are point supported only at the corners, while BD-2 shells have four additional point supports at the mid-points of the four edges.

(ii) Lamination: - $+45^0/-45^0$ (AP)(AS), $0^0/90^0$ (CP)(AS),$+45^0/-45^0/+45^0$(AP)(SY), $0^0/90^0/0^0$(CP) (SY)

(iii) Velocity of impact (m/s): - 1, 2, 3, 5, 7, 10

(iv) Details of shell geometry: - a = 1.0m, b =1.0m, t=0.02m, c=0.2m

(v) Material details: - E_{11}=120GPa, E_{22}= 7.9 GPa, G_{12}= G_{23}= G_{13}= 5.5GPa

ν_{12} = 0.30, ρ = 1.58x10^{-5}N-sec^2/cm^4

The converged value for a time step Δt=3μs is adopted in the present analysis.

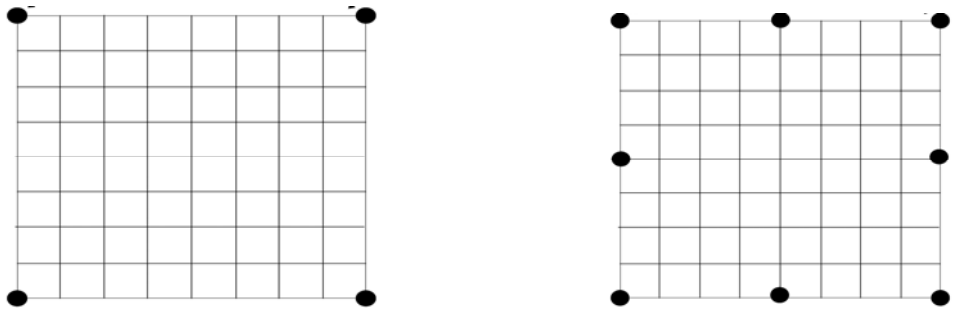

Figure 7.1 Arrangement of boundary conditions

7.3 RESULTS AND DISCUSSION

The result of Table 7.1 shows that the natural frequency values of corner point supported cylindrical shell obtained by the present formulation agree closely to those reported by Narita and Leissa (1984). Thus, the correct incorporation point supported boundary condition in the present code is established.

The finite element mesh adopted in the present study is based on force and displacement convergence criteria. All the results of contact force and displacement that are presented in tabular form are arrived at after the study of time step convergence. Some typical results are represented graphically also. Time histories of contact force and displacement for BD-1 shell options are shown in Figure 7.3 to 7.6 whereas the same for BD-2 shell options are represented in Figure 7.8 to 7.11. When low velocity normal impact response of Point-supported shells is studied being struck by the spherical impactor centrally, it is observed that the contact force shows a sort of parabolic variation with a single peak. After a given time span which is 100μs or less the contact force converges to a null value. It is interesting to note that higher the impact velocity higher is the contact force as expected, but the force dies down to a null value earlier. This behavior may be attributed to the fact that the higher the velocity more rapid is the elastic

rebound of the impactor followed by detachment which causes contact force to decay out. It is also very interesting to observe that the time instant corresponding to peak contact force and that for peak displacement do not match. This is because the resultant displacement at any time instant is a cumulative effect of the instantaneous contact force value and the inertia effect of the previous instant. The figure showing the transient displacement reflects the fact that vibration continues even after the force dies down with successively occurring peak though the peak values are less in magnitude than the highest peak which occurs a bit after the instant of maximum contact force but before the full decay of it.

The displacement histories of several points (Figure 7.3) are studied along with the node of impact (node-1). It may be noted that at some of the points, e.g. Node-2 and 8, the displacement at some instant may exceed the same occurring at the point of impact. But such displacements will never govern the design as they are always less that the absolute maximum displacement occurring at the point of contact. Important information regarding the deflection of Node- 2, 3, 8 and 9 is these points suffers stress reversal which is never seen to occur at node of impact.

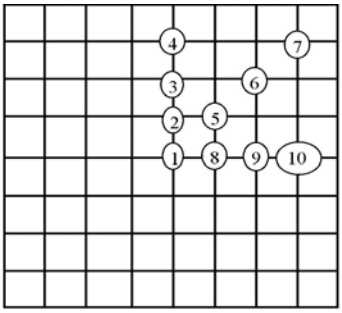

Figure 7.2 Points at which displacements are calculated

To estimate the equivalent static load (ESL) corresponding to a particular impact velocity, a concentrated load at the center (point of impact) is applied and adjusted the yield a central displacement equal to the maximum dynamic displacement. It is further explored to estimate the magnitude of the central displacement when the peak contact force is applied at the point of

impact as a static concentrated load. The central displacement obtained under such a load when divides the maximum dynamic displacements yields dynamic magnification factor (DMF). These two parameters will help to design the shell by static load without doing the detail dynamic analysis. The variations of maximum contact force, maximum dynamic displacement and equivalent static load (ESL) with impactor velocity are almost linear and are increasing functions of impactor velocity for both the boundary conditions. However the dynamic magnification factor (DMF) and the impactor velocity shows a logarithmic relation and the DMF is a decreasing function of velocity for the same. All these variations are represented in Figure 7.7 for BD-1 shells and in Figure 7.12 for BD-2 shells.

Some typical response patterns of corner supported shells under impact loading are shown below.

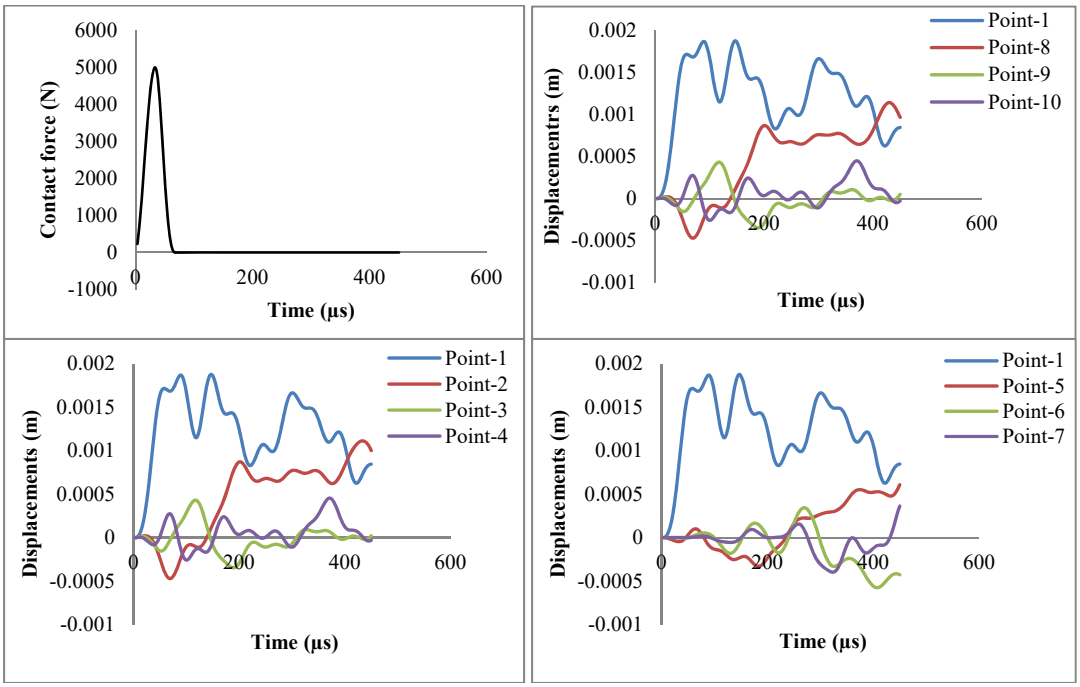

Figure 7.3 Impact response of point-supported anti-symmetric angle ply (APAS/BD-1) composite hypar shells for impact velocity 10m/s

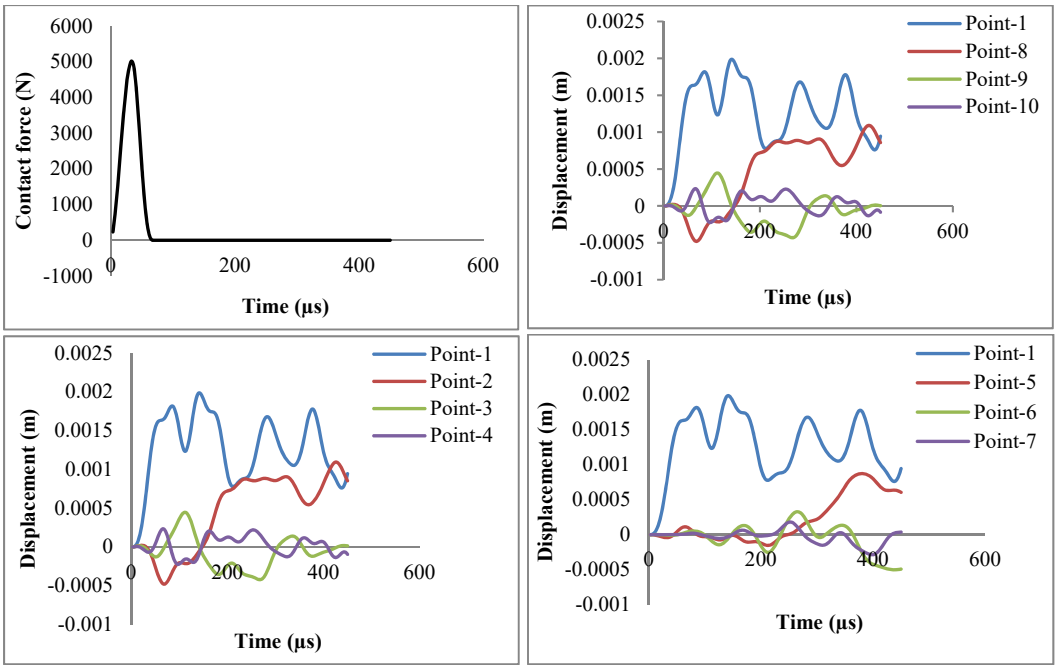

Figure 7.4 Impact response of point-supported anti-symmetric cross ply (CPAS/BD-1) composite hypar shells for impact velocity 10m/s

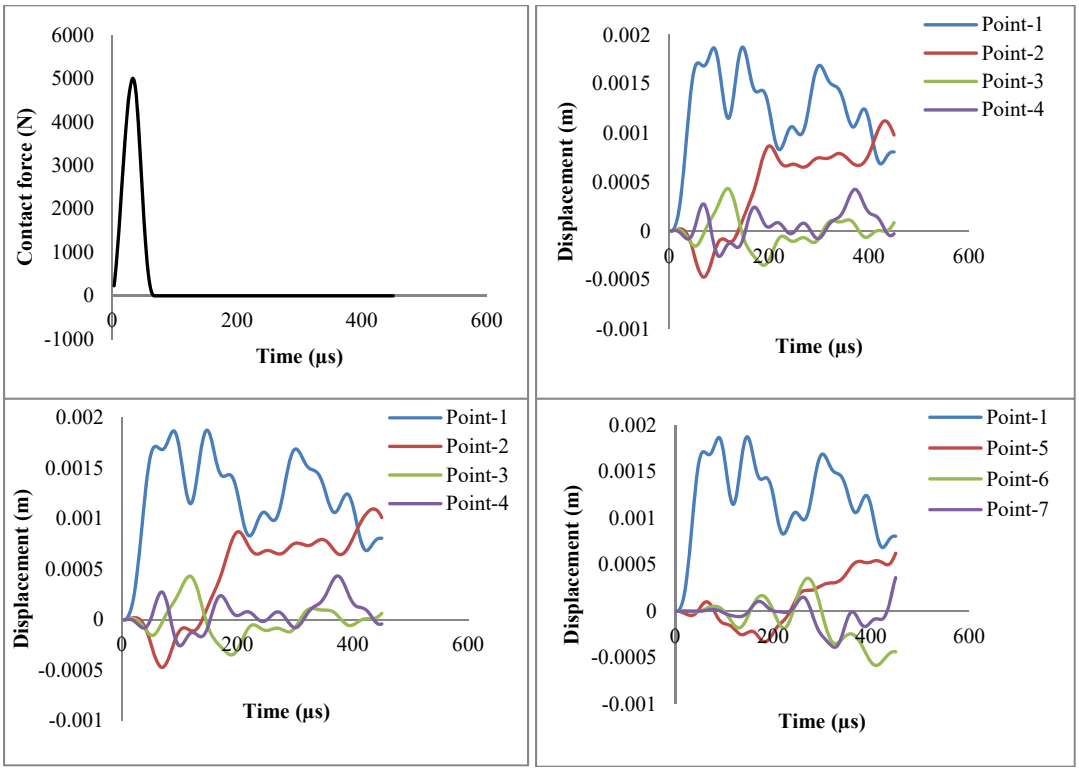

Figure 7.5 Impact response of point-supported symmetric angle ply (APSY/BD-1) composite hypar shells for impact velocity 10m/s

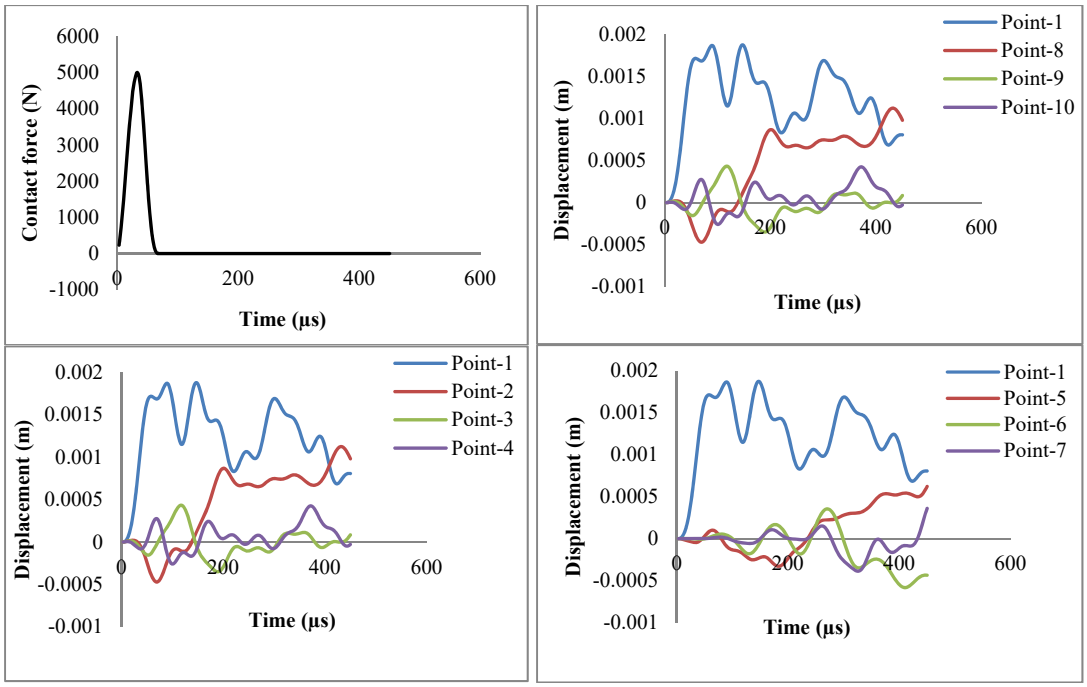

Figure 7.6 Impact response of point-supported symmetric cross ply (CPSY/BD-1) composite hypar shells for impact velocity 10m/s

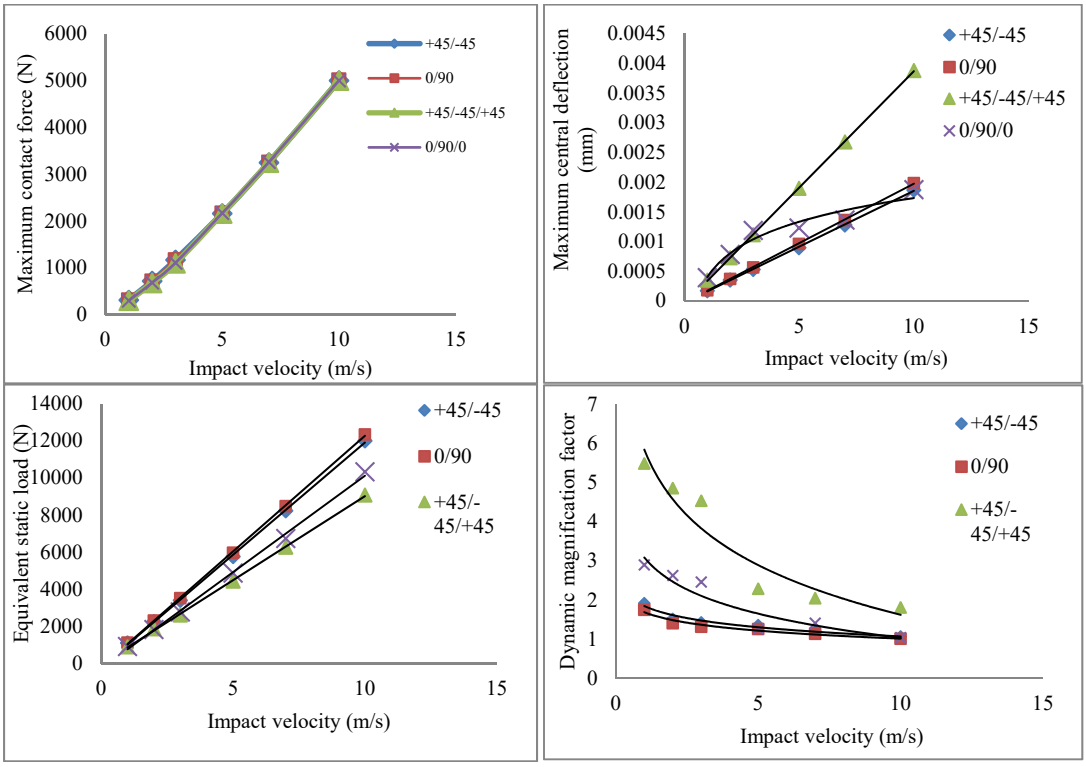

Figure 7.7 Variation of maximum contact force, maximum dynamic displacement, equivalent static load and dynamic magnification factor with velocity for point-supported composite hypar shells of BD-1 shell option

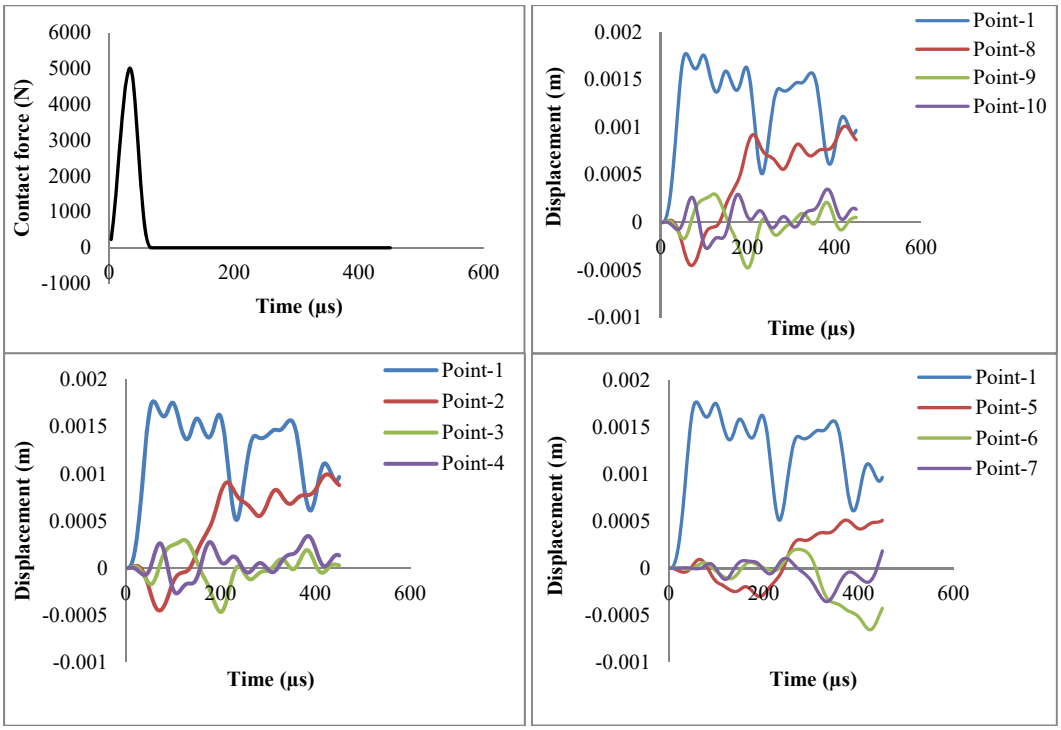

Figure 7.8 Impact response of point-supported anti-symmetric angle ply (APAS/BD-2) composite hypar shells for impact velocity 10m/s

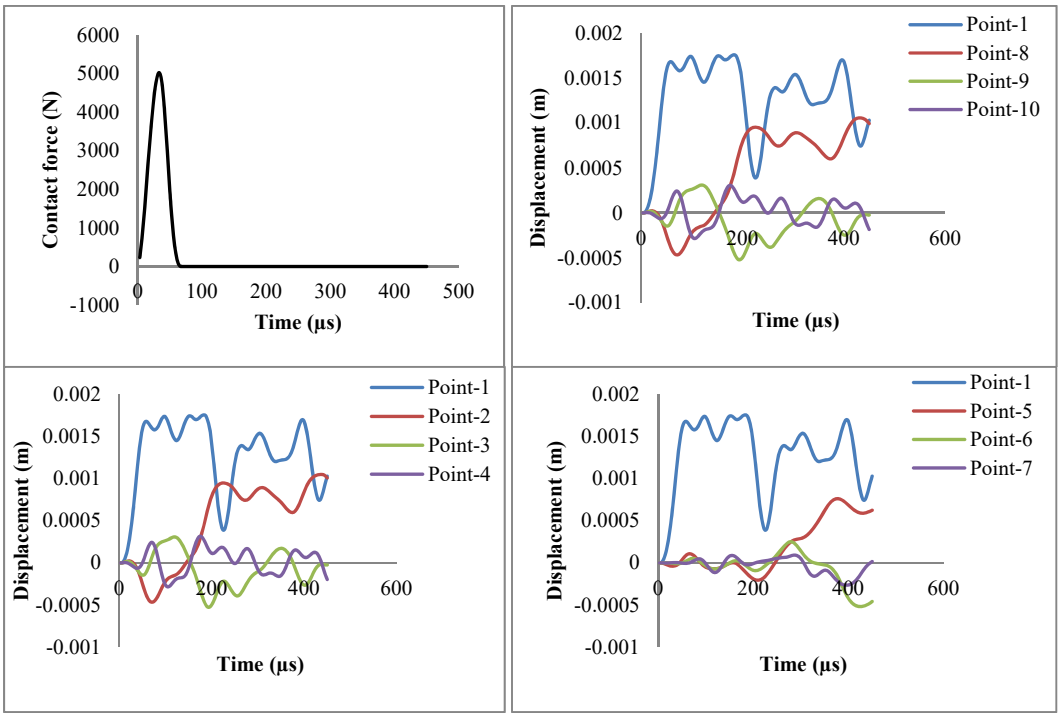

Figure 7.9 Impact response of point-supported anti-symmetric cross ply (CPAS/BD-2) composite hypar shells for impact velocity 10m/s

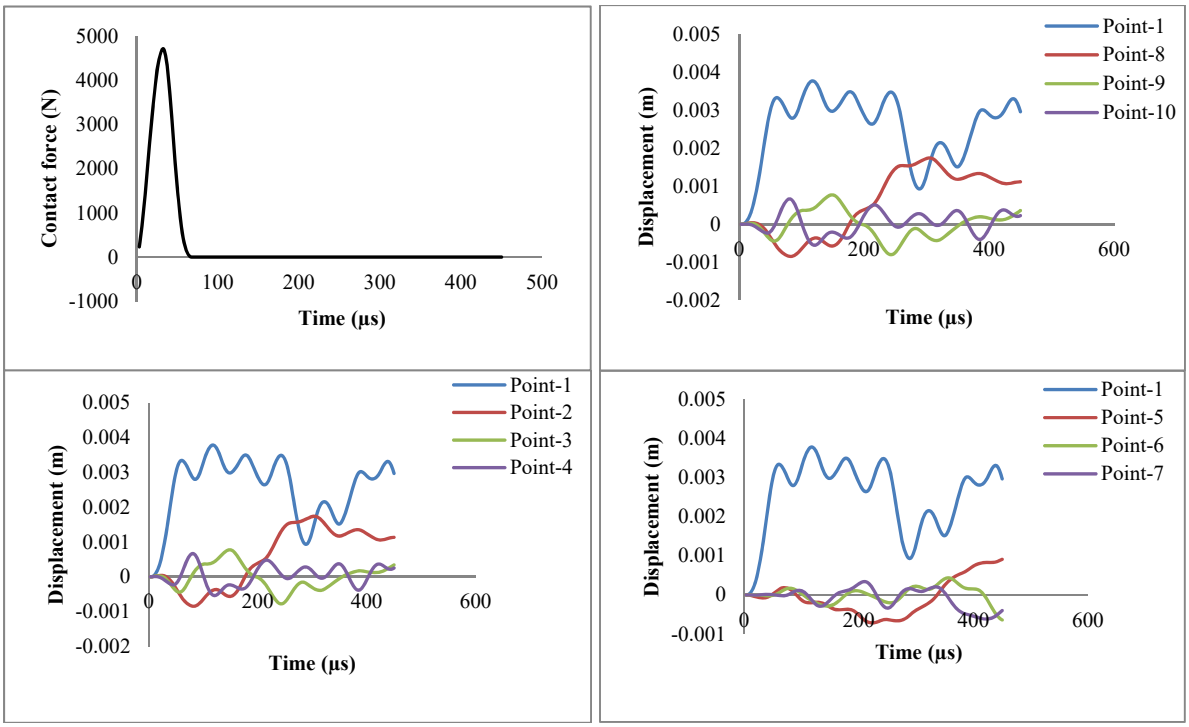

Figure 7.10 Impact response of point-supported symmetric angle ply (APSY/BD-2) composite hypar shells for impact velocity 10m/s

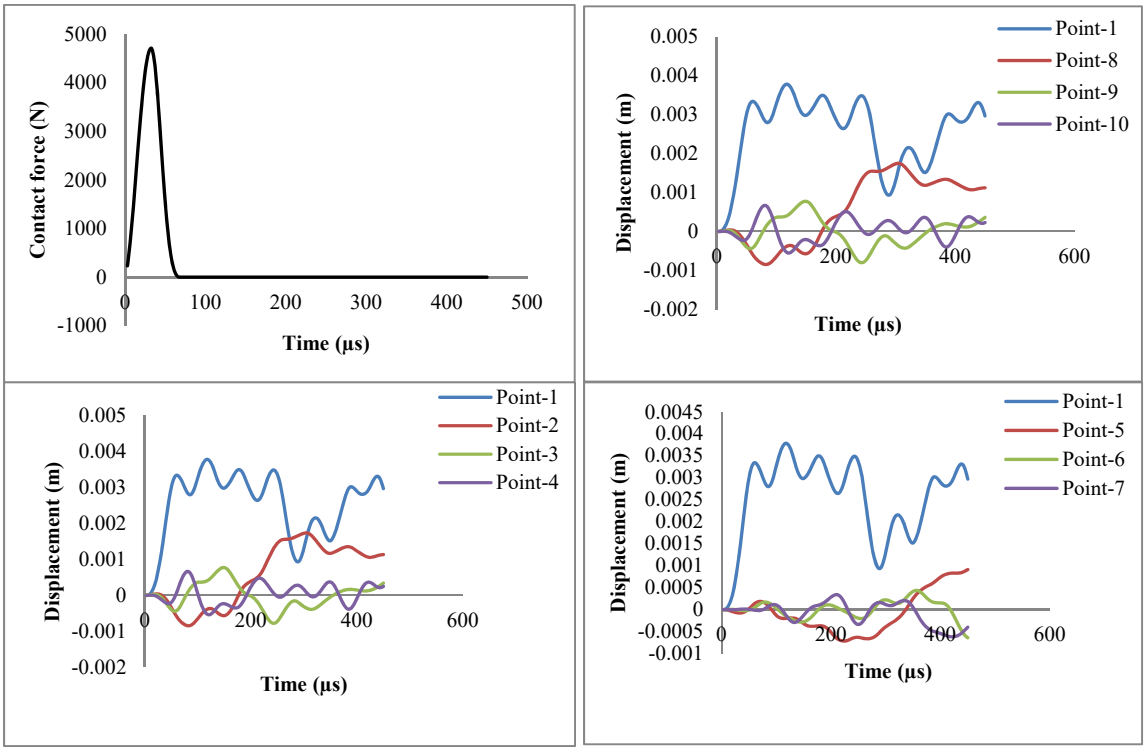

Figure 7.11 Impact response of point-supported symmetric cross ply (CPSY/BD-2) composite hypar shells for impact velocity 10m/s

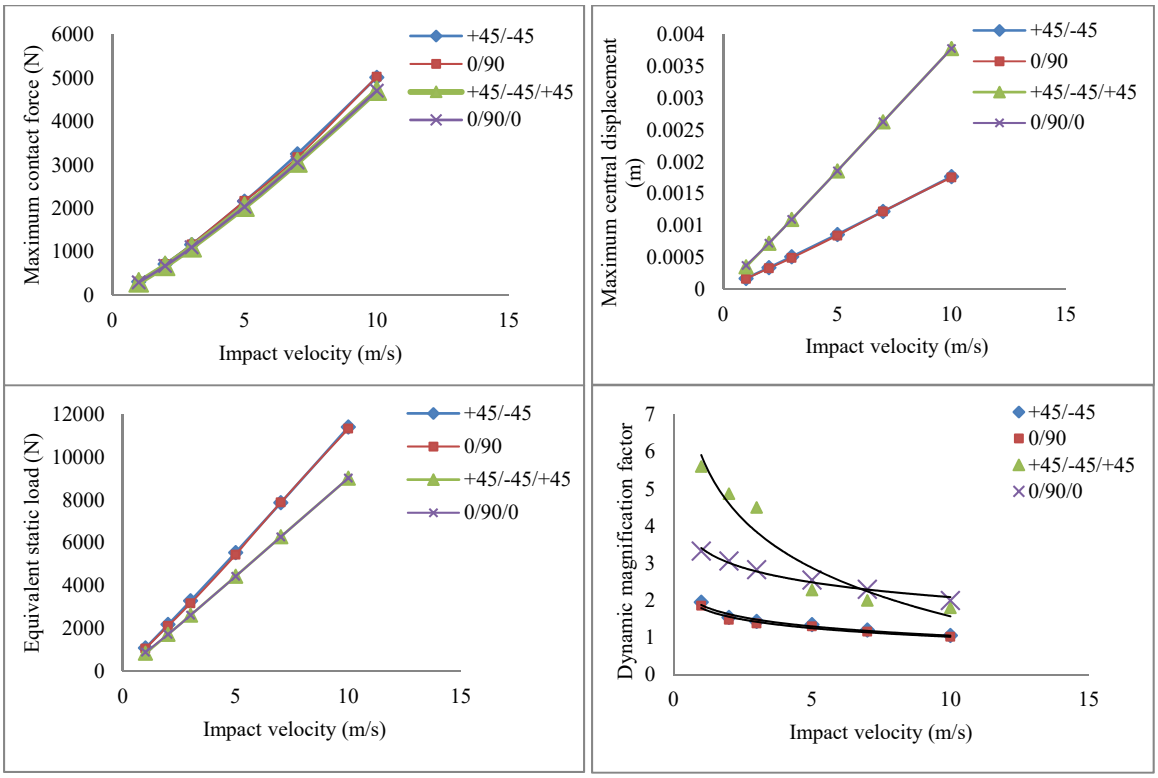

Figure 7.12 Variation of maximum contact force, maximum dynamic displacement, equivalent static load and dynamic magnification factor with velocity for point-supported composite hypar shells of BD-2 shell option

7.3.1 *Effect of stacking sequence on impact response*

The relative performances of cross-ply and angle-ply shells under impact may be studied by keeping the number of laminae same in both the cases. It is observed that for BD-1 two and three-layered laminates, angle-ply shows better performance than cross-ply and yields lesser deflection values. The maximum contact force generated at the point of impact is higher in case of CP shells in contrast to AP shells though the contact force dies down more or less at equal paces. While discussing the results of BD-2 two and three-layered laminates, deflections and contact forces of AP and CP shells are quite comparable. Thus conclusively one may infer that for BD-1 edge conditions angle ply laminates may be preferred over cross ply ones if one has the

option to choose.

Table 7.2 Maximum contact force, maximum dynamic displacement, equivalent static load, dynamic magnification factor for different velocities of the impactor for BD-1 shell

Boundary condition and ply orientation			Velocity(m/s)	Maximum impact load(N)	Maximum dynamic displacement(m)	Equivalent static load (N)	Dynamic magnification factor
BD-1	Anti-symmetric ply	$0^0/90^0$	1	310.824	0.000181	1124	1.754
			2	716.848	0.000373	2317	1.409
			3	1170.221	0.000566	3516	1.32
			5	2168.200	0.000961	5969	1.264
			7	3257.591	0.001365	8478	1.14
			10	5015.142	0.001987	12342	1.013
		$+45^0/-45^0$	1	309.835	0.000172	1104	1.92
			2	714.222	0.000351	2253	1.52
			3	1165.861	0.00053	3402	1.43
			5	2160.158	0.000898	5764	1.36
			7	3247.508	0.001281	8222	1.21
			10	5002.12	0.001868	11990	1.07
	Symmetric ply	$0^0/90^0/0^0$	1	296.573	0.000392	915	2.960
			2	680.355	0.000783	1829	2.630
			3	1105.675	0.001190	2780	2.460
			5	2168.200	0.001230	4873	1.410
			7	3257.591	0.001365	6732	1.260
			10	5002.12	0.001876	10330	1.042
		$+45^0/-45^0/+45^0$	1	294.407	0.000350	892	5.49
			2	675.097	0.000727	1864	4.86
			3	1096.942	0.001116	2607	4.54
			5	2160.158	0.001898	4433	2.29
			7	3247.508	0.002681	6263	2.05
			10	5002.12	0.003884	9073	1.81

Table 7.3 Maximum contact force, maximum dynamic displacement, equivalent static load, dynamic magnification factor for different velocities of the impactor for BD-2 shell

Boundary condition and ply orientation		Velocity (m/s)	Maximum impact load(N)	Maximum displacement (m)	Equivalent static load (N)	Dynamic magnification factor
		1	310.358	0.000164	1058	1.858
		2	716.129	0.000329	2122	1.477
		3	1169.694	0.000492	3174	1.380
	$0^0/90^0$	5	2169.357	0.000844	5445	1.301
		7	3176.346	0.001224	7897	1.160
	Non-	10	5029.359	0.001785	11342	1.021
	Symmetric	1	309.421	0.000169	1089	1.949
	Ply	2	713.923	0.000339	2187	1.541
	$+45^0/-45^0$	3	1166.147	0.000511	3292	1.436
		5	2162.702	0.000861	5547	1.346
		7	3253.985	0.001221	7877	1.200
BD-2		10	5013.577	0.001772	11416	1.055
		1	296.056	0.000373	890	3.33
		2	676.383	0.000721	1720	3.06
	$0^0/90^0/0^0$	3	1101.179	0.001098	2620	2.83
		5	2037.332	0.001860	4439	2.55
		7	3055.144	0.002632	6281	2.30
	Symmetric	10	4708.150	0.003785	9033	2.00
	ply	1	294.204	0.000352	840	5.50
		2	676.383	0.000721	1721	4.87
	$+45^0/-45^0/+45^0$	3	1101.179	0.001098	2621	4.50
		5	2037.332	0.001860	4441	2.28
		7	3055.144	0.002633	6287	2.00
		10	4708.150	0.003785	9025	1.80

Table 7.4 Working equations relating different design parameters with impact velocity (v_i)

BD-1 shell	BD-2 shell
$F = 10.79v_i^2+401.05\ v_i -136.525$	$F = 11.615\ v_i^2+380.6\ v_i -101.37$
$\delta = 1x10^{-6}\ v_i^2+0.001\ v_i -4.667$	$\delta = 1x10^{-6}\ v_i^2+0.001\ v_i$
(This equation is not valid for $0^0/90^0/0^0$ shell)	
$ESL = 9.549\ v_i^2+995.25\ v_i -52.907$	$ESL = 4.31\ v_i^2+981.85\ v_i -48.776$
$DMF = -.835\ln(v_i)+3.117$	$DMF = -0.782\ln(v_i)+3.247$

F = Maximum contact force; δ = Maximum dynamic displacement

7.3.2 Effect of number of boundary constraints on impact response

BD-1 shells have the smaller number of boundary constraints than BD-2 shells. The results of maximum downward deflections in Table 7.2 and Table 7.3 show that under impact loading the deflection decreases as the number of support constraints increases, which is quite natural. In cases of symmetric plies both for angle and cross ply options, downward deflections are more or less same for BD-1 and BD-2. When the rate of increment of deflection due to increase in impact velocities are checked, it is found that rate of deflection increases with the increment of impact velocity up to 5m/s. But the rate of increment in deflection decreases after 5m/s impact velocity. This shows the deflections in the lower impact velocity levels are affected by numbers of boundary constraints but as the velocity increases and approaches towards high velocity impact, it becomes independent of numbers of boundary constraints. That is the effect of impact becomes more localised. From the above discussion it can be also concluded that in case of symmetric ply shell option increment in boundary constraint does causes significant improvement in stiffness.

7.3.3 Responses of different composite shells in terms equivalent static load (ESL) and dynamic magnification factor (DMF)

From the definition of ESL as discussed it can be easily understood that the shell suffering higher deflection will be subjected to higher equivalent static load. This quantity has been calculated to make the design procedure simpler. It is evident that the shell subjected to higher ESL will generate higher bending moments and normal forces. Here again the repetition of the same interpretation may not be insignificant that for two-layered unsymmetrical ply of BD-1 and BD-2 shells CP shell options are under higher loading (ESL) than AP shell options. Difference in ESL for BD-1 and BD-2 three-layered symmetric ply of CP and AP shell options is not too

significant. While comparing the ESL between BD-1 and BD-2 shells it can be noticed that BD-2 shells are under lower load as the deflection of this shell is lower than BD-1.

When DMF are studied, it can be seen that though the maximum dynamic deflections are lower in BD-2 shell option than BD-1 shells, dynamic magnification is higher in BD-2 option. While comparing the results with CP shells with AP shells, AP shells shows higher dynamic magnification though its deflection is lower than CP shells in BD-1 option. It may be noted that in case of BD-2 shells DMF of AP and CP plies are at par when anti-symmetrically laid. When the symmetric ply shell option is compared in this regard with anti-symmetric ply shells it is the symmetric ply which shows higher dynamic magnification factor in both the boundary conditions, but symmetric ply AP shells show higher value than CP shells in lower level of impact velocity but in higher impact velocity DMF of AP shells drops down below the CP shells (Fig-14). It is interesting to notice here that for all shell options there is a considerable drop in DMF when the impact velocity is equal to or higher than 5m/s.

7.3.4 Performances of different shell options

The depth of a shell surface is mostly governed by the maximum values of deflection and different shell actions. These are dependent on the contact force, ESL and DMF. To get an idea of the performance of different shell options with respect to the four above mentioned governing quantities, Table 7.5 assigns ranks to different shell combinations, from 1 to 8, in ascending order of magnitude of these parameters.

Table 7.5 Ranks of different shell combinations in terms of deflection, ESL and DMF

Shell options	Governing shell actions				Sum of ranks	Ranks in terms of sum of ranks
	Deflection (m)	Contact force (N)	ESL (N)	DMF		
ASCP/BD-1	4	8	8	1	21	6
ASAP/BD-1	3	6	7	3	19	5
SYCP/BD-1	8	4	4	5	21	6
SYAP/BD-1	5	2	3	7	17	3
ASCP/BD-2	1	7	5	2	15	1
ASAP/BD-2	2	5	6	4	17	3
SYCP/BD-2	7	3	2	6	18	4
SYAP/BD-2	6	1	1	8	16	2
∑CP = 75	∑AP = 69		∑SY = 72	∑AS = 72	∑BD-1 = 78	∑BD-2 = 66

To obtain an overall picture of how the different shell options perform in terms of the governing impact response parameters, they are ranked according to the sum of ranks for individual governing impact response parameters in Table 7.5. It can be noted that the ASCP/BD-2 option is the best choice as far as the deflection criteria is concern and it also emerges as the best choice as per the overall criteria. The first three choices of shells as per their rank in terms of sum of ranks are ASCP/BD-2, SYAP/BD-2 and SYAP/BD-1, ASAP/BD-2. As per rank based on sum of ranks, SYAP/BD-1 and ASAP/BD-2 stands in same position. Though the shell option in the first and third rank also stands in first and third position as per the deflection criteria but the shell option in second rank is not within first three as far as deflection is concern.

The facts discussed above show that the deflection criterion may not be considered as the only governing factor in impact response of the hypar shell roof. It may be also noted that the boundary conditions and ply orientations are also the essential factors to be considered.

Sum of the rank of AP shells is 69, and for CP shells 75. This implies that the performance of AP shells is comparatively better than CP shells under impact load. Sum of the rank of symmetric

ply (SY) and asymmetric ply (AS) are 72. These indicate that performance of SY and AS shells are similar for sudden impact. Increase in boundary constraints improves the impact behavior of skewed hypar shell roofs as it can be found that sum of rank of BD-1 and BD-2 shells are 78 and 66 respectively.

These facts help to conclude that while selecting a shell option for skewed hypar geometry from the available options as discussed in this thesis a designer is free to choose symmetric or asymmetric ply options. But it always better to have angle ply (AP) than a cross ply (CP) shell. Increase in number of supports increases the number of boundary constraints is proofed to be better but it also depends on the actual site condition and other functional requirements.

7.4 CONCLUSIONS

The following conclusions can be drawn from this study:

1. The present formulation can be applied to study the impact response of point-supported composite skewed hypar shells, which is evident from the close agreement of the present results with the published ones.
2. Under the influence of normal low velocity impact the contact force shows a parabolic combined loading and unloading curve with a single peak for the practical class of shells considered here. Higher magnitude of impact velocity results in higher value of the peak contact force. However, due to a sharp elastic rebound the total duration of contact force is less for higher velocity of impactor.
3. The time instants at which the maximum contact force and the maximum dynamic displacement occur show a phase difference and interestingly in some cases the maximum displacement and hence stresses may occur even after the contact force dies down totally

.Thus it is concluded that the study should be continued only after when the major peaks of the dynamic displacement die down and not after the full decay of the contact force only.

4. The maximum contact force, the peak dynamic displacement and the equivalent static load are all increasing functions of impactor velocity, the relations being almost linear. However, the dynamic magnification factor shows a logarithmically decreasing tendency with increase of the velocity of impact.
5. The displacement histories of several points (Figure 7.3) are studied along with the node of impact (node-1). It may be noted that at some of the points, e.g. Node-2 and 8, the displacement at some instant may exceed the same occurring at the point of impact. But such displacements will never govern the design as they are always less that the absolute maximum displacement occurring at the point of contact.
6. Table 7.5 shows that only the increase or decrease in boundary constraints may not be the only governing factor of deflection characteristics of a shell. This requires more detail study.
7. Though the symmetric and asymmetric plies show comparable performance, angle ply shell performs bit better than cross ply shell.
8. It is also clear from the results that increase in boundary constraints gives better performance under impact load but it should also comply with the other functional requirements of the site.

Chapter 8

IMPACT PERFORMANCE OF COMPOSITE HYPAR SHELL ROOF UNDER OBLIQUE IMPACT WITH FRICTION

8.1 GENERAL

Behavior of skewed hypar shell under low velocity oblique impact is studied and presented in this chapter. Dry friction has been considered which depends on normal pressure of contact but is nearly independent of sliding speed.

The problem used to validate the oblique impact formulation and those solved to study the behavior of skewed hypars subjected to oblique impact are presented in Section 8.2. The results and the related discussions are furnished in Section 8.3. The conclusions of major engineering significance find place in Section 8.4.

8.2 NUMERICAL EXAMPLES

Problems are solved to validate the present finite element code and to numerically explore the different behavioral aspects of composite skewed hypar shell roof under low-velocity impact with an obliquity. Problem of impact response of composite plate, solved earlier by Tu and Chow (1999) serves as the benchmark to validate the correct incorporation of oblique impact formulation considering the effect of friction for simply-supported boundary condition. The detail of the benchmark problem is furnished in Figure 8.1.

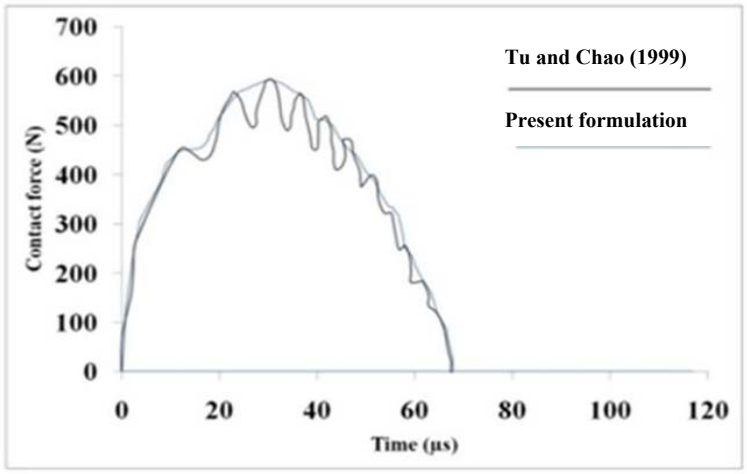

E_1=128 GPa. E_2=E_3=8 GPa. G_{12}=G_{13}=4.5 GPa. G_{23}=1.6 GPa. ν_{12}=ν_{23}=ν_{31}= 0.28, γ =1515 kg/m^3, μ_1 =0.2, μ_2 =0.4, a =150 mm b =150 mm, h =9.95 mm, D_s =25.4 mm m_s= 0.125kg, v_x= 20.0 m/s v_z= 5.0 m/s

Figure 8.1 Contact force history of a simply supported plate under oblique impact

Besides the aforementioned problem, responses of skewed hypar shells being impacted at the central point are also studied for two different ply options combining simply supported boundary condition. Six impact velocities with four different angle of impact are considered. The details of which are furnished below.

i)	Boundary conditions	Simply-supported (SS)
ii)	Laminations	+45°/-45° (Angle ply or AP)0°/90° (Cross ply or CP)
iii)	Velocity of impact (m/s)	1, 2, 3, 5, 7, 10
iv)	Angle of impact (θ_i)	0^0, 15^0, 30^0, 45^0
iv)	Details of shell geometry	a = 1.0m, b =1.0m, t=0.02m, c=0.2m

8.3 RESULTS AND DISCUSSION

8.3.1 Results of benchmark problems

Figure 8.1 presents diagrammatically the results of the benchmark problem including the published ones and those obtained by the present approach. The contact force history obtained by the present approach for a simply-supported composite plate under oblique impact considering

the effect of friction shows a good agreement with that reported by Tu and Chao (1999). This confirms the correct incorporation of the oblique impact formulation considering the effect of friction for simply-supported boundary condition in the present finite element code. Here the authors have taken the liberty of converting the hypar shell configuration to plate assigning a zero value to the curvature.

8.3.2 General behavior of the hypar shells under oblique impact

The finite element mesh implemented in the present study is based primarily on force and displacement convergence criteria. All the results of contact force and displacement that are presented are arrived at only after the study of time step convergence.

Table 8.2 and 8.3 contains the maximum values of the contact force, maximum dynamic displacement for different impact velocities and different angle of impact for simply-supported boundary condition. The values of equivalent static loads and dynamic magnification factors (as explained hereafter) are also furnished in the tables.

Contact force and displacement histories are studied on the central point where the impactor strikes the shell. Typical time histories of contact force and displacement for simply-supported shell are shown in Figure 8.2 and Figure 8.3 for different impact angle and for 10m/s impact velocity only.

While studying low velocity impact response, struck by the spherical impactor centrally, it is observed that the contact force follows a parabolic variation having a single peak. After some time both for angle and cross ply shell the contact force converges to zero value for normal impact around or less than 60μs, whereas, the oblique impact dies down at about 35μs. It is interesting to note that higher the impact velocity, higher is the contact force, but the force dies

down to zero relatively faster (although such pictorial representation is not furnished here to maintain brevity). This behavior may be attributed to the rapid elastic rebound of the impactor with the increment in the velocity value followed by detachment which causes contact force to decay out. It is also worth noting that the time instants corresponding to peak contact forces and peak displacements at the centre point do not match. This is because the resultant displacement at any time instant is a cumulative effect of the instantaneous contact force value and the inertia effect of the previous instant. The figures showing the transient displacement show that vibration continues even after the force dies down with successively occurring peaks, though the peak values are less in magnitude than the highest peak which occurs a bit after the instant of maximum contact force but before the full decay. It is to be noted that the contact forces and the transient displacements do not exhibit any tendency of local reversal. The peak transverse contact force in oblique impact is considerably low than normal impact as component of the impact is shared in tangential direction. Contact force decreases as the obliquity increases.

Table 8.1 Maximum contact force, maximum dynamic displacement, equivalent static load, dynamic magnification factor for different velocities of the impactor for simply supported angle ply (SS/AP) hypar shell

Velocity of impact (m/s)	Maximum contact force (N)				Maximum displacement (m)				Equivalent static load (N) (ESL)				Dynamic magnification factor (DMF)			
	$\theta_i = 0^0$	$\theta_i = 15^0$	$\theta_i = 30^0$	$\theta_i = 45^0$	$\theta_i = 0^0$	$\theta_i = 15^0$	$\theta_i = 30^0$	$\theta_i = 45^0$	$\theta_i = 0^0$	$\theta_i = 15^0$	$\theta_i = 30^0$	$\theta_i = 45^0$	$\theta_i = 0^0$	$\theta_i = 15^0$	$\theta_i = 30^0$	$\theta_i = 45^0$
1	309.3	112.8	104.7	86.0	0.00017	0.00003	0.00003	0.00003	2074	427.2	421.0	364.2	3.76	1.533	1.440	2.283
2	713.6	265.6	246.7	276.7	0.00034	0.00007	0.00007	0.00008	4206	911.1	895.1	1030.9	2.97	1.306	1.226	1.9428
3	1165.9	436.5	406.6	332.2	0.00050	0.00011	0.00011	0.00010	6204.7	1407.4	1382.7	1200	2.76	1.035	1.322	1.227
5	2162.3	822.4	770.2	622.8	0.00086	0.00019	0.00019	0.00016	10638.4	2395.1	2333.3	2012.3	2.58	1.14	1.061	1.355
7	3252.5	1255.2	1161.6	951.4	0.00123	0.00028	0.00027	0.00024	15237.4	3444.4	3382.7	2913.6	2.31	0.863	1.137	1`.052
10	5010.8	1961.3	1815.5	1473.7	0.00180	0.00041	0.00040	0.00035	22207.5	5098.8	4975.3	4308.6	2.03	0.93	0.864	1.131

θ_i = Angle of impact measured with vertical axis

Table 8.2 Maximum contact force, maximum dynamic displacement, equivalent static load, dynamic magnification factor for different velocities of the impactor for simply supported cross ply (SS/CP) hypar shell

Velocity of impact (m/s)	Maximum contact force (N)				Maximum displacement (m)				Equivalent static load (N) (ESL)				Dynamic magnification factor (DMF)			
	$\theta_i = 0^0$	$\theta_i = 15^0$	$\theta_i = 30^0$	$\theta_i = 45^0$	$\theta_i = 0^0$	$\theta_i = 15^0$	$\theta_i = 30^0$	$\theta_i = 45^0$	$\theta_i = 0^0$	$\theta_i = 15^0$	$\theta_i = 30^0$	$\theta_i = 45^0$	$\theta_i = 0^0$	$\theta_i = 15^0$	$\theta_i = 30^0$	$\theta_i = 45^0$
1	310.2	112.4	104.5	86.0	0.00017	0.00003	0.00004	0.00003	1627.5	341.2	360.8	312.7	2.84	1.17	1.26	1.32
2	715.8	264.5	246.2	202.2	0.00034	0.00008	0.00008	0.00007	3333.3	782.4	665.7	665.7	2.25	1.02	1.27	1.16
3	1169.6	436.6	407.0	332.4	0.00055	0.00010	0.00012	0.00011	5411.8	1039.2	1196.1	1039.2	2.1	0.81	1.00	1.04
5	2169.1	818.2	768.2	622.7	0.00090	0.00022	0.00021	0.00021	8843.1	2098.0	2098.0	2098.0	1.97	0.89	0.83	0.94
7	3261.3	1250.0	1158.0	950.8	0.00139	0.00031	0.00031	0.00027	13627.5	3039.2	3029.4	2627.5	1.77	0.69	0.89	0.82
10	5025.0	1951.3	1810.3	1472.7	0.00190	0.00045	0.00045	0.00039	18598.0	4441.2	4411.8	3862.7	1.56	0.74	0.69	0.88

θ_i = Angle of impact measured with vertical axis

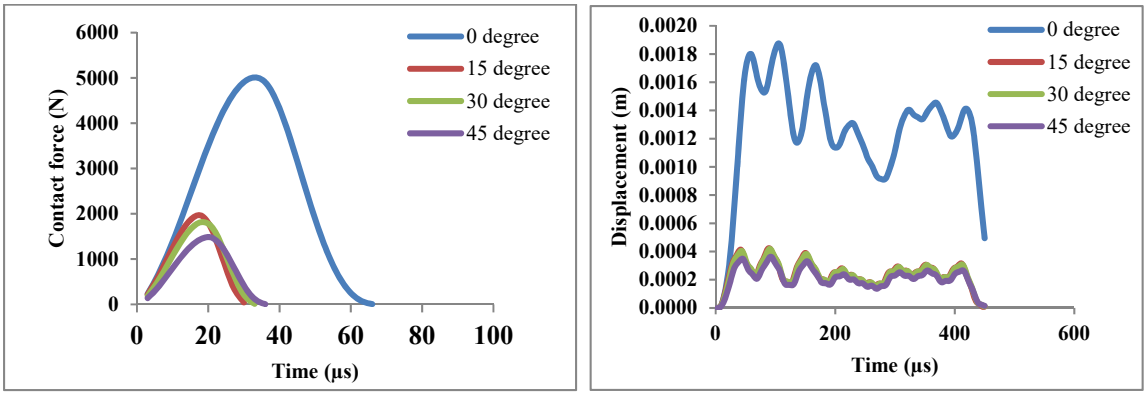

Figure- 8.2 Impact response of simply supported angle ply (SS/AP) composite hypar shells for impact velocity 10 m/s

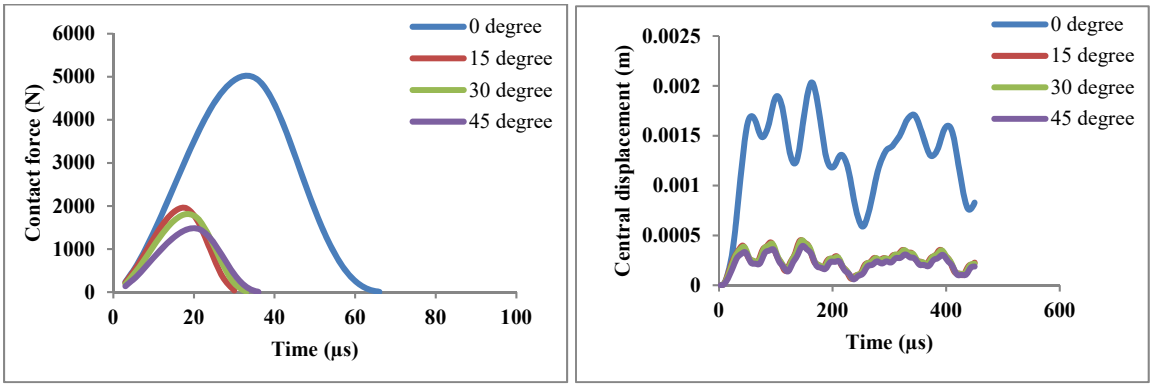

Figure- 8.3 Impact response of simply supported angle ply (SS/CP) composite hypar shells for impact velocity 10 m/s

8.3.3 Equivalent Static Load and Dynamic Magnification Factor

To estimate the equivalent static load (ESL) corresponding to a particular impact velocity, a concentrated load at the centre (point of impact) is applied and adjusted the yield a central displacement equal to the maximum dynamic displacement. It is further explored to estimate the magnitude of the central displacement when the peak contact force is applied at the point of impact as a static concentrated load. The central displacement obtained under such a load when divides the maximum dynamic displacements yields dynamic magnification factor (DMF).The variations of maximum contact force, maximum dynamic displacement and equivalent static load (ESL) with impact velocity, shown in Figure 8.4 and Figure 8.5, are almost linear and are increasing functions of impact velocity. However, the dynamic magnification factor (DMF) and the impact velocity shows a logarithmic detrimental relation with impact velocity. This enables the designer to practice the static approximation of the problem.

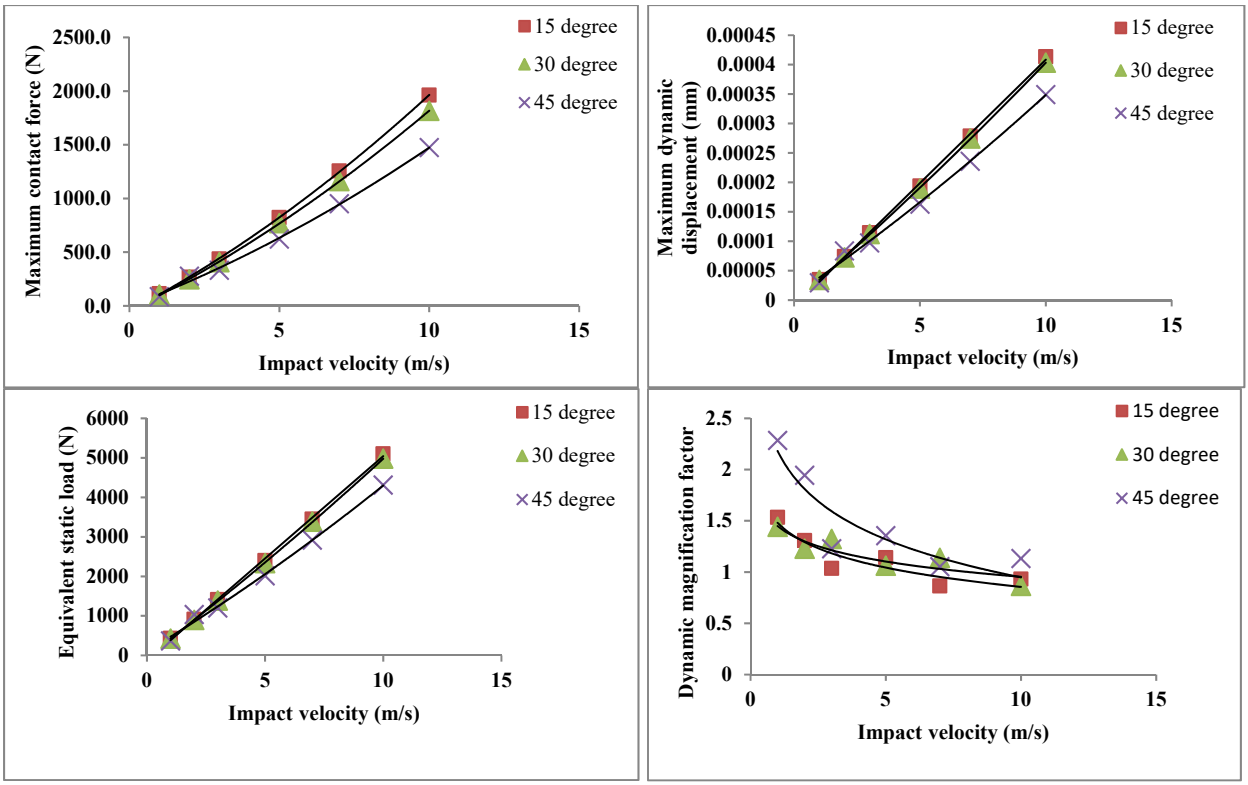

Figure- 8.4 Variation of maximum impact load, maximum displacement, equivalent static load and dynamic magnification factor with velocity for simply supported angle ply (SS/AP) composite hypar shells

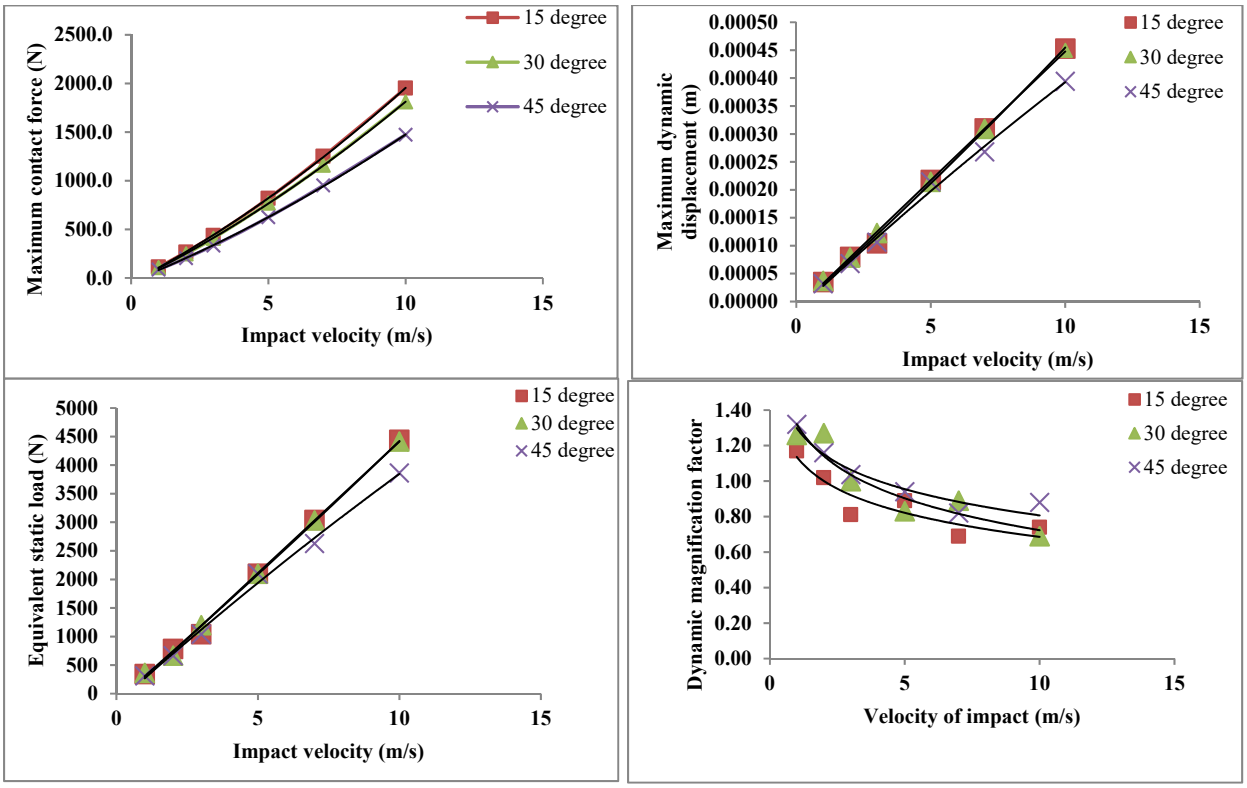

Figure- 8.5 Variation of maximum impact load, maximum displacement, equivalent static load and dynamic magnification factor with velocity for simply supported anti-symmetric cross ply (SS/ASCP) composite hypar shells

8.3.4 Comparative performance of angle ply and cross ply shell

The behavior of the impact response of simply supported cross (SS/CP) and angle ply (SS/AP) shell may be studied through Figure 8.2 and Figure 8.3 and Table 8.2 and Table 8.3. The nature of contact force and dynamic displacement for SS/ CP shell is more or less similar to what is discussed before for SS/AP shell. One interesting difference is that for SS/ CP shell the peak dynamic displacement does not only show a phase lag with respect to the peak contact force but by the time displacement value reaches the peak, the contact force value dies down totally. This shows that the after-effect of impact are some times more severe than the shell response during the impact and study of displacement variation even after the contact force decays to a null value

is absolutely necessary. However, after passage of some more time the subsequent local maxima which are obtained do not touch the peak.

The dependence of the maximum contact force, the peak dynamic displacement and the equivalent static load (ESL) on the impactor velocity in case of simply supported cross ply (SS /CP) shell are comparable to what is observed in case of simply supported angle ply (SS/AP) shell.

While comparing the equivalent static (ESL) load it was observed that the value of the same is little higher in case of SS/AP shell option and difference increases with increase of impact velocity. Difference of ESL value between two shell options remains more or less same with change of impact angle.

When dynamic magnification factor (DMF) was compared between two shell options it was found that dynamic magnification factor is higher in case of SS/AP shell in compare to SS/CP shell. It is interesting to note that DMF value sometimes is less than unity in case of oblique impact with high impact velocity.

8.4 CONCLUSIONS

The following conclusions can be drawn from this study:

1. The present formulation can be applied to study the response of simply supported composite skewed hypar shell under oblique impact, which is evident from the close agreement of the present results with the published one.
2. Under the influence of low velocity oblique impact the contact force shows a parabolic combined loading and unloading curve with a single peak for simply supported shell considered here for all values of impact angles. Higher magnitude of impact velocity results in higher value of the peak contact force. However, due to a sharp elastic rebound the total

duration of contact force is less for higher velocity of impactor. Value of the peak contact force decreases with increase in angle of impact. Such decrement occurs in case oblique impact as only a component (vertical) contributes in normal impact.

3. The time instants at which the maximum contact force and the maximum dynamic displacement occur show a phase difference and interestingly in some cases the maximum displacement and hence stresses may occur even after the contact force dies down totally .Thus it is concluded that the study should be continued only up to the time when the major peaks of the dynamic displacement die down and not up to the full decay of the contact force only.
4. The maximum contact force, the peak dynamic displacement and the equivalent static load are all increasing functions of impactor velocity, the relations being almost linear. However, the dynamic magnification factor shows a logarithmically decreasing tendency with increase of the velocity of impact.
5. For SS/ CP shell the peak dynamic displacement does not only show a phase lag with respect to the peak contact force but by the time displacement value reaches the peak, the contact force value dies down totally. This shows that the after-effect of impact are some times more severe than the shell response during the impact and study of displacement variation is required even after the contact force decays to a null value
6. Equivalent static (ESL) load is little higher in case of SS/AP shell than in case of SS/CP and the difference increases with increment of impact velocity. This confirms that the SS/AP shell performs better in terms of load carrying capacity.

7. Dynamic magnification factor is higher in case of SS/AP shell compared to SS/CP shell. It is interesting to note that DMF value sometimes is less than unity in case of oblique impact with high impact velocity.

Chapter 9

CONCLUSION AND FUTURE SCOPE

9.1 GENERAL

In this chapter a general conclusion on the outcome of the present thesis and the significant contribution made by the author through the present study is presented. The chapter ends with the future scope of the present work.

9.2 GENERAL CONCLUSION

Considering the results presented and analyzed in the present study in different chapters following general conclusion may derived.

1. Close agreement of the results obtained by the present method with those available in the published literature establishes the correctness of the approach use here.
2. Under the influence of the low velocity impact the contact force shows a parabolic combined loading unloading curve with a single peak for the practical class of shells considered in this study. Higher magnitude of impact velocity results in higher value of the peak contact force. However, due to a sharp elastic rebound the total duration of contact force is less for higher velocity of impactor.
3. The time instants at which the maximum contact force and the maximum dynamic displacement occur show a phase difference and interestingly in some cases the maximum displacement and hence stresses may occur even after the contact force dies down totally .Thus it is concluded that the study should be continued only after when the major peaks of the dynamic displacement die down and not after the full decay of the contact force only.

4. The maximum contact force, the peak dynamic displacement and the equivalent static load are all increasing functions of impactor velocity, the relations being almost linear. However, the dynamic magnification factor shows a logarithmically decreasing tendency with increase of the velocity of impact.
5. Though the symmetric and asymmetric plies show comparable performance, angle ply shell performs bit better than cross ply shell.
6. The displacement histories of several other nodes are studied along with the node of impact. Interestingly in some of the nodes, other than node of impact, the displacement at some instant exceed the same occurring at the point of impact. Though such displacements will never govern the design as they are always less that the absolute maximum displacement occurring at the point of contact.
7. Increase or decrease in boundary constraints may not be the only governing factor of deflection characteristics of a shell but increase in boundary constraints gives better performance under impact load but it should also comply with the other functional requirements of the site.
8. It is interesting to note that DMF value sometimes is less than unity in case of oblique impact with high impact velocity.

9.3 SIGNIFICANT CONTRIBUTION MADE THROUGH PRESENT THESIS

A skewed hypar shell which is easy to be fabricated apart from being aesthetically appealing should find greater application in the industry as felt by the author. The principal contribution of the author lies in carrying out an in-depth study of laminated composite skewed hypar shell subjected to impact loading by varying parameters like staking sequence, boundary condition,

impact velocity and angle of impact. A thesis in engineering on shells should preferably end up with suggesting pin pointed recommendations which will help confident use of the shell in practical field. The ranks proposed in the present thesis for choosing the optimum shell option among a number of choices in terms of contact force, impact deflection, equivalent static load and dynamic magnification factor should act as design aids to practicing engineers. In a nut shell, the contribution made through the present work is about exploring the impact behavior of a shell configuration not reported in the past and suggesting design guidelines to practicing engineers to use those shells confidently for which design codes are not available.

9.4 FUTURE SCOPE

Impact on composite shell surface may lead to localized damages in forms of delamination and failure of matrix or fiber. The present work may be continued to explore these post impact effects. Linear and nonlinear first ply failure and progressive failure analyses may be carried out under impact loading as an extension of the present research. The complicated aspects like impact induced dynamic instability problems and analyzing shells having different edges with different constraints may be taken up for future study. These are indicative areas where future research may be carried out and the above list is not exhaustive.

REFERENCES

1. Abrate, S., Impact on laminated composite materials. *Applied Mechanics Review* 44 (1991) 155-190.
2. Abrate, S., Impact on laminated composites : recent advances. *Applied Mechanics Review* 47 (1994) 517-544.
3. Abrate, S., Modeling of impacts on composite structures, Composite Structures, 51(2001) 129–138.
4. Ansari, Md Chakraborty M., Iqbal, M.A., An experimental and finite element investigation of the ballistic performance of laminated GFRP composite target, *Composites Part B: Engineering*, In Press,(2017).
5. Ansari,Md., M. Chakrabarty., A. Influence of projectile nose shape and incidence angle on the ballistic perforation of laminated glass fiber composite plate. *Composite Science and Technology,*142 (2017) 107-116.
6. Boria, S., Scattina, A., Belingardi, G., Impact behavior of a fully thermoplastic composite, *Composite Structures*,167 (2017) 63-75.
7. Cantwell, W.J., Morton, J., Detection of impact damage in CFRP laminates, *Composite Structures*, 3(1985) 241-257.
8. Chakraborty, D., Delamination of laminated fiber reinforced plastic composites under multiple cylindrical impact, *Materials and Design* 28 (2007) 1142–1153.

9. Chen, S., Zang, M., Wang, Di., Zheng, Z., Zhao, C., Finite element modeling of impact damage in polyvinyl butyral laminated glass, *Composite Structures*, 138, 15 (2016) 1-11.
10. Choi, H.Y., Chang F.K., A model for predicting damage in graphite/ epoxy laminated composites resulting from low-velocity point impact, *Journal of Composite Materials*, 26 (1992) (14) 2134–2169.
11. Choi, H.Y., Downs, R.J., Chang, F.K.. A new approach toward understanding damage mechanisms and mechanics of laminated composites due to low-velocity impact: Part I—experiments, *Journal of Composite Materials*, 25 (1991) 992–1011.
12. Choi, I.H. Geometrically nonlinear transient analysis of composite laminated plate and shells subjected to low-velocity impact, *Composite Structures*, 142 (2016) 7-14.
13. Choi, I.H. Lim, C.H. Low-velocity impact analysis of composite laminates using linearized contact law. *Composite Structures* 66 (2004) 125–132.
14. Christoforou, A.P., Swanson, S.R., Analysis of simply supported orthotropic cylindrical shells subjected to lateral impact loads, *ASME, Journal of Applied Mechanics*, 57 (1990) 376-382.
15. Chun, L.U., Lam, K.Y., Dynamic response of fully-clamped laminated composite plates subjected to low-velocity impact of a mass, *International Journal of Solids and Structures*, (1998) 35(11) 963-979.
16. Dobyns, A.L., Analysis of simply supported orthotropic plates subjected to static and dynamic load, *AIAA Journal*, 1981, 19(5), 642-650.
17. Elber, W., Failure mechanics in low-velocity impacts on thin composite plates, *NASA, Technical Paper* (1983) 2152.

18. Elder, D., Thomson, R., Scott, M.L., Comparison of composite damage predictions between a 2D, 3D LS-Dyna simulation and experimental results for a low speed impact event, In: Proceedings of *Tenth Australian International Aerospace Congress (AIAC- 10)*, Brisbane, Australia, 2003.
19. Elder, David J., Thomson, R., S. Nguyen Minh, Q. Murray Scott, L. Review of delamination predictive methods for low speed impact of composite laminates, *Composite Structures* 66 (2004) 677–683.
20. Evci, Celal., Thickness-dependent energy dissipation characteristics of laminated composites subjected to low velocity impact, Composite Structures, 133 (2015) 508-521.
21. Fan, Y., Wang, H., Nonlinear low-velocity impact analysis of matrix cracked hybrid laminated plates containing CNTRC layers resting on visco-Pasternak foundation, *Composites Part B: Engineering,*117 (2017) 9-19.
22. Farooq, U., Gregory, K., Finite Element Simulation of Pseudo Damage Induced Quasi Static Indentation of Fibrous Composite Panels Under Variable Shape Indentors, *European Journal of Scientific Research,* 25 (1) (2009), 77-85.
23. Farooq, U., Myler, P., Finite element simulation of damage and failure predictions of relatively thick carbon fibre-reinforced laminated compositepanels subjected to flat and round noses low velocity drop-weight impact, *Thin-Walled Structures,*104, (2016) 82-105.
24. Farooq, U., Myler, P., Ply level failure predictio of carbon fibre reinforced laminated composite panels subjected to low velocity drop-weightimpact using adaptive meshing techniques, *Acta Astronautica,* 102 (2014) 169-177.

25. Ganapathy, S., Rao, K.P., Interlaminar Stresses in laminated composite plates, cylindrical/ spherical shell panels damaged by low-velocity impact, *Composite Structures* (1997) 38(1-4) 157-168.
26. Ganapathy, S., Rao, K.P., Failure analysis of laminated composite cylindrical/spherical shell panels subjected to low-velocity impact, Computers, *Computers and Structures*, (1998) 68, 627-641.
27. Ghasemnejad, H., Furquan, A.S., M. Mason, P.J. Charpy impact damage behaviour of single and multi-delaminated hybrid composite beam structures, *Materials and Design,* 31 (2010) 3653–3660.
28. Goldsmith,W., '*Impact' Edward Arnold*, London,1960.
29. Gong, S.W., Toh, S.L., Shim, V.P.W., Impact response of laminated shells with orthogonal curvature, *Composites Engineering* 4(2) (1994) 247-266.
30. Greve, L. Pickett,A.K., Payen, F., Experimental testing and phenomenological modeling of the fragmentation process of braided carbon/epoxy composite tubes under axial and oblique impact, *Composites: Part B* 39 (2008) 1221–1232.
31. Gupta , N.K., Madhu, K., An experimental study of normal and oblique impact of hard-core projectile on single and layered plate, *International Journal of Impact Engineering*, 9 (5-6), (1997) 395-414.
32. Gupta, N.K., Madhu,V., Normal and oblique impact of a kinetic energy projectile on mild steel plates, *International Journal of Impact Engineering*, 12(3) (1991) 333-343.
33. Haro, Edison E., Jerzy A., Szpunar, Akindele, G., Odeshi, Ballistic impact response of laminated hybrid materials made of 5086-H32 aluminum alloy, epoxy and Kevlar fabrics

impregnated with shear thickening fluid, *Composites Part A: Applied Science and Manufacturing,* 87,(2016), 54-65.

34. He, W., Guan, Z., Li, X., Liu, D., Prediction of permanent indentation due to impact on laminated composites based on an elasto-plastic model incorporating fiber failure, *Composite Structures*, 96(2013) 232-242.
35. Her, S., Liang,Y., The finite element analysis of composite laminates and shell structures subjected to low velocity impact, *Composite Structures,* 66 (2004) 277–285.
36. Hertz, H., On the contact of elastic solids. *Journal fur die reine und angewandte Mathematik*, 92 (1881) 156-171.
37. Hosson, O.H., Tarfaoui, M., Moumen, E.I., A progressive damage modeling in laminated composites under slamming impact water for naval applications, *Composite Structures*, 167 (2017) 178-190.
38. Hwang, W.C., Sun C.T., Failure analysis of laminated composites by using iterative three-dimensional finite element method. *Computers and Structures*,33 (1989) 41-47.
39. Icardi, U., C^0 plate element based on strain energy updating and spline interpolation, for analysis of impact damage in laminated composites, *International Journal of Impact Engineering*, 34 (2007) 1835–1868.
40. Isaac, C. W., Oluwole, O., Energy absorption improvement of circular tubes with externally press-fitted ring around tube surface subjected under axial and oblique impact loading, Thin-Walled Structures, 109 (2016) 352-366.

41. Ivancevic, D., Smojver, I., Explicit multi-scale modeling of impact damage on laminated composites – Part II: Multiscale analyses, *Composite Structures,*145, (2016) 259-268.
42. Ivanez, I. Moure, M.M. Garcia-Castillo, S.K. Sanchez-Saez, S. The oblique impact response of composite sandwich plates, *Composite Structures,* 133 (2015) 1127-1136.
43. Jafari, A.A., Khalili, S.M., Azarafza, R. R., Transient dynamic response of composite circular cylindrical shells under radial impulse load and axial compressive loads, *Thin-Walled Structures,* 43 (2005) 1763–1786.
44. Johnson, Alastair F., Holzapfel, M., Modelling soft body impact on composite structures, Composite Structures 61 (2003) 103–113.
45. Johnson, A.F., Holzapfel, M., Influence of delamination on impact damage in composite structures, *Composites Science and Technology*, 66 (2006) 807–815.
46. Kavousi Sisi, M., Shakeri, M. Sadighi, M. Dynamic response of composite laminated beams under a synchronous/repeated low-velocity impacts of multiple masses, *Composite Structures,* 132 (2015) 960-973.
47. Keer, L.M., Schonberge, W.P., Smooth indentation of a isotropic cantilever beam, *International Journal of Solids and Structures,* 22 (1986) 87-103.
48. Kistler, L.S., Waas, A.M., Impact response of cylindrically curved including a large deformation scaling study, *International Journal of Impact Engineering*, 21 (1998) (1-2) 61-75.
49. Krishnamurthy, K.S., Mahajan, P., Mittal, R.K., A parametric study of the impact response and damage of laminated cylindrical composite shells, *Composites Science and Technology* 61 (2001) 1655–1669.

50. Krishnamurthy, K.S., Mahajan , P., Mittal, R.K., Impact response and damage in laminated composite cylindrical shells, Composite Structures, 59 (2003) 15–36

51. Li , S., Reid, S.R., Zou, Z., Modelling damage of multiple delaminations and transverse matrix cracking in laminated composites due to low velocity lateral impact, *Composites Science and Technology,* 66 (2006) 827–836.

52. Li, D.H., Liu, Y., Zhang, X., Low-velocity impact responses of the stiffened composite laminated plates based on the progressive failure model and the layerwise/solid-elements method, *Composite Structures,* 110 (2014) 249-275.

53. Li, S., Reid, S.R., Zou, Z., Modelling damage of multiple delaminations and transverse matrix cracking in laminated composites due to low velocity lateral impact, *Composites Science and Technology,* 66 (2006) 827–836.

54. Liao, B.B., Liu, P.F., Finite element analysis of dynamic progressive failure of plastic composite laminates under low velocity impact, *Composite Structures,* 159 (2017) 567-578.

55. Lin, J.H. Lee, Y.J. Use of statical indentation law in the impact analysis of composite laminated plates and shells, *ASME, Journal of Applied Mechanics*, 57(1990) 787-789.

56. Liu, P.F., Liao, B.B., Jia, L.Y., Peng, X.Q., Finite element analysis of dynamic progressive failure of carbon fiber composite laminates under low velocity impact, *Composite Structures,* 149 (1) (2015) 408-422.

57. Liu, Chunchuan, Li, Fengming, Huang, Wenhu, Transient impact responses of laminated composite cylindrical shells, *Theoretical and Applied Mechanics Letters,* 1,(3) (2011) Article 031004.

58. Lou, X., Cai, H., Yu, P., Jiao, F., Han, X., Failure analysis of composite laminate under low-velocity impact based on micromechanics of failure, *Composite Structures,* 163 (2017) 238-247.

59. Luo, R.K., Green, E.R., Morrison, C.J., An approach to evaluate the impact damage initiation and propagation in composite plate, *Composite Part B* 32(2001) 513-520.

60. Madjidi, S., Arnold, W.S., Marshall, I.H., Damage tolerance of GSM laminates subject to low velocity oblique impact, *Composite Structures,* 34(1996) 101-116.

61. Mahanta, B.B. Chakraborty, D., Dutta, A., Accurate prediction of delamination in FRP composite laminates resulting from transverse impact, *Composites Science and Technology* 64 (2004) 2341–2351.

62. Malekzadeh, K., Khalili, M.R., Olsson, R., Jafari, A., Higher-order dynamic response of composite sandwich panels with flexible core under simultaneous low-velocity impacts of multiple small masses *International Journal of Solids and Structures* 43 (2006) 6667–6687.

63. Malik, M.H., Arif, A.F.M., Al-Sulaiman, F.A. Z., Khan,. Impact resistance of composite laminate flat plates- A parametric sensitivity analysis approach, *Composite Structures,* 102 (2013)138-147.

64. Marcon, B., Fouvry, S., Sassy,O., Guegan, J., Daniel, G. Fracture mechanics of impacted laminated glass subjected to various fatigue stressing conditions, *Engineering Fracture Mechanics,* 127 (2014) 71-82.

65. Mijia, Y., Pizhong, Q., Higher-order impact modeling of sandwich structures with flexible core. *International Journal of Solids and Structures* 42 (2005) (10), 5460–5490.

66. Mills, N.J., Wilkes, S., Derler, Flisch, S. A., FEA of oblique impact tests on a motorcycle helmet, *International Journal of Impact Engineering* 36 (2009) 913–925.

67. Narita, Y., Leissa, A.W., Vibrations of point-supported shells of rectangular platform, *Earthquake Engineering and Structural Dynamics*, vol. 12, pp. 651-661, 1984.

68. Natsuki, T., Yoshizawa, K., Bao, L.M., Ni, Q.Q., Theoretical analysis of low-velocity impact response in two-layer laminated plates with an elastic medium layer, *Composite Structures*, 162 (2017) 308-312.

69. Navarro, P., Aubry, J., Marguet, S., Ferrero, J.-F., Lemaire, S., Rauch, P., Semi-continuous approach for the modeling of thin woven composite panels applied to oblique impacts on helicopter blades, *Composites Part A: Applied Science and Manufacturing,* 43 (6) (2012) 871-879.

70. Newton, I., Philosophiae Naturalis Principia Mathematica, (1687) , Imprimatur, Londini

71. Olsson, R., Donadon, Mauricio V., Falzon, Brian G., Delamination threshold load for dynamic impact on plates, *International Journal of Solids and Structures*, 43 (2006) 3124–3141.

72. Paruka, P., Shah, Mohd Kamal Mohd, Mannan, Md Abdul, Influence of Axial and Oblique Impact Loads on Crush Response Properties of Square Tube Structures Made with FRP Pultruded Composites, *Procedia Engineering,* 68 (2013) 572-578.

73. Perez, Marco A. Martínez, X. Oller,S. Gil, L. Rastellini, F. Flores, F. Impact damage prediction in carbon fiber-reinforced laminated composite using the matrix-reinforced mixing theory, *Composite Structures*, 104 (2013) 239-248.

74. Poisson, S.D., Traite DE Mechanique, Paris, Bachelier Impremeur-Libraire 1833 (Second Edition)

75. Puente, L., Zaera J. R., Navarro, C., An analytical model for high velocity impacts on thin CFRPs woven laminated plates, *International Journal of Solids and Structures* 44 (2007) 2837–2851.

76. Puente. Lopez, Zaera,J., R. Navarro,C. Experimental and numerical analysis of normal and oblique ballistic impacts on thin carbon/epoxy woven laminates, *Composites: Part A* 39 (2008) 374–387

77. Qatu M.S., Leissa A.W., Natural frequencies for cantilevered doubly-curved laminated composite shallow shells., *Computers Structures*,17(1991) (3) 227-256.

78. Rajbhandari , S. P., Parametric finite element modellingof monolithic composite structures for impact damage, Master of Engineering thesis, Royal Melbourne Institute of Technology, Melbourne, Australia, 2003.

79. Ramkumar, R.L., Thakur R. Y., Dynamic response of a curved laminated plate subjected to low velocity impact. *Journal of Engineering Materials and Technology*, Transactions of the ASME 109 (1987) 67-71.

80. Rekerby, D.G., Macmilan, N.H., On the oblique impact of a rigid sphere against a rigid plastic solid, *International Journal of Mechanical Siences,* 22(1979) 491-498.

81. Santos, R.A.M., Reis, P.N.B., Santos, M.J. Coelho, C.A.C.P., Effect of distance between impact point and hole position on the impact fatigue strength of composite laminates, *Composite Structures,*168 (2017) 33-39.

82. Saravanos, D., Christoforou, A., Andreas P., Low-energy impact of adaptive cylindrical piezoelectric–composite shells, *International Journal of Solids and Structures,* 39 (2002) 2257–2279.

83. Schoeppner, G.A., Abrate, S., Delamination threshold load for low velocity impact on composite laminates, *Composites Part A,* (2000) 31, 903-915.

84. Setoodeh, A.R., Malekzadeh, P., Nikbin, K. Low analysis of laminated composite plates using a 3D elasticity based layer wise FEM ,*Materials & Design,* 30(9) (2009) 3795-3801.

85. Shim, V.P.W., Toh, S.L., Gong, S.W., The elastic impact response of glass/epoxy laminated ogival shells, International Journal of Impact Engineering, 18 (1996) (6) 633-655

86. Shivakumar, K.N., Elber, W,. Illg, W., Prediction of low-velocity impact damage in thin circular laminates, *AIAA Journal* 23 (1985) 442- 449.

87. Shu, D., Stronge,W.J., Yu, T.X., Oblique impact at the tip of a cantilever, *International Journal of Impact Engineering*, 12(1) (1991) 37-47.

88. Spottwood, S. Michael., Palazotto, Anthony N., Progressive failure analysis of a composite shell, *Composite Structures*, 53(2001) 117-131.

89. Sun, C.T., Chottopadhyay, S., Dynamic response of anisotropic laminated plates under initial stresses to impact of masses, *Journal of Applied Mechanics*, Transactions of the, ASME,1975,42,693-698.

90. Sun, C.T., Chen, J.K., On the impact of initially stressed composite laminates, *Journal of Composite Material,* 19 (1985) 490-503

91. Sunderarajan, G., Shewmon, P.G., Oblique impact on a hard ball against ductile semi infinite target materials- Experiment and analysis, *International Journal of Impact Engineering*, 6(1) (1986) 3-22.

92. Tabacu, S. Analysis of circular tubes with rectangular multi-cell insert nder oblique impact loads, *Thin-Walled Structures,* 106 (2016)129-147.

93. Tan, T.M., Sun, C.T., Use of statical indentation laws in the impact analysis of laminated composite plate, *Journal of Applied Mechanics*. 52 (1985) 6-12.

94. Timoshenko, S. P. and Goodier, N. J., (195 l), Theory of Elasticity, McGraw-Hill, New York.

95. Tita, V., Carvalho, J. de, Dirk Vandepitte, Failure analysis of low velocity impact on thin composite laminates: Experimental and numerical approaches, *Composite Structures*, 83 (2008) 413–428.

96. Toh, S.L., Gong, S.W., Shim, V.P.W., Transient stress generated by low velocity impact on orthotropic laminated cylindrical shell, *Composite Structures*, 31(1995) (3),213-228.

97. Tu, C.Y., Chao, C.C., Three-dimensional contact dynamics of laminated plates: Part 2. Oblique impact with friction, *Composites: Part B* 30 (1999) 23–41.

98. Vaziri, R., Quan, X., Olson, M.D., Impact analysis of laminated composite plates and shells by super finite elements, *International Journal of Impact Engineering*, (1996) 18 (7) 765-782.

99. Vlasov, V.Z., 1958, 'Allegemeine Schalen theorie und ihre anwendung in dar technik', Akademie-Verlag GmBH, Berlin

100. Wang, C.Y., Yew C.H., Impact damage in composite laminates. *Computers and Structures* 37 (1990) 967-982.

101. Wang, D., Yang, J., Sun, Y., Influence of the middle weak layer on the impact behavior of laminated structures, *Acta Mechanica Solida Sinica*, 26 (3) (2013) 263-276.

102. Wu, H.Y. Chang, F.K. Transient dynamic analysis of laminated composite plates subjected to transverse impact, *Computers and Structures*, 31(1989) 453-466.

103. Xiao, S., Chen, P., Ye, Q., Prediction of damage area in laminated composite plates subjected to low velocity impact, *Composites Science and Technology*,98 (27) (2014) 51-5

104. Xie, W., Zhang, W., Kuang, N., Li, D., Huang, W., Gao, Y., Ye, N., Guo, L., Ren, P.,

Experimental investigation of normal and oblique impacts on CFRPs by high velocity steel sphere, *Composites Part B: Engineering*, 99 (2016) 483-493.

105. Xu, J., Askari, A., Weckner, Olaf S. S., Peri-dynamic Analysis of Impact, Damage in Composite Laminates, *Journal of Aerospace Engineering*, ASCE, (2008) 187- 194.

106. Yang, S., Chalivendra, Vijaya B. Kim, Yong K., Fracture and impact characterization of novel auxetic Kevlar/Epoxy laminated composites, *Composite Structures*,16(2017)120-129.

107. Yang, S.H., Sun, C.T., Indentation law for composite laminates, *Composite Material: Testing and Design.*, ASTME STP 787 (1982) 425-449.

108. Yokoyama, N.O., Donadon, M.V., Almeida de, S.F.M., A numerical study on the impact resistance of composite shells using an energy based failure model, *Composite Structures* 93 (2010) 142–152.

109. Zhang, X., Hao, H., Ma, G., Laboratory test and numerical simulation of laminated glass window vulnerability to debris impact, International *Journal of Impact Engineering,* 55, (2013) 49-62.

110. Zhao, G.P., Cho, C.D., Damage initiation and propagation in composite shells subjected to impact, *Composite Structures,* 78 (2007) 91–100.

111. Zheng, C. Ren, M., Zhao,W., Chen, H., Delamination prediction of composite filament wound vessel with metal liner under low velocity impact, *Composite Structures,* 75 (2006) 387–392.

112. Zheng, D., Binienda,W.K., Effect of permanent indentation on the delamination threshold for small mass impact on plates, *International Journal of Solids and Structures,* 44 (2007) 8143–8158.